Interactive comment on "Analysis of multiple new-particle growth pathways observed at the US DOE Southern Great Plains field site" by Anna L. Hodshire et al.

Anonymous Referee #1

Received and published: 19 April 2016

This article presents an important study of growth pathways of nanoparticles, comparing field measurements with results from process modeling. It is well writing and falls within the scope of the journal. While both modeling uncertainties and lack of some key measurements do not allow for closure, uncertainties and limitations are fully acknowledged and discussed. This discussion of limitations is an important aspect of the article, identifying key unknowns holding back out current understanding of nanoparticle growth and signaling ways forward for future work. I recommend this article for publication in ACP with minor revisions.

Scientific Comments 1. GR methods

Page 12 lines 1-5: There are many methods that can be used to calculate GR from measured size distributions. Why is this method used as opposed to e.g. continuous dDp/dt using the mode diameter or using the leading edge of the banana instead of the mode diameter? An evaluation of how the assumptions in this method chosen compare with the way MABNAG calculates GR would show whether any of the systematic discrepancy between measured and modeled GRS is due to method differences instead of missing species as implicitly assumed in later sections. Part of the consistent under prediction of GR from MABNAG compared to these measurements could be due to systematic differences from the method of GR calculation. MABNAG measures wet diam. Temperature of saturators in CPCs of the SMPSs could mean measuring dry diam. For the compositions observed do you have an estimate of how much this could be affecting the particle diameters and thus GRs?

We have reconsidered our GR methods for this work. We have completed the leading edge method and the mode diameter method for each day, as well as made a linear growth rate based upon visual inspection, all for the D_p range of 10-20 nm. We have made figures showing the results of each method (see below) and have included these figures in the supplementary information. It can be seen from the figures that the leading edge and the D_p-mode methods, although fully automated and thus theoretically better than the visual method, do not perfectly

track the growing distribution well. We have added the following text to the discussion on calculating the observed growth rates:

"There is considerable noise in the SMPS data (Figure 1, a-c), especially for May 9 and May 11, due possibly to the hypothesized mixing down of particles and possible inhomogeneities in the air mass. For this reason, we have calculated the growth rate between 10-20 nm for each using three different methods. The first method, referred to here as the leading edge method, is adapted from Lehtipalo et al. (2014) and finds the time at which the binned aerosol distribution between 10-20 nm reaches one half of its maximum $dN/dlogD_p$ for each bin. A linear fit between the bin's median diameter and the associated time determines the growth rate. The second method, referred to here as the D_p-mode method, tracks the change in diameter of the maximum $dN/dlogD_p$ of the aerosol size distribution between 10-20 nm; a linear fit between the diameters and time determines the growth rate. When plotted against the size distribution (see supplement, Figures S1-S3), it is seen that the leading edge and D_p mode method both do not always track the growing size distribution well. For this reason, we have included a third method, which we call the visual method, in which we have made a linear growth rate between 10-20 nm for each day based upon visual inspection of the size distribution (see supplement, Figure S1-S3), using Eq. (3):

$$GR_{obs} = dDp/dt \sim = \Delta Dp/\Delta t \qquad (3)$$

These three methods provides a range of growth rates (Table 3) for the particles between 10-20 nm; the specific results for each day will be discussed in section 3. We do not attempt to provide uncertainty estimates for each method, due to the overall noise in the data. Instead, we present the ranges of calculated growth rates as a possible range of the actual growth rates. May 9 and May 11 tend to have higher growth rates: this could be from the influence of the continued mixing down from nucleation aloft and not actually representative of the growth rates of the particles forming near the surface."

In re the SMPS measurements: the measurements were made at ambient dew point. If the temperature inside the trailer were equal to the ambient temperature, then measurements would have been carried out at ambient relative humidity as well. As an approximation, we have assumed that particle sizes in the SMPSs were equal to particle sizes in ambient air (i.e., water was neither lost nor gained; if particles were wet in the ambient they were equally wet in the DMAs). The temperatures in the trailer should be close to that of the ambient temperatures. We have modified the text to make this more clear, "For all systems, filtered ambient air was used for the DMA sheath air, without adjusting the water vapor partial pressure. Therefore, the

relative humidity was close to ambient relative humidity, and particle water content was close to that in the atmosphere."

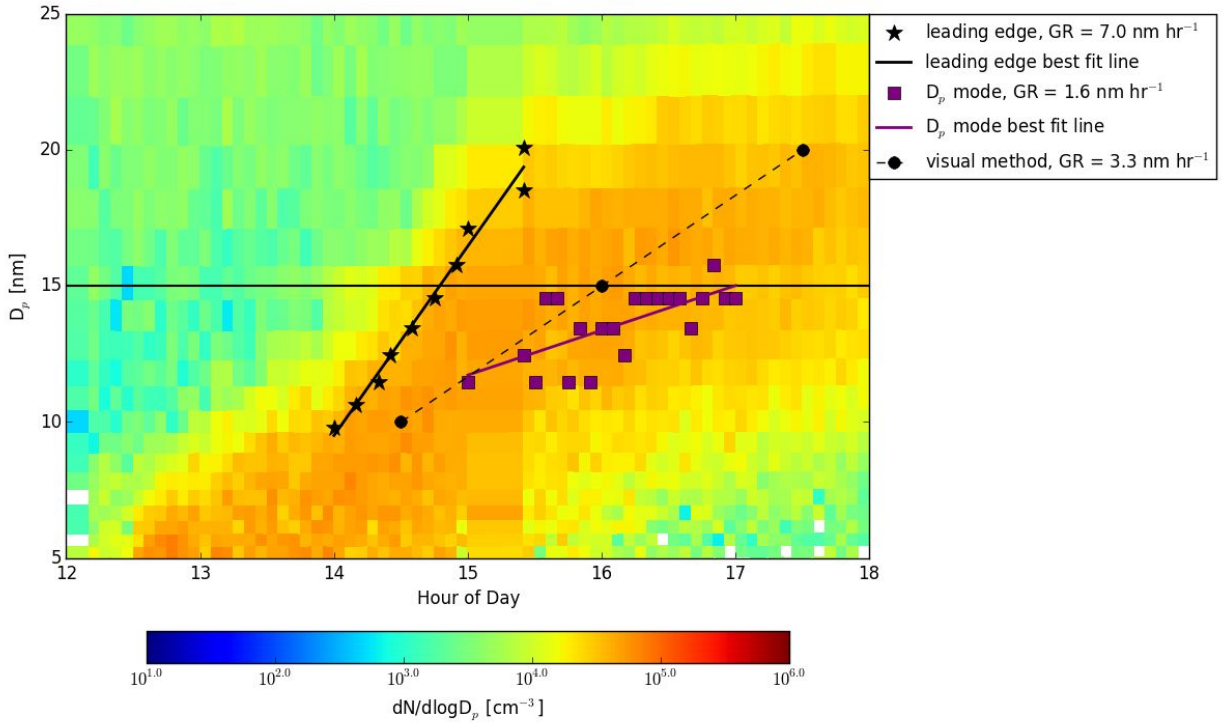

Figure S1. The results of the three growth rate calculations for April 19, 2013. The x-axis represents CDT time. The line at 15 nm D_p is to guide the eye.

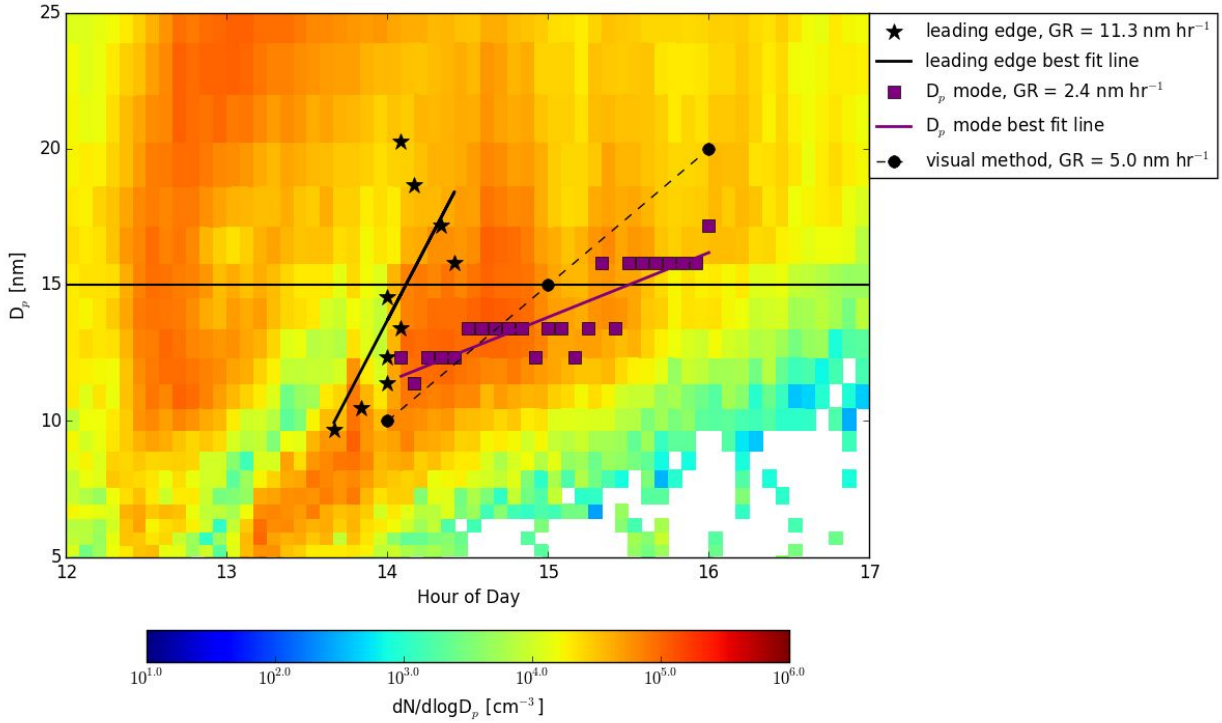

Figure S2. The results of the three growth rate calculations for May 9, 2013. The x-axis represents CDT time. The line at 15 nm D_p is to guide the eye.

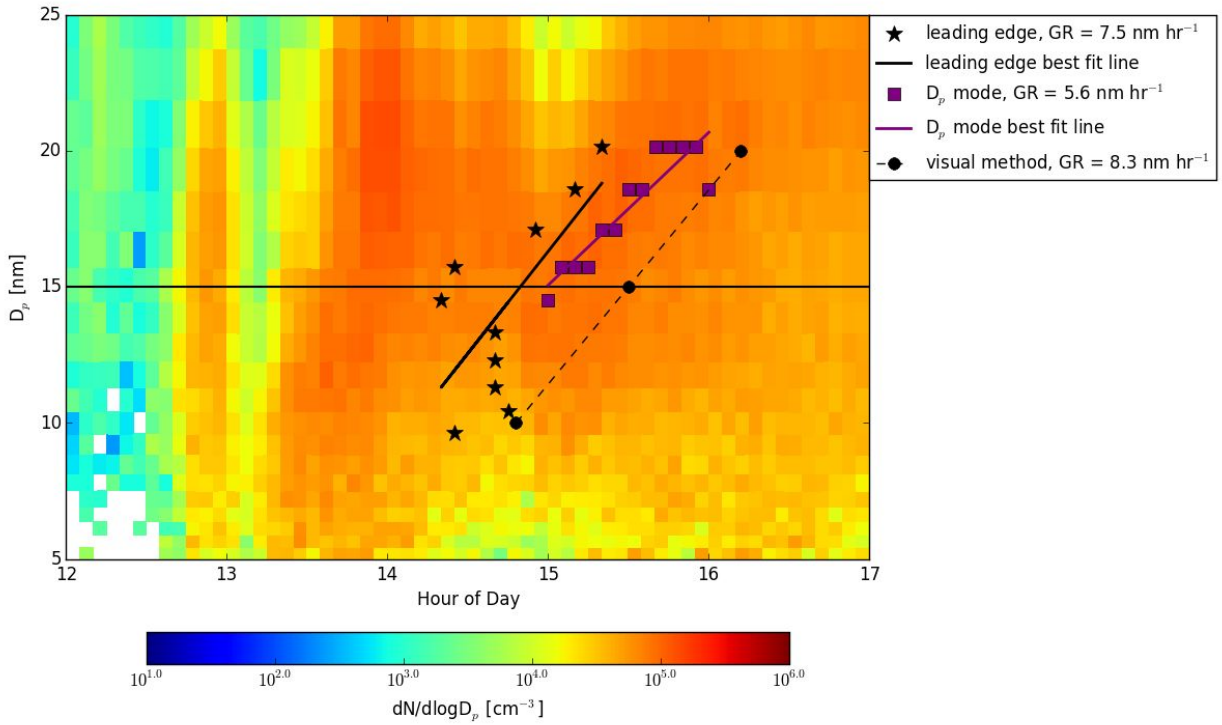

Figure S3. The results of the three growth rate calculations for May 11, 2013. The x-axis represents CDT time. The line at 15 nm D_p is to guide the eye.

2. GR uncertainties

Page 12 paragraph 2: This range of GRs given by the 3 diameter ranges is not a measure of uncertainty, but is presented almost like an uncertainty in the results and evaluation section. Table 3 would be more useful if it showed which GR comes from which diameter range. Is there any trend in how GR varies over the diameter range? A more continuous dDp/dt plotted as a function of Dp would give a clearer view of this and could be usefully compared with how the MABNAG GRs vary with size and an experimental view on whether the reduction of the Kelvin effect with size (line 15) is a significant contributor or not.

See our response to the first half of your first comment under ***Scientific Comments 1. GR methods*** in re the issue of using a range of growth rates; we instead have chosen to present a variety of growth rate methods and their results to show the possible variety in growth rates. Given the variety from just using different methods due to the noise in the SMPS data, we are hesitant to attempt to calculate growth rates at different size ranges, as this will introduce further uncertainties. We do not feel that we can confidently determine any changes in the growth rate from possible Kelvin effects at smaller sizes based on these uncertainties.

Page 15 line 5: 50% MABNAG GR uncertainty from ELVOC concentration uncertainty would lead to a maximum GR of 2.1 nmph, which is still lower than the measured 3nm GR. It needs to be stated clearly that this uncertainty in the ELVOC concentration cannot alone account for the model-measurement discrepancy in this case.

We have added the following to the discussion: "However, even a 50% underprediction of the contribution from ELVOCs to growth would lead to a maximum growth rate of 2.1 nm hr^{-1}, which is on the low end of the growth-rate range that we have calculated from the measurements. Thus, our low bias in growth rate for this day may not be from the ELVOC concentration uncertainties alone."

Page 15 line 9 and lines 16-19 : If LVOC and SVOC contribute more to growth as the particle size increases we would expect the modeled GR to deviate more from the measured result at larger sizes, especially for the case where organics dominate growth. Is this apparent in the data?

For the three days that are analysed here, getting growth rates much past 20 nm in diameter is tenuous, at best. By the time all three days begin to reach sizes beyond 20 nm in diameter, the amount of noise in the SMPS data increases, making the automated growth rate methods' results (e.g. the leading edge and D_p-mode methods) more uncertain. Furthermore, none of the days analysed here grow significantly past ~35 nm. April 19 does not grow far enough past 20 nm to confidently get a growth rate even from the visual method. (The strong growth seen until about hour 18 ends at around 22 nm D_p.)

Similarly, the strong growth seen for the 2nd event of May 9 ends at around 20 nm by about hour 15; the SMPS data at higher D_p at later times shows a very similar number concentration across several D_p bins, making it difficult to pick out a possible growth events.

It is possible to estimate the growth rate for May 11 using the visual method; we obtain a growth rate of around 3 nm hr^{-1} between 20-30 nm between hours ~16-19. This is slower than the growth rate calculated for May 11 using the visual method between 10-20 nm; that growth rate was found to be 8.3 nm hr^{-1}. (It should be noted that for May 11, we likely have a lot of pre-existing aerosol from the first event in the 20-30 nm bins during this time period, making growth-rate calculations less trustworthy.) Across cases and days, if the aerosol grows past 20 nm, MABNAG predicts a growth rate in the 20-30 nm range that is essentially the same (usually slightly slower but only by a few percent) as what is predicted for the 10-20 nm range. Given our uncertainties in the SMPS data, we cannot estimate whether or not the modelled GRs deviate more from the measured GRs at larger sizes.

Page 15 line 26: What is the uncertainty on the cluster CIMS SA measurement and also for the ammonia and amine concentrations on page 16 line 35?

The uncertainty on the Cluster CIMS SA measurements is given in the SI of Chen et al. (2013). We have added the following to the discussion of the Cluster CIMS: "The detection of sulfuric acid in the CIMS has been quantified and calibrated, and the uncertainties for the concentrations of the monomers and dimers of sulfuric acid are estimated to be factors of 1.5 and 3, respectively (Chen et al., 2012)."

The uncertainty for the data set from the AmPMS for the SGP campaign (ammonia and amine concentrations) is given in the SI of Freshour et al. (2014). We have added the following to the discussion of the AmPMS: "Uncertainties in the AmPMS data for this campaign is discussed further in Freshour et al. (2014) and is estimated to be +150/-60%, overall."

Page 18 lines 27-36: RH uncertainty on MABNAG GR would be more usefully included quantitatively in the discussion of GRs for the separate case. This and the ELVOC concentration uncertainty (put at 50% earlier in the manuscript), the oxalic acid factor 100 uncertainty and perhaps other sources of uncertainty could allow a fuller basis for comparison between model and measurements if they were included quantitatively in the results.

One major difficulty in qualitatively including uncertainties for each day for the different uncertain variables is that we do not know the PDFs of these uncertainties. For instance, is the likelihood of oxalic acid equally distributed between 1x and 100x? Could it in reality be lower than 1x or higher than 100x--and so forth for the other uncertain factors. It is beyond the scope of this paper to attempt to fully map out each uncertain variable in its entirety, and we currently do not have a good enough understanding of the uncertainty spaces of our parameters. Instead, discussing the qualitative uncertainties addresses what limitations we have in this study, without introducing further layers of uncertainty by attempting to quantify each uncertain parameter.

Page 12 lines 5-10: Hypothesis that double nucleation is mixing of nucleation event that occurred higher up + later event lower down seems plausible for May 9th, but May 11th both events show particles growing from the smallest sizes. The plots in fig1. are composite plots from multiple SMPSs – could the larger concentrations at larger sizes on May 11th 1st nucleation event be a compatibility issue between SMPSs (i.e. could the SMPS measuring at larger sizes be measuring with a higher efficiency – perhaps because of unaccounted for diffusion losses in the sampling lines?)

We put a large effort into comparing the responses of the 3 SMPS instruments for the size ranges where they overlap, and it was seen that the SMPS systems are in reasonable agreement for these overlapping size ranges. Thus we are confident that the measurements are reasonably accurate, and that the higher concentrations at larger sizes for the first nucleation event of May 11 are not due to SMPS compatibility issues.

May 11th 2nd nucleation event: condensation/coagulation sink from 1st nucleation event will likely be affecting the GR making it appear smaller than it would be for a single event – some estimation of the size of this effect would be useful as it would further increase the difference between the measured GR and the MABNAG modeled GR

MABNAG does not rely on the condensation sink explicitly to make its predictions. We use the measured gas-phase species to drive MABNAG. The condensation sink from the first event would have affected the measured gas-phase sulfuric acid etc on that day, and thus this condensation sink is implicitly included in the MABNAG simulations.

3. Other

Page 7 paragraph 4: Some discussion on the accuracy of MEGAN2.1 estimations of monoterpine emissions and concentrations and applicability for this site/study is necessary to give confidence in their use.

Guenther et al. (2012) provides an discussion of the various uncertainties related to the MEGAN2.1 model; however, they defer to Lamb et al. (1987) and state that , "the uncertainty estimate of a factor of three can be associated with the annual global emissions" of monoterpenes. However, as far as we are aware, no regional studies have been done to determine what uncertainties should be associated with the SGP region in regards to MEGAN model output. Thus, an uncertainty factor of three for the annual global emissions is the best we have at the moment.

We have added the following to the methods discussion of MEGAN: "For a discussion on the uncertainties associated with emissions from MEGAN2.1, see Guenther et al. (2012). "

Page 9 paragraph 1: What was the basis for choosing 20 molecules as the initial particle size? How does this choice affect the modeled results?

Choosing 20 molecules of each species as the initial particle size is arbitrary and creates a particle that is ~3 nm in diameter. The choice of molecules in the 3 nm particle has negligible influence on the growth rate and composition in the 10-20 nm size range.

We have added the following to the text: "MABNAG also requires an initial particle size and composition; for simplicity in this study, the initial particle is formed from 20 molecules of each input species, creating a particle approximately 3 nm in diameter. The choice of molecules in forming the initial particle has negligible influence on the growth rate and composition in the 10-20 nm size range."

Page 12 line 5: On what is the assertion that nucleation potentially occurred aloft based?

The assertion that nucleation potentially occurred aloft is based on tethered balloon data that measured particle size distributions that was taken on May 12. We have added further details to the text as follows: "Similar to May 9 and May 11, the SMPS data for May 12 shows what appears to be two nucleation events occurring at the surface where the SMPS collected size distributions. Tethered-balloon flight profiles for May 12 indicate that nucleation potentially occurred aloft. These observations will be described in detail in a manuscript currently in preparation (Craig, et al., 2016, in preparation), but are briefly described here: The balloon payload consisted of two portable condensation particle counters (model 3007, TSI, Inc.) operating at different minimum size-cut points, which allowed the vertically-resolved measurement of 10 to 20 nm diameter particle number concentrations, $N_{10\text{-}20nm}$. On May 12, high concentrations of particles in this size range were detected at 600 m above ground level, exactly coincident with, or slightly prior to, ground-level observations of high concentrations of $N_{10\text{-}20nm}$. We hypothesize the following explanation for the "double" nucleation events observed on May 9, 11, and 12: Nucleation and growth begins to occur aloft in the residual layer. Once the mixed-layer depth grows into the residual layer, these new particles (that may have already grown to ~10 nm) then mix down and are measured at the surface. This hypothesis is supported by the presence of a high concentration of larger particles (D_p = 10-30 nm) that have already undergone growth at the "beginning" of the first event as measured by the SMPS on May 9 and May 11. Then, the second event, which presumably begins near the surface, shows a high concentration of freshly growing particles (3-5 nm, close to the limit of the SMPS detection) before larger particles appear."

Page 16 line 18: GR for ammonium sulfate case shows better model-measurement agreement than for the growth by organics case. SA/amine/organic growth on p17 also shows better agreement. Comment on why this might be?

We expect to do well for an inorganic ammonium-sulfate system, as gas-phase measurements are complete, and the thermodynamic properties and chemical interactions of ammonia/ammonium and sulfuric acid/sulfate are well-known. Growth by organics is much more difficult to constrain especially under this particular modelling framework given the uncertainties discussed throughout the paper (properties, LVOCs/SVOCs etc.). Given these limitations, it is unsurprising that we do not model the growth rates well for the growth by organics case.

We do not necessarily agree that we do much better for the SA/base/organics growth case than we do for the growth by organics case. We appear to do worse in terms of underpredicting growth rates for the SA/base/organics growth case than we do for the organics case. However, we do see a reasonable amount of sulfate and base in the particle phase for many of the sensitivity cases, which once again is likely due to our ability to model inorganic ammonium-sulfate cases well.

Page 17 line 16: The base simulation predicts GR that are way too low compared to measured GR. Therefore the relevance of the composition from this model seems tenuous. In general, different MABNAG simulations have better/worse agreement with the measured GR and also predict different compositions – more could be made of which compositions are more likely to be accurate based on this.

We do not see one set of assumptions in MABNAG that best captures all three days, and the only cases that had completely unreasonable results were the MAL_LoVP/100ox cases for May 9. Many cases tended to predict similar particle compositions and growth rates with only slight differences from case to case. Given this, the qualitative nature of the TDCIMS data, and that we are not including higher volatility organics (LVOCs and SVOCs) in the model and do not know whether we are accounting for the nitrogen species whose signal often shows up strongly in the TDCIMS, we cannot make definite model-to-observational comparisons and instead present these results as the basis of further research, especially into the areas that we are limited by (i. e. higher volatility organics, etc.).

We have added the following to the discussion for May 11:
"We do note that as MABNAG appears to be underpredicting the growth rates more than for April 19 or May 9 that the MABNAG-predicted particle compositions (Figures 6 and 7) are possibly less representative of the actual particle compositions. However, we reiterate our hypothesis that the underpredictions could be from the nitrogen-containing species that are detected in the TDCIMS but are not accounted for in MABNAG, as well as our uncertainty in ELVOC concentrations and lack of LVOCs, SVOCs, and accretion reactions. Furthermore, this day shows a more variable particle-phase spectrum than April 19 or May 9, as well as a more poorly defined second growth event (Figure 1c), making the observed growth rates difficult to

determine. The TDCIMS particle composition information is only qualitative. Thus, we will not speculate what differences are possible between observed and modelled particle composition."

We have also added the following sentence to the end of the first paragraph of our synthesis section: "We do not see that one set of assumptions in MABNAG best captures all three days (Figures 3, 5, and 7), and instead present these results as a basis for further research, especially into the contribution of higher-volatility organic species to growth."

Page 17 line 18: This sentence should include the fact that there are significant additional unknown growth pathways (N, LVOC, SVOC) as well

We do mention the N uncertainty in the previous paragraph, "The TDCIMS negative ion data also indicate the presence of nitrate; as stated previously, we hesitate to attribute significant growth from nitrate due to the unknown sensitivity of the TDCIMS to nitrate." We have modified the paragraph that page 17/line 18 was in to read, " Conversely, MABNAG predicts roughly 5-25% of the moles in the particle to be from ELVOCs, with the lowest relative ELVOC contribution seen in MAL_LoVP/100ox cases. Since the TDCIMS shows a variable amount of organics throughout the event, and we do not know the actual individual contributions from ELVOCs and organic acids, nor are we accounting for any higher-volatility neutral organic species (e.g. LVOCs and SVOCs), we cannot conclude which set of organics inputs best captures this day and do not exclude any set of inputs for being unrealistic."

Technical Comments

Page 9 line 21: SVOC doesn't seem to be defined here or earlier and should be

Done

Page 7 lines 10-11: "estimated uncertainty in oxalic acid . . . is approximately a factor 100 lower" is unclear. Need a better way of saying the oxalic acid concentrations could be up to 100x larger than measured as done later on page 11

We have modified the text: "Therefore, the estimated systematic uncertainty in the oxalic acid concentration measured via nitrate chemical ionization is approximately up to a factor 100 times lower than reported, indicating that the actual concentration could be up to 100 times higher than observed."

Page 13 line 16: Reference needed for sulfuric acid concentration of 2e-6 leading to 0.2nmph growth rate

This GR was calculated using the growth rate formula for the kinetic regime,

$$dDp/dt = ([H_2SO_4])*(Mw*c*alpha) / (2*rho)$$

Assuming accommodation coefficient alpha = 1; c = sqrt((R*T)/(pi*Mw)); assuming T = 283 K; R = gas constant; Mw = molecular weight of sulfuric acid; $[H_2SO_4]$ = concentration of sulfuric acid; and rho = density of sulfuric acid. This leads to a GR closer to about 0.1 nm hr^{-1}; we have altered the text to reflect that as well as give more information.

The text now reads as follows: “Some notable features of the gas-phase data for April 19 (Figure 2a-b) include relatively low sulfuric-acid concentrations (~2×10^6 cm^{-3}), which should only contribute to growth rates of about 0.08 nm hr^{-1} (assuming kinetic regime growth, an accommodation coefficient of 1, and a temperature of 283 K), or approximately 10% of the observed rates.”

Review of Analysis of multiple new-particle growth pathways observed at the US DOE Southern Great Plains field site by Hodshire et al.

This article adds to the understanding of particle growth processes in the atmosphere. The article is well written and the topic fits to the scope of the journal. The article gives valuable, yet qualitative information about the growth pathways of nanoparticles, which is derived from both measurement and modelling. I find it especially important that the authors show that the major growth mechanism can vary even at the same site and the same season.

The major weakness of this study is the missing reliable measurement of organic compounds of different volatilities. However, I find that the authors are well aware of the limitations, which are acknowledged appropriately and discussed extensively. Therefore I recommend the article to be published in Atmospheric Physics and Chemistry with minor revisions.

General comments and questions:

-how representative were the 3 discussed cases in light of the whole measurement period? Can you estimate which growth pathway was the most important at this site? What determines the prevailing growth mechanism, the sulfuric acid concentration?

During the campaign, 13 possible new-particle formation events were observed. We selected the 3 events that we did because all of the instruments available were working and the TDCIMS was measuring the sizes of the growing nucleation mode. As our growth hypotheses are based on the particle compositions obtained from the TDCIMS, it was important to have data from the smaller, growing particles. For the 10 events that were not analyzed in the paper, the TDCIMS was measuring at a large (~40 nm) particle size for the event and thus the particle compositions of the growing particles was not captured for the most part. Also, some of these events were not captured by our other instruments due to instrument failure. There were a few events in which the TDCIMS captured particles at the end of the growth event (e.g. when the growing particles reached ~40 nm) but at the larger particle sizes, there is more potential for contamination from the background accumulation-mode aerosols as the TDCIMS tends to take in significantly larger particles than the nominal 40 nm particles at these larger size cuts. With all of these considerations, we do not have the ability to estimate the more important growth pathway(s) for SGP during this campaign.

Regarding what determines the prevailing growth mechanism: We have sulfuric acid measurements for the entire campaign except during occasional periods of instrument failure. We do not currently have ELVOC estimates for the entire campaign, as we obtained the monoterpene emissions data from MEGAN from GEOS-Chem for only the three days

considered. Nor do we have any measurements or estimates of higher volatility organics (e.g. LVOCs or SVOCs) that can contribute to growth at larger particle sizes, as has been often brought up in the text. We do see that for the day that showed growth by primarily organics, the ELVOC estimated concentration at the beginning of the event is the highest of the three days and the sulfuric acid concentration at the beginning of the event is the lowest of the three days and that for the ammonium sulfate growth day, the sulfuric acid concentration is the highest out of the three days. Both the organic acid and ELVOC estimated concentrations are higher for the ammonium sulfate day than for the growth by sulfuric-acid/bases/organics, and yet we see significantly more organics for the growth by sulfuric-acid/bases/organics day. It is difficult to draw any conclusions based on only three days as to what determines the prevailing growth mechanism.

-you have particle size distribution measurements from 1.9nm-528nm, yet you report only the growth rate between 10-20nm, why? It would be very interesting to see how the growth rate (and the primary growth mechanism, if you can get that information) changes with particle size

We selected the range 10-20 nm for a few different reasons. We do not see significant growth past ~20 nm for April 19, and we wish to remain consistent in our analysis across the three days. Our analysis of particle composition is somewhat constrained to this smaller size range: our hypotheses of growth mechanisms are based upon the TDCIMS data. During the campaign, the TDCIMS was set to measure at ~40 nm mode diameter when new-particle formation events were not ongoing, and set to measure smaller particle sizes (usually around ~20 nm) when the onset of a new-particle formation event was detected. The smaller size selection was chosen in order to determine what species were in the freshly growing particles. Unfortunately, not all of the events were detected in real-time, and several new-particle formation events occurred without concurrent TDCIMS measurements in the smaller size ranges--these days were not a part of this paper's analyses. Thus we cannot categorically state how the primarily growth mechanism(s) change with particle size, since we do not have TDCIMS data that tracks the growing particles beyond the ~20 nm range for the new-particle formation events.

We have added the following to the text: "We have calculated the observed growth rates between 10-20 nm for each day of our analysis from the SMPS data (Figure 1, a-c). This size range is used since we constrain our analysis of particle composition to the TDCIMS data. During the NPFS campaign, the TDCIMS was set to measure at ~40 nm mode diameter when new-particle formation events were not ongoing. Then, when the onset of a new-particle formation event was detected, the TDCIMS was set to measure smaller particle sizes, around 20 nm mode diameter, in order to determine what species were in the freshly growing particles. Thus, our growth rate calculations represent the size range that the TDCIMS measured in during the events of our analysis."

-can you estimate how accurately was the sulfuric acid concentration measured and how the uncertainties in the total sulfuric acid concentrations affect your conclusions

The uncertainty on the Cluster CIMS SA measurements is given in the SI of Chen et al. (2013). We have added the following to the discussion of the Cluster CIMS: "The detection of sulfuric acid in the CIMS has been quantified and calibrated, and the uncertainties for the concentrations of the monomers and dimers of sulfuric acid are estimated to be factors of 1.5 and 3, respectively (Chen et al., 2013)."

Regarding how the uncertainties of total sulfuric acid concentrations affect our conclusions: consider April 19 as an example. If we assume irreversible condensation (reasonable, given the particle sizes), an accommodation coefficient of 1, and a temperature of ~10 C, the reported sulfuric acid concentration of $2x10^6$ molecules cm^{-3} will lead to a growth rate of ~0.1 nm hr^{-1} by sulfuric acid condensation alone. The concentration of sulfuric acid dimer tends to be at least 2-3 orders of magnitude lower than the concentrations of sulfuric acid monomer throughout the campaign, and often falls beneath the detection limit. Thus, we'll assume that any uncertainty in the dimer concentrations are negligible compared to uncertainties in the monomer concentrations. Under these assumptions, the sulfuric acid could be up to ~$3x10^6$ molecules cm^{-3}, leading to a growth rate of ~0.12 nm hr^{-1}, a ~20% increase in growth from sulfuric acid alone. We have updated our growth rate calculations (please see our response to your final comment for more details on the growth rates) to include three growth rate methods; for April 19, these three methods yield a possible growth rate range of 1.6-7.7 nm hr^{-1}. So even at the low end of this range, 1.6 nm hr^{-1}, the contribution to growth from sulfuric acid goes from contributing 6.25% to 7.5% towards the total growth rate with a 50% increase in sulfuric acid contribution. This difference is too small when compared to our other uncertainties (including what the actual observed growth rate is) to account for any possible underpredictions in the MABNAG-predicted growth rates.

Similarly, the growth rate for May 9, the day that shows the most growth from sulfuric acid, only has about 0.8 nm hr^{-1} of growth coming from condensation of sulfuric acid, assuming the reported concentration of ~$2x10^7$ molecules cm^{-3}. A 50% increase in the sulfuric acid concentration to ~$3x10^7$ molecules cm^{-3} leads to a growth rate of ~1.2 nm hr^{-1}, a 50% increase in the growth rate from sulfuric acid. Thus, the uncertainties in sulfuric acid contribute to smaller uncertainties in growth rates than the other uncertainties discussed in the text.

-based on the text and the showed results it seems that each of the considered days had a predominant growth-mechanism, however, the other compounds also had a minor, but distinct contribution. Therefore, I think it is wrong to say 'growth by organics alone' (as you do in the

abstract) for April 19. I think you need to change the abstract and heading in chapter 3 to say 'Growth primarily by organics' and maybe even add 'with a small contribution from sulfuric acid and ammonia'

We have modified the abstract and heading for chapter 3 to reflect that we see growth primarily from organics.

-the mechanism on May 9: should it be ammonium sulfate or sulfuric acid and ammonia? Maybe also mention the contribution from amines which seems to be non-negligible

We have changed the heading to be Growth by primarily sulfuric acid and ammonia; we indicate in the text of this subsection that amines (and organics) appear to make a small but non-negligible contribution, as well: "A small, but non-trivial, amount of organics and amines are seen in the particle phase as well."

-you claim that on May 11 the mechanism was sulfuric acid/amines/organics, although you say in the text you cannot assess the relative importance of ammonia to amines based on TDCIMS, and also MABNAG predicts both in the particle phase. So why not sulfuric acid, ammonia, amines and organics (or just call it mixed as in the synthesis chapter).

We have changed the abstract and the text to reflect that we see a contribution from bases, instead of only amines.

-there is currently almost no discussion on how the results of this study compare to other recent field and laboratory measurements about nanoparticle growth rates, compositions and proposed growth mechanisms. I suggest the authors could include a short chapter on that before the conclusions section to give an idea how widely representative their results are.

We have added the following brief section:

4. The Southern Great Plains: Comparison to other campaigns

The New Particle Formation Study provided unique insights into new-particle formation events for the region during the spring of 2013, as both gas-phase and particle-phase measurements were taken concurrently in order to assess the species contribution to growth. We see that from three days of the campaign where all instruments were running, three different

dominant growth mechanisms are present, from growth by primarily organics to growth by primarily ammonium sulfate to a mixture of growth from organics, sulfuric acid, and bases.

Previous field campaigns have taken place to similarly assess the growth of new-particle formation events in the continental boundary layer. A review paper by Kulmala et al. (2004) and references therein considered over 100 field campaigns, both long-term and intensive, primarily at continental boundary layer sites. Growth rates were found to be mainly within the 1-20 nm hr^{-1} range in the mid-latitudes, and our events are within this range. Furthermore, for campaigns in which growth rates and gas-phase sulfuric acid were measured, it was found that sulfuric acid tended to account for only 10-30% of the observed growth rates (Kulmala et al., 2004); although water and ammonia accounted for some of the remaining growth, organic compounds are thought to comprise the remaining growth. Studies within the past few years have reported growth from either primarily organics (e.g. Smith et al., 2008b; Kuang et al., 2010; Riipinen et al., 2011; Pierce et al., 2012) or inorganic components, primarily sulfate or ammonium sulfate (e.g. Bzdek et al., 2012).

On-line particle-composition measurements of sub-micron aerosols are a relatively new and still-evolving measurement technique. Smith et al. (2004) reported the first such measurements, using the TDCIMS to examine 6-20 nm particles. Another recently developed instrument is the Nano Aerosol Mass Spectrometer (NAMS) (Wang et al., 2006; Wang and Johnston et al., 2006; Pennington and Johnson, 2012), which reports quantitative elemental composition of nanoparticles in the 10-30 nm range. Of the recent studies that have used combined gas-phase measurements with particle-phase measurements (using either the TDCIMS, NAMS, or both) to determine dominant growth mechanisms (e.g. Smith et al., 2008b; Bzdek et al., 2012; Bzdek et al., 2014), this study is, to our knowledge, unique in reporting distinctly different dominant growth pathways for separate yet temporally closely spaced new-particle growth events. However, it is highly unlikely that SGP is truly unique in this regard; instead the findings of this paper point towards the value of investigating more field sites influenced by mixtures of anthropogenic and biogenic emission using similar combinations of gas-phase and particle-phase measurements.

Specific comments:

-your abstract is too long: you could leave out rows 26-30, which is more like introductory material and is indeed repeated in the introduction chapter.

We feel that lines 26-30 briefly supply important motivation for this particular piece in work, in other words, assessing the contribution of growth from these different pathways. As such, we have chosen to leave these sentences in the abstract.

-the four pathways mentioned in the abstract (row 26-29) and introduction (p.3, row 5-9) seem to be missing the interaction between sulfuric acid and bases (which is mentioned elsewhere, though)

We have altered the discussion on sulfuric acid in abstract to read, "condensation of sulfuric acid vapor (and associated bases when available)", and the discussion in the intro to read, "Irreversible condensation of sulfuric acid vapor (produced through gas-phase oxidation of SO_2 by the hydroxyl radical) is known to be a major contributor to growth. The effective equilibrium vapor pressure of sulfuric acid in the presence of tropospheric water vapor is negligible compared to ambient sulfuric acid concentrations (Marti et al., 1997), and sulfuric acid readily condenses to the smallest stable particles, often forming inorganic salts with associated bases when available."

-you could leave out 'analysis of' from the title. It would make it more concise and put emphasis on the fact that you found several different pathways (just a suggestion, though)

Done.

-p. 8, row 5. Please use SI units

Done.

-p. 13, row 10 citation

This was fixed after the pre-ACPD review.

-it should be mentioned in the abstract and table 3 what size range you considered

Done.

-this reviewer found it confusing that you report a range of GRs for each event. Before carefully reading the methods I did not understand where this range came from. Why not give a mean value and then list all the considered size ranges (10-15, 15-20 and 10-20) in table 3, so you also get a feeling of the variation.

We have reconsidered our GR methods for this work. We have completed the leading edge method and the mode diameter method for each day, as well as made a linear growth rate based upon visual inspection, all for the D_p range or 10-20 nm. We have made figures showing the results of each method (see below) and have included these figures in the supplementary information. It can be seen that the leading edge and the D_p mode methods, although fully automated and thus theoretically better than the visual method, do not always track the growing distribution well. We have added the following text to the discussion on calculating the observed growth rates:

"There is considerable noise in the SMPS data (Figure 1, a-c), especially for May 9 and May 11, due possibly to the hypothesized mixing down of particles and possible inhomogeneities in the air mass. For this reason, we have calculated the growth rate between 10-20 nm for each using three different methods. The first method, referred to here as the leading edge method, is adapted from Lehtipalo et al. (2014) and finds the time at which the binned aerosol distribution between 10-20 nm reaches one half of its maximum $dN/dlogD_p$ for each bin. A linear fit between the bin's median diameter and the associated time determines the growth rate. The second method, referred to here as the D_p-mode method, tracks the change in diameter of the maximum $dN/dlogD_p$ of the aerosol size distribution between 10-20 nm; a linear fit between the diameters and time determines the growth rate. When plotted against the size distribution (see supplement, Figures S1-S3), it is seen that the leading edge and D_p mode method both do not always track the growing size distribution well. For this reason, we have included a third method, which we call the visual method, in which we have made a linear growth rate between 10-20 nm for each day based upon visual inspection of the size distribution (see supplement, Figure S1-S3), using Eq. (3):

$$GR_{obs} = dDp/dt \sim = \Delta Dp/\Delta t \qquad (3)$$

These three methods provides a range of growth rates (Table 3) for the particles between 10-20 nm; the specific results for each day will be discussed in section 3. We do not attempt to provide uncertainty estimates for each method, due to the overall noise in the data. Instead, we present the ranges of calculated growth rates as a possible range of the actual growth rates. May 9 and May 11 tend to have higher growth rates: this could be from the influence of the continued

mixing down from nucleation aloft and not actually representative of the growth rates of the particles forming near the surface."

Regarding the SMPS measurements: the measurements were made at ambient dew point. If the temperature inside the trailer were equal to the ambient temperature, then measurements would have been carried out at ambient relative humidity as well. As an approximation, we have assumed that particle sizes in the SMPSs were equal to particle sizes in ambient air (i.e., water was neither lost nor gained; if particles were wet in the ambient they were equally wet in the DMAs) because the temperatures in the trailer should be close to that of the ambient temperatures. We have modified the text to make this more clear, "For all systems, filtered ambient air was used for the DMA sheath air, without adjusting the water vapor partial pressure. Therefore, the relative humidity was close to ambient relative humidity, and particle water content was close to that in the atmosphere."

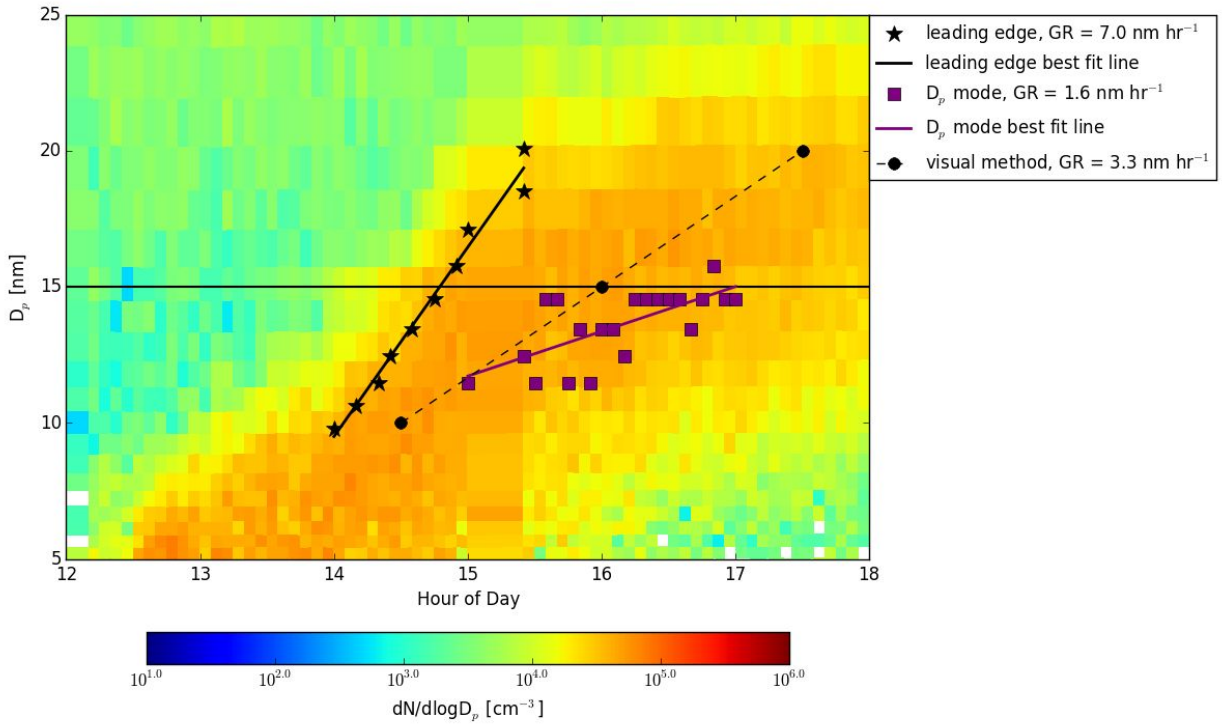

Figure S1. The results of the three growth rate calculations for April 19, 2013. The x-axis represents CDT time. The line at 15 nm D_p is to guide the eye.

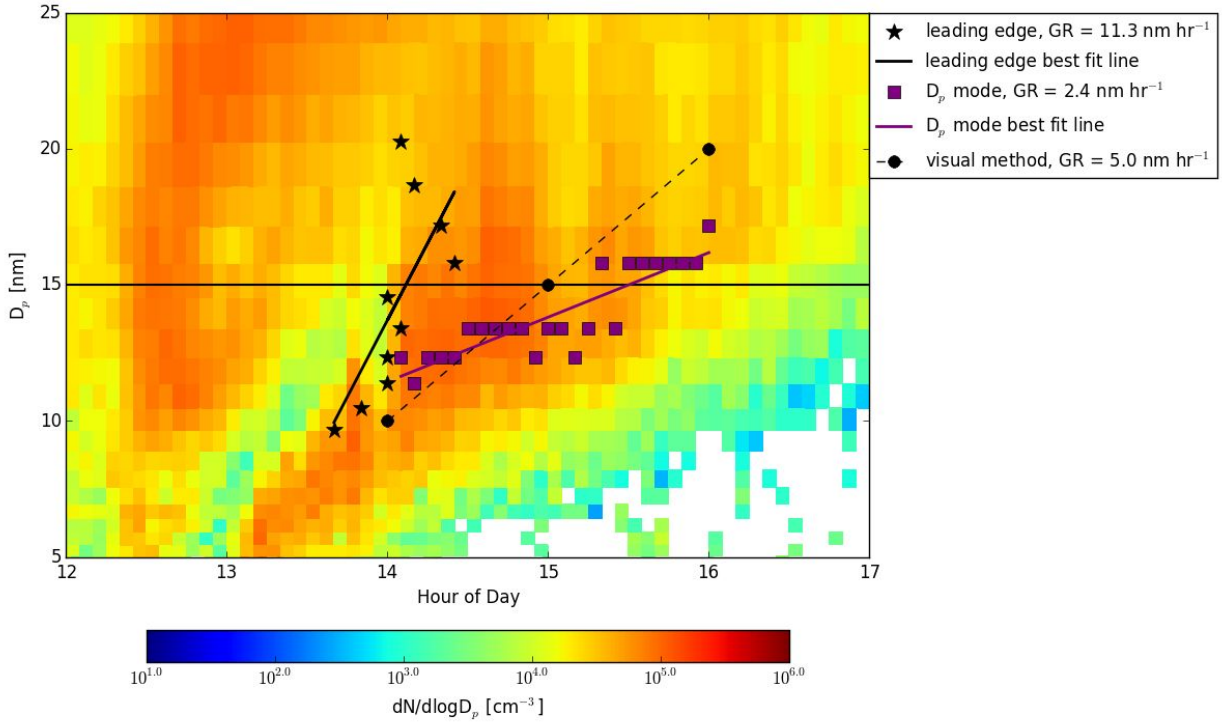

Figure S2. The results of the three growth rate calculations for May 9, 2013. The x-axis represents CDT time. The line at 15 nm D_p is to guide the eye.

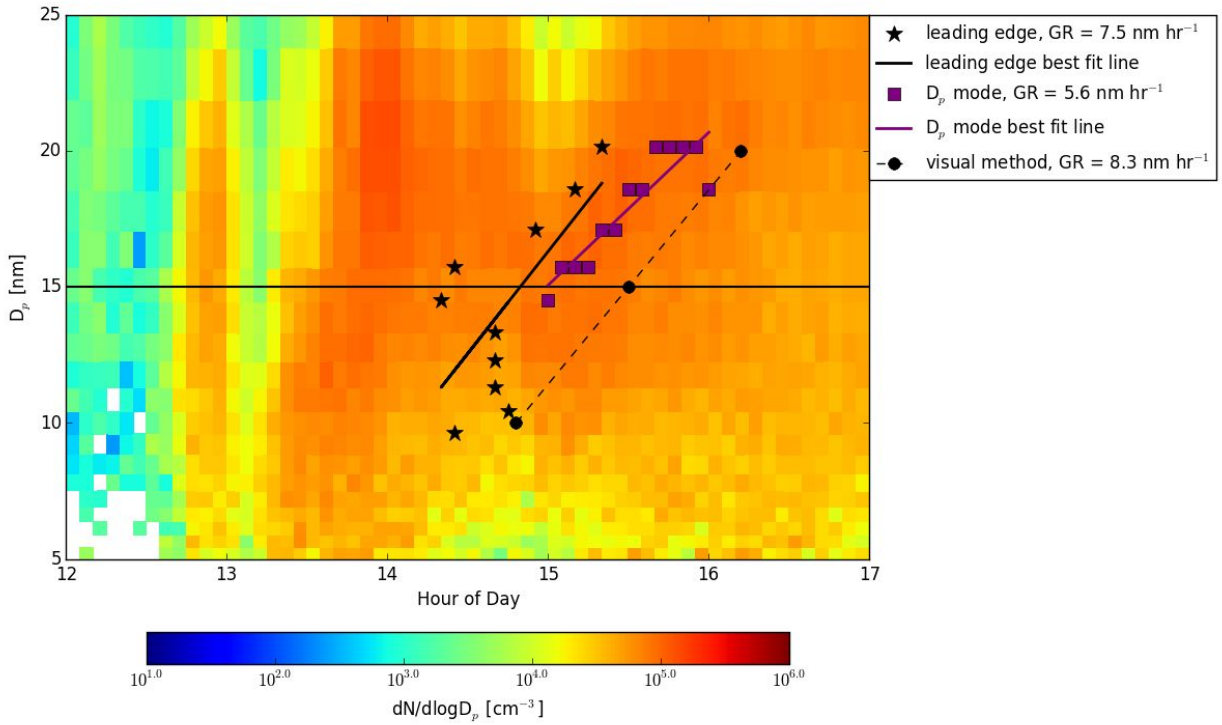

Figure S3. The results of the three growth rate calculations for May 11, 2013. The x-axis represents CDT time. The line at 15 nm D_p is to guide the eye.

Interactive comment on "Analysis of multiple new-particle growth pathways observed at the US DOE Southern Great Plains field site" by
Anna L. Hodshire et al.

Anonymous Referee #4

Received and published: 10 May 2016

This is a very nice paper that combines measurements with modelling. It is based in a technically challenging frontier of aerosol science: determining and verifying the composition of the smallest nucleating particles. It is generally well-defined and clearly written. The authors acknowledge the limitations of their methods and describe the approximations and assumptions they have relied on.

My major concern in this paper relates to the way in which the findings are communicated to the reader. Rather than having a huge data dump, it would be better to both group and separate the scenarios/simulations more clearly. Some methods are suggested below:

In Tables 4-6, for each group of three simulations, the first and last identifiers are constant and the middle one changes. Either change the order of the identifiers or the order in which the simulations are presented. I think it would be clearer to have all the MAL simulations first, divided into thirds by 1ox/10ox/100ox, each of which is further divided based on DMA_L and TMA_L. After that, a similar breakdown of MAL_LoVP, then OX, then OX_LoVP. This would give a logical progression, while still leaving the reference scenario in second place on the list. However, the authors may prefer to use another system based on what they feel is the most important characteristic to group simulations for important comparisons. Based on my reading, it seems that the characteristics change from case to case, and so the ordering may be less important from that perspective.

We have changed Tables 4-6 to Figures 3, 5, and 7. Figures 3, 5, and 7 display both the mole fractions and mass fractions of each species' contributions to the particle for each case. This more clearly communicates how the relative amounts of each species may or may not change across different assumptions. We have further grouped all malonic cases together and all oxalic cases together, instead of grouping MAL/OX then MAL_LoVP/OX_LoVP cases together.

Add vertical lines between the case identifiers and growth rates, and between growth rates and mole fractions.

ACP provides strict formatting guidelines for tables; unfortunately, “Vertical lines must be avoided”. However, we have translated these tables into Figures 3, 5, and 7, thus removing the tables entirely.

Please colour code the simulations which differ significantly from the base case, or which provide the best reproduction of observations; at the very least, those which are discussed in-depth in the text. Refer to the cases by colour in the figure caption, for ease of understanding.

Deviations should hopefully be more apparent with the new figures (Figures 3, 5, and 7).

Add explanatory text to the captions of Tables 4-6. As a general rule, a caption should provide enough information that the item can be at least minimally understood without any other context.

Tables 4-6 have been replaced with Figures 3, 5, and 7. We believe that the captions provided for each of these figure gives a clear explanation of each case and case identifier.

Using T to represent Total amines measured at SGP is quite confusing in the text, because it usually means Temperature (as it does in Table 1, for example). Maybe use TAm?

We agree and have changed all instances of T and L to Tam and Lam in the text and figures.

Use the format A.B × 10C in e.g. Table 1. ($\times$ in LaTeX, Insert →Symbol →× in MS Word)

Your suggested format is correct under ACP guidelines. The numbers have been reformatted in both the tables and text.

In Figure 1, please add units to the colour bar for panels (a)-(c) (and it would be better to label the colour bar as “log N”, or to only label whole powers of ten).

Done.

In panel (f) of Figures 2-4, ELVOCs and organic acids seem to be the same colour. Is this intentional? The mole fractions are shown separately in Tables 4-6, so I assume they can be distinguished at all.

The ELVOCs are a dark green color, and the organic acids are a bright lime green color. There is so little organic acid in the particle phase throughout the shown MABNAG simulations that it cannot be seen for Figure 2 or 6; the predicted organic acid mole fraction is slightly distinguishable in Figure 4.

I would like to see an explicit equation for "the same calculations as used for April 19". I'm more of a physicist than a chemist, and while I tinkered around with the numbers in some of the tables, I couldn't reproduce 12.5% by mole. Of course, there were quite a lot of scenarios in the tables, so it was hard to be sure exactly which numbers I was meant to be using…

We have determined that our calculations for the formation of organic salts are tenuous, given the many uncertainties associated with the organic acids as model inputs (e.g. concentration and chemical properties uncertainties). It is clear that (excluding the few unrealistic cases in which organic acid dominated the particle growth and particle growth rates exceeded 40-50 nm hr^{-1}) organic acids tend to contribute very little to the particle on both a molar and mass basis (see Figures 3, 5, and 7). Thus, we have removed the detailed discussions upon the possible numerical upper bounds of organic salt contribution to particle growth for each day and instead have made note of the small contributions of organic acids to particle growth and thus small contributions of organic salts to particle growth for each case day. For April 19, we state, "The majority of our simulations predict that less than 1% of the particle is organic acid by mole; thus, the contribution to particle growth from organic salt formation would be negligible, even when including the contribution from associated bases. Thus, we expect the majority of growth from organics to be coming from non-reactive organics (ELVOCs in our simulations) for this day." For May 9, we state, "However, given that most cases predict negligible (<3% by mole) of the particle to be composed of organic acid, the contribution to particle growth from organic salt formation is still predicted to be minor for this day." And for May 11, we state, "The majority of our simulations predict <5% by mole of the particle to be organic acid, thus again leading to only minor contributions from organic salt formation to particle growth."

The growth rates listed in Table 3 show a single number, whereas the text references three different numbers for each day. It would be better to see those numbers explicitly rather than be given a range.

We have revised our growth rate estimates for this work. We have decided to use three different methods of determining the growth rate: the leading edge method, the Dp mode method, and a visual method. We have inserted the following into the discussion on calculating observed growth rates:

"There is considerable noise in the SMPS data (Figure 1, a-c), especially for May 9 and May 11, due possibly to the hypothesized mixing down of particles and possible inhomogeneities in the air mass. For this reason, we have calculated the growth rate between 10-20 nm for each using three different methods. The first method, referred to here as the leading edge method, is adapted from Lehtipalo et al. (2014) and finds the time at which the binned aerosol distribution between 10-20 nm reaches one half of its maximum $dN/dlogD_p$ for each bin. A linear fit between the bin's median diameter and the associated time determines the growth rate. The second method, referred to here as the D_p-mode method, tracks the change in diameter of the maximum $dN/dlogD_p$ of the aerosol size distribution between 10-20 nm; a linear fit between the diameters and time determines the growth rate. When plotted against the size distribution (see supplement, Figures S1-S3), it is seen that the leading edge and D_p mode method both do not always track the growing size distribution well. For this reason, we have included a third method, which we call the visual method, in which we have made a linear growth rate between 10-20 nm for each day based upon visual inspection of the size distribution (see supplement, Figure S1-S3), using Eq. (3):

$$GR_{obs} = dDp/dt \sim = \Delta Dp/\Delta t \qquad (3)$$

These three methods provides a range of growth rates (Table 3) for the particles between 10-20 nm; the specific results for each day will be discussed in section 3. We do not attempt to provide uncertainty estimates for each method, due to the overall noise in the data. Instead, we present the ranges of calculated growth rates as a possible range of the actual growth rates. May 9 and May 11 tend to have higher growth rates: this could be from the influence of the continued mixing down from nucleation aloft and not actually representative of the growth rates of the particles forming near the surface."

We have also included in the supplement a figure for each day that shows the results and best-fit lines of these three methods, included below.

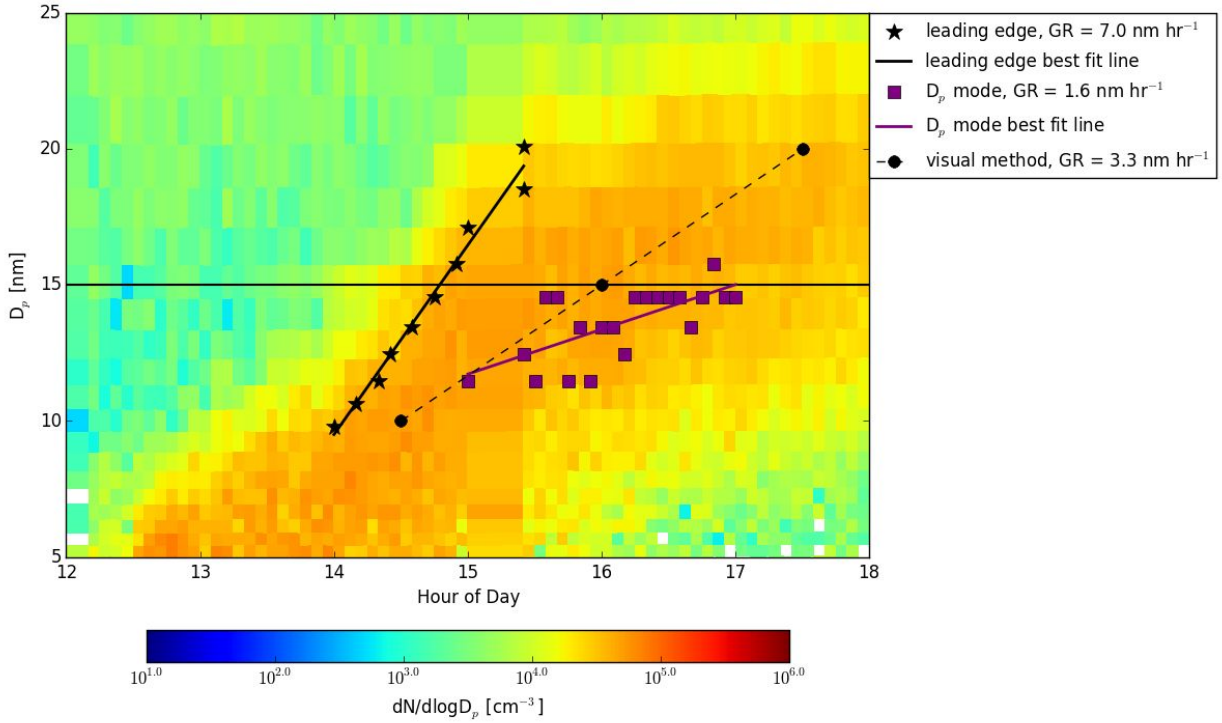

Figure S1. The results of the three growth rate calculations for April 19, 2013. The x-axis represents CDT time. The line at 15 nm D_p is to guide the eye.

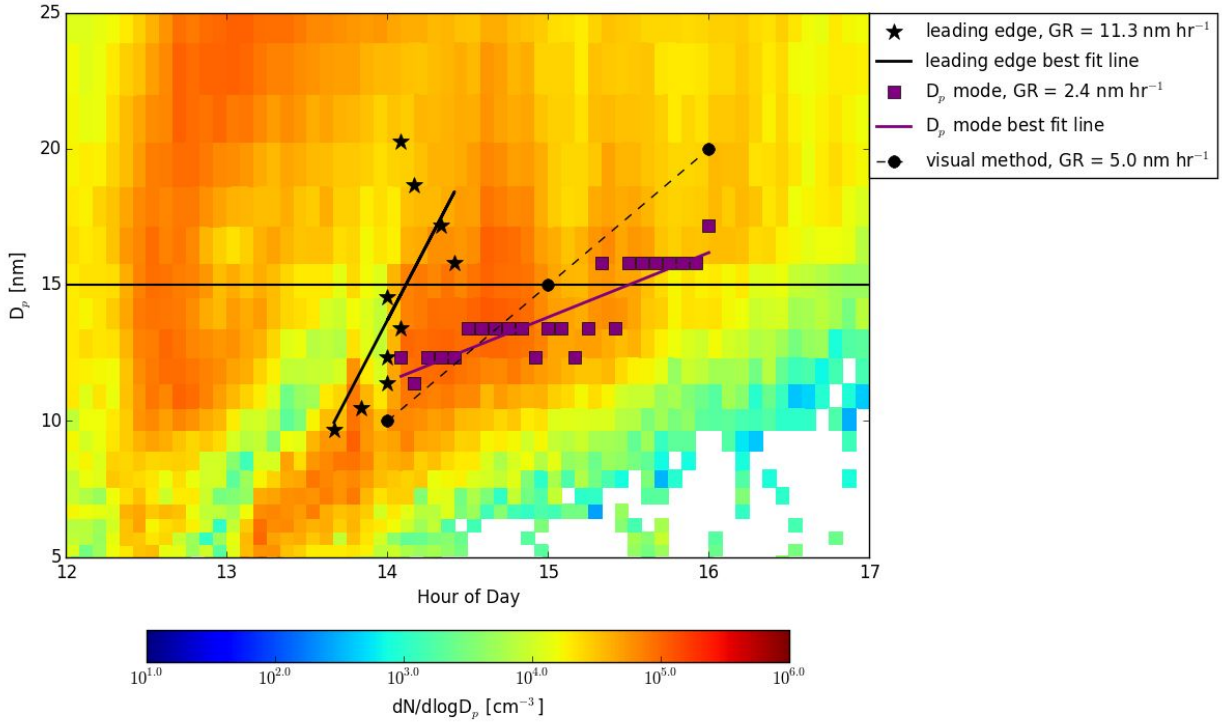

Figure S2. The results of the three growth rate calculations for May 9, 2013. The x-axis represents CDT time. The line at 15 nm D_p is to guide the eye.

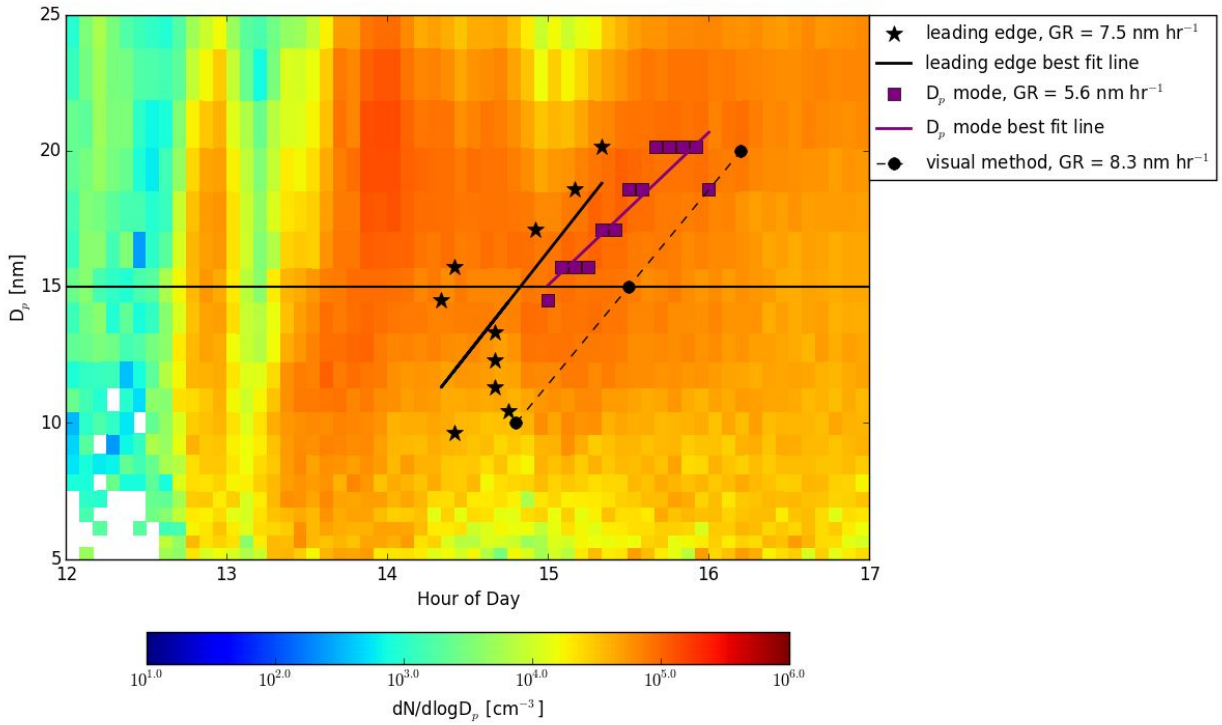

Figure S3. The results of the three growth rate calculations for May 11, 2013. The x-axis represents CDT time. The line at 15 nm D_p is to guide the eye.

Aside from these minor concerns, I found the paper interesting and feel that it makes an important contribution to its field. I would recommend that it be published subject to minor revisions.

Multiple new-particle growth pathways observed at the US DOE Southern Great Plains field site

Anna L. Hodshire[1], Michael J. Lawler[2, a], Jun Zhao[3, b], John Ortega[2], Coty Jen[3, c], Taina Yli-Juuti[4], Jared F. Brewer[1], Jack K. Kodros[1], Kelley C. Barsanti[5, d], Dave R. Hanson[6], Peter H. McMurry[3], James N. Smith[7], Jeffery R. Pierce[1]

[1]Department of Atmospheric Science, Colorado State University, Fort Collins, 80523, USA
[2]Atmospheric Chemistry Observations & Modeling, National Center for Atmospheric Research, Boulder, 80305, USA
[3]Department of Mechanical Engineering, University of Minnesota-Twin Cities, Minneapolis, 55455, USA
[4]Department of Applied Physics, University of Eastern Finland, Kupio, FI-70211, Finland
[5]Department of Civil and Environmental Engineering, Portland State University, Portland, 97201, USA
[6]Department of Chemistry, Augsburg College, Minneapolis, 55454, USA
[7]Department of Chemistry, University of California, Irvine, 92697-2025, USA
[a]now at Department of Chemistry, University of California, Irvine, 92697-2025, USA
[b]now at School of Atmospheric Sciences, Sun Yat-sen University, Guangzhou, 510275, China
[c]now at Environmental Science, Policy, and Management, University of California, Berkeley, 94720-3114, USA
[d]now at Chemical and Environmental Engineering, University of California, Riverside, 92521, USA

Correspondence to: Anna L. Hodshire (hodshire@rams.colostate.edu)

Abstract. New-particle formation (NPF) is a significant source of aerosol particles into the atmosphere. However, these particles are initially too small to have climatic importance and must grow, primarily through net uptake of low-volatility species, from diameters ~1 nm to 30-100 nm in order to potentially impact climate. There are currently uncertainties in the physical and chemical processes associated with the growth of these freshly formed particles that lead to uncertainties in aerosol-climate modeling. Four main pathways for new-particle growth have been identified: condensation of sulfuric acid vapor (and associated bases when available), condensation of organic vapors, uptake of organic acids through acid-base chemistry in the particle phase, and accretion of organic molecules in the particle phase to create a lower-volatility compound that then contributes to the aerosol mass. The relative importance of each pathway is uncertain and is the focus of this work.

The 2013 New Particle Formation Study (NPFS) measurement campaign took place at the DOE Southern Great Plains (SGP) facility in Lamont, Oklahoma, during spring 2013. Measured gas-and particle-phase compositions during these new-particle growth events suggest three distinct growth pathways: (1) April 19 shows growth by primarily organics; (2) May 9 shows growth by primarily sulfuric-acid/ammonia; and (3) May 11 shows growth by primarily sulfuric-acid/bases/organics. To supplement the measurements, we used the particle-growth model MABNAG (Model for Acid-Base chemistry in NAnoparticle Growth) to gain further insight into the growth processes on these three days at SGP. MABNAG simulates growth from (1) sulfuric-acid condensation (and subsequent salt formation with ammonia or amines); (2) near-irreversible condensation from non-reactive extremely-low-volatility organic compounds (ELVOCs); and (3) organic-acid condensation and subsequent salt formation with ammonia or amines. MABNAG is able to corroborate the observed differing growth pathways, while also predicting that ELVOCs contribute more to growth than organic salt formation. However, most MABNAG

Jan Hamer 6/13/2016 2:03 PM
Deleted: Analysis of multiple

Anna Hodshire 5/5/2016 10:45 AM
Deleted: alone

Anna Hodshire 5/5/2016 10:51 AM
Deleted: amines

model simulations tend to underpredict the observed growth rates between 10-20 nm in diameter; this underprediction may come from neglecting the contributions to growth from semi-to-low-volatility species or accretion reactions. Our results suggest that in addition to sulfuric acid, ELVOCs are also very important for growth in this rural setting. We discuss the limitations of our study that arise from not accounting for semi- and low-volatility organics, as well as nitrogen-containing species beyond ammonia and amines in the model. Quantitatively understanding the overall budget, evolution, and thermodynamic properties of lower-volatility organics in the atmosphere will be essential for improving global aerosol models.

1. Introduction

Atmospheric aerosols can affect climate directly, through the absorption and scattering of solar radiation (Rosenfeld et al., 2008; Clement et al. 2009), and indirectly, by modifying cloud properties (Charlson et al., 1992). Both of these effects depend on aerosol particle size, with particles with diameters larger than 50-100 nm dominating the effects. Larger particles scatter and absorb radiation more efficiently than smaller particles (Seinfeld and Pandis, 2006), and particles with diameters larger than 50-100 nm have the potential to act as cloud condensation nuclei (CCN; a full list of all abbreviations used in the paper is listed in Appendix A) (e.g., Seinfeld and Pandis, 2006). CCN number and activity are instrumental in determining cloud properties, including precipitation and albedo (Rosenfeld et al., 2008; Forster et al., 2007). The predictions of these aerosol impacts on climate remain amongst the largest uncertainties in climate models (Boucher et al., 2013). Thus, in order to better constrain the climate effects of aerosols, atmospheric particle size distributions must be accurately modeled.

The majority of atmospheric aerosols originate from photochemically driven new-particle formation (NPF) (e.g., Spracklen et al., 2008; Pierce et al., 2009). NPF is regularly observed to occur throughout the troposphere (e.g. Kulmala et al., 2004; Kuang et al., 2010). We distinguish between nucleation and NPF as follows: Nucleation is the formation of stable particles ~1 nm in diameter from gas-phase sulfuric-acid molecules and stabilizing vapors that could include water, ammonia, amines, diamines, and oxidized organic molecules (e.g. Kirkby et al., 2011; Chen et al., 2012; Almeida et al., 2013; Riccobono et al., 2014; Jen et al., 2016). NPF, however, includes the growth of these stable nuclei to sizes frequently observed in the atmosphere (larger than 3-10 nm). In order to grow to climate-relevant sizes, new particles must grow through uptake of vapors while avoiding being lost to coagulation by larger particles. This competition between growth and coagulational scavenging depends primarily on initial and final particle size, growth rate, and the concentration of pre-existing aerosols (Kerminen et al., 2004; Pierce et al., 2007; Kuang et al., 2010; Westervelt et al., 2013; Westervelt et al., 2014). Large impacts of NPF on CCN are most favorable under conditions of fast particle growth rates and low pre-existing aerosol concentrations (small coagulation sinks). Thus, it is important to understand both particle growth and the time-evolving particle size distributions in order to model the resulting CCN concentrations from new-particle events accurately. In this work, we focus upon the growth of particles from these NPF events.

Particle growth from NPF events is chemically complex and poorly understood. Irreversible condensation of sulfuric acid vapor (produced through gas-phase oxidation of SO_2 by the hydroxyl radical) is known to be a major contributor to growth. The effective equilibrium vapor pressure of sulfuric acid in the presence of tropospheric water

vapor is negligible compared to ambient sulfuric acid concentrations (Marti et al., 1997), and sulfuric acid readily condenses to the smallest stable particles, often forming inorganic salts with associated bases when available. However, observed particle growth often exceeds that which can be explained by the condensation of sulfuric acid alone (Weber et al., 1997; Stoltzenburg et al., 2005; Riipinen et al., 2007; Iida et al., 2008; Kuang et al., 2010; Smith et al. 2010; Pierce et al., 2012). These and other studies have shown that the uptake of low-volatility organic vapors is also important and even explains the majority of growth for some regions (e.g., Smith et al., 2008a; Kuang et al., 2009; Riipinen et al., 2011; Bzdek et al., 2014; Xu et al., 2015). Growth by organics may involve a large number of species and multiple growth pathways (Riipinen et al., 2012). We propose that particle growth rate can be modelled as the sum of the following processes: irreversible condensation of sulfuric acid (GR_{H2SO4}), reversible or nearly irreversible condensation of semivolatile or low-volatility organic compounds ($GR_{org\ cond}$), uptake of organic acids through acid-base chemistry in the particle-phase ($GR_{acid\text{-}base}$), and growth from the accretion of two or more organic molecules in the particle phase to form a lower-volatility compound that can then contribute to aerosol mass (GR_{accret}):

$$GR = GR_{H2SO4} + GR_{org\ cond} + GR_{acid\text{-}base} + GR_{accret} \quad (1)$$

The contribution of atmospheric vapors to observed growth rates through condensation of these organic vapors (without reactions in the particle phase) depends heavily upon the volatility of the organics in the gas phase. It is estimated that the equilibrium vapor pressure required for near-irreversible condensation of vapors onto nanoparticles (defined here to be aerosol particles with an ambient diameter less than 50 nm) must be around 10^{-7} Pa ($\sim 10^{-12}$ atm) or less, corresponding to a saturation concentration of 10^{-4}-10^{-3} μg m^{-3} (Donahue et al., 2011; Pierce et al., 2011).

The presence of essentially non-volatile organic vapors in the atmosphere, referred to here as extremely low-volatility organic compounds (ELVOCs), defined to have saturation concentrations of around 10^{-4} μg m^{-3} or less (Murphy et al., 2014), have been detected in both laboratory and ambient measurements (Ehn et al., 2012; Zhao et al., 2013, Jokinen et al., 2015). Ehn et al. (2014) proposed a possible chemical pathway in which large atmospheric organic parent molecules (e.g. terpenes) undergo initial oxidation to form peroxy radicals followed by rapid autoxidation (self reaction), creating highly oxygenated, yet still large (e.g., 10 carbons) molecules. This pathway has since been confirmed by Jokinen et al. (2014) and Rissanen et al. (2014). Jokinen et al. (2015) determined ELVOC yields from five major biological volatile organic compound (BVOC) species from both ozonolysis and OH oxidation, including isoprene and 4 monoterpenes (limonene, alpha-pinene, myrcene, and beta-pinene). The ELVOC yield for isoprene from the two oxidation pathways is low (0.01% and 0.03%, respectively); however, since isoprene emissions are the highest among all non-methane BVOCs (Guenther et al., 2004), these pathways could contribute an appreciable amount of ELVOCs in high isoprene-emitting regions (e.g., Yu et al., 2014). The monoterpenes have much higher ELVOC yields, ranging from 0.12% to 5.3%, dependending on both the monoterpene structure and oxidation pathway. Subsequent global aerosol simulations have indicated that the ELVOCs produced from the observed monoterpene yields increased NPF and growth globally, which in turn increased total number

concentrations across most of the continental regions and moderately increased the number of CCN (Jokinen et al., 2015).

Ammonia can form inorganic salts in atmospheric particles with sulfuric acid and nitric acid (Jaeschke et al., 1998; Seinfeld and Pandis, 1998); these reactions shift the equilibrium of ammonia (the partitioning species) to the particle phase, as the inorganic salts are lower in volatility than their individual constituents (Pankow, 2003; Pinder et al. 2007). Amines (nitrogen-containing bases with at least one carbon) and organic acids also are observed in growing new atmospheric particles (e.g., Mäkelä et al, 2001; Smith et al., 2008a; Smith et al., 2010; Wang et al., 2010; Tao et al., 2015). Since the vapor pressures of these compounds are higher than is favorable for contributing to new-particle growth by non-reactive condensation alone, the formation of organic salts (formed from organic acids reacting with either amines or ammonia) has been suggested as a potential mechanism for reducing the volatility of these compounds (Barsanti et al., 2009). The presence of these organic-acid and base species in the particle phase depends on the thermodynamic properties of these species (volatility and pKa) (Barsanti et al., 2009) as well as the amount of sulfuric acid, which will preferentially react with bases.

Accretion products are formed from a large variety of reactions, through which organic molecules may contribute to particle mass by reactions between organic molecules that reduce the volatility of the parent molecules (Barsanti and Pankow, 2004; Pun and Seigneur, 2007). Assessing the tendency of atmospheric molecules to undergo accretion reactions via thermodynamic considerations showed that glyoxal and methylglyoxal and acetic, malic, maleic, pinic, and likely other similar mono- and di-carboxylic acids have the thermodynamic potential to contribute significantly to particle growth under the right kinetic conditions (Barsanti and Pankow, 2004; 2005; 2006). Matsunaga et al. (2005) found that small multifunctional compounds (e.g. methylglyoxal) in the ambient atmosphere had a much higher particle-phase affinity than predicted by their Henry's law constants; they proposed oligomerization as a possible pathway. Several laboratory studies have confirmed the presence of accretion products in secondary organic aerosols (SOA) formed from a variety of precursor species (Limbeck et al., 2003; Tolocka et al., 2004; Heaton et al., 2007; Wang et al., 2010). On a mass basis, polymers and oligomers have been found to account for up to 50% of the SOA formed from ozonolysis (Gao et al., 2004; Kalberer et al., 2004; Hall and Johnston et al., 2011). Wang et al. (2010) directly observed oligomers from glyoxal reactions in growing particles from 4-20 nm in diameter, indicating that accretion products have the potential to contribute to new-particle growth. While there are studies showing that accretion could be an important process for particle growth, there are still many uncertainties associated with it.

Despite the growing body of evidence for multiple growth pathways for new-particle growth, current global and regional model studies of aerosol impacts focus on growth through the condensation of vapors only, generally sulfuric acid and lumped organics (e.g. Yu et al., 2011; D'Andrea et al., 2013; Jokinen et al., 2015; Scott et al., 2015). Often, global and regional models with online aerosol microphysics have made simplified assumptions about SOA yields and the size-dependent uptake of organic vapors to particles. Many microphysics models assume fixed SOA yields (e.g., Pierce et al, 2009; Spracklen et al., 2010; Spracklen et al., 2011; Westervelt et al., 2013), as size- and volatility-resolved vapor condensation/evaporation is a computationally burdensome system; others explicitly include volatility-dependent yields (e.g., Zaveri et al., 2008; Yu et al., 2011). The fixed-yield models either treat

SOA as ideally semi-volatile, with the assumption that organic vapors reach instantaneous equilibrium with the aerosol and condense proportionally to the pre-existing particle mass distribution, or the models assume that the SOA is effectively non-volatile and condenses proportionally to the pre-existing Fuchs-corrected surface area (Pierce et al., 2011; Riipinen et al., 2011; Zhang et al., 2012a).

Generally, regional and global models do not account explicitly for the possible particle-phase reactions (organic acid-base chemistry and oligomerization) with some exceptions (e.g. Carlton et al 2010). To our knowledge, no regional or global modelling study has investigated the role of these particle-phase reactions on new-particle growth. The studies discussed above are simply attempting to account for all growth via traditional non-reactive gas-phase condensation. On the other hand, there are several process-based box models that implicitly or explicitly simulate particle-phase processes in addition to condensation and non-reactive partitioning, including the oligomer formation framework of Pun and Seigneur (2007) and Ervens et al. (2010); the kinetic modelling framework of Pöschl et al. (2007), extended by Shiraiwa and co-workers to build multi-layer kinetic models of gas-aerosol interactions (Shiraiwa et al., 2009; 2010; 2012); and the Model for Acid-Base chemistry in NAnoparticle Growth (MABNAG; Yli-Juuti et al. (2013)), a single-particle growth model that simulates particle-phase acid-base reactions as well as condensation/evaporation. These detailed, process-based aerosol models may be used to determine the relative contributions of the various potential growth pathways (GR_{H2SO4}, $GR_{org\ cond}$, $GR_{acid\text{-}base}$, GR_{accret}) but to our knowledge have not been used extensively in conjunction with detailed measurements of growth events. Ultimately, well-tested and measurement-informed process-based models should be used in the future to create next-generation particle-growth schemes for more realistic global and regional aerosol models.

In this study, we seek to understand the species and mechanisms that drove the growth of new particles observed during the Southern Great Plains (SGP) New Particle Formation Study (NPFS) in April-May 2013 in Oklahoma, USA. We attempt to find closure in particle growth rates and particle composition between a state-of-the-art process-based growth model (MABNAG) and detailed measurements of particle growth, particle composition, and gas-phase species. We consider GR_{H2SO4}, $GR_{org\ cond}$, and $GR_{acid\text{-}base}$. We do not consider GR_{accret} as we do not have sufficient measurements to constrain these rates. Through this closure process, we provide estimates of the dominant species and mechanisms for three specific growth events observed during the study. Section 2 provides an overview of our measurement and modelling methods. Section 3 closely examines three NPF events observed during the NPFS at SGP and compares these events to modelling results using MABNAG. Conclusions and future work are discussed in Section 4.

2. Methods

The Southern Great Plains (SGP) New Particle Formation Study (NPFS) took place from April 13 to May 24, 2013 (http://www.arm.gov/campaigns/sgp2013npfs). The primary objectives of the campaign were to study the formation and evolution of aerosols and the impacts of the newly formed particles on cloud processes. The majority of the measurements (and all of those used in this work) took place at the US Department of Energy (DOE) Atmospheric Radiation Measurement (ARM) SGP Central Facility in the Guest Instrument Facility. The site is representative of the large Great Plains region, with agricultural activities, such as cattle and pig husbandry, as well

as oil and gas extraction. To our knowledge, the nucleation and growth in the Great Plains region has not been studied in detail. For more information on the site and campaign, visit the DOE and campaign report websites (http://www.arm.gov/sites/sgp and http://www.arm.gov/campaigns/sgp2013npfs). Thirteen new-particle formation events were observed during the NPFS. In this paper, we focus on three new-particle formation events that occurred on April 19, May 9, and May 11; these were the days where NPF was observed and all the available equipment was operating properly. Figure 1 shows the observed size distributions and derived back trajectories from the HYbrid Single-Particle Lagrangian Integrated Trajectory (HYSPLIT) model (Draxler and Rolph, 2012; Rolph, 2012) for these three days. These data will be described in detail later.

2.1 Measurements

During the 6-week campaign, 13 new-particle formation events were observed at Lamont by a battery of three Scanning Mobility Particle Sizers (SMPS) operated in parallel. They included the DEG SMPS (a TSI 3085 Nano DMA operated with a laboratory prototype laminar flow diethylene glycol condensation particle counter detector; Jiang et al.(2011); 1.9-13.6 nm mobility diameter), a Nano SMPS (a TSI 3085 Nano DMA operated with a TSI 3025A laminar flow ultrafine butanol CPC detector; 2.8-47 nm mobility diameter), and a conventional SMPS (a home-built long column DMA with dimensions similar to the TSI 3071 with a TSI 3760 CPC detector; 23-528 nm mobility diameter). For all systems, filtered ambient air was used for the DMA sheath air, without adjusting the water vapor partial pressure. Therefore, the relative humidity was close to ambient relative humidity, and particle water content was close to that in the atmosphere.

Nanoparticle composition data were collected using the Thermal Decomposition Chemical Ionization Mass Spectrometer (TDCIMS) (Voisin et al., 2003; Smith et al., 2004). For the observations reported here, we used the recently developed time-of-flight mass spectrometer version of the instrument (TOF-TDCIMS) (Lawler et al., 2014). The TDCIMS measures the molecular composition of size-selected atmospheric nanoparticles in near-real-time. It performs this measurement by first charging and size-selecting nanoparticles using unipolar chargers and differential mobility analyzers, respectively. Charged, size-selected particles are collected by electrostatic precipitation onto a platinum filament for approximately 30 min. Following this, the filament is moved into the ion source of a chemical ionization mass spectrometer and undergoes a current ramp to reach an estimated maximum temperature of 600 °C. This heating thermally desorbs and/or decomposes the sample to produce gas phase analyses. Two different chemical ionization reagents are used to detect the chemical species desorbed from the sample: $H_3O^+(H_2O)_n$ (n=0-3), hereafter referred to as "positive ion chemistry", detects base compounds such as ammonia and amines as well as carbonyl-containing compounds and some alcohols; $O_2^-(H_3O)_n$ (n=0-3), hereafter referred to as "negative ion chemistry", detects organic and inorganic compounds with acid groups, as well as other oxygenated compounds with high electron affinities. During the campaign, the instrument cycled roughly hourly between positive and negative ion chemistry. We classify the detected ions into the following categories: ammonia, amine/amide, organics with sulfur, organics with nitrogen, organics without sulfur or nitrogen, sulfate, and nitrates that are either oxidized (no carbons) or inorganic (see Figures 2, 4, and 6, panels (c)-(d)). At the present time, we have not identified marker compounds for the condensation of ELVOCs; however, a prior laboratory study has

shown that the detection of organic acids in nanoparticles correlates with the early growth of nanoparticles from the oxidation of a-pinene (Winkler et al., 2012). We are also unable to distinguish between the oxidized nitrates and the inorganic nitrates; thus we have grouped these ions together (the nitrate (ox/inorg) category in Figures 2, 4, and 6, panels (c)-(d)).

Ambient gas-phase sulfuric acid (both monomers and dimers), malonic acid, and oxalic acid were measured with the Cluster CIMS using nitrate core ion (present primarily as dimer, $HNO3{\bullet}NO_3^-$) as the chemical ionization reagent ion (Zhao et al., 2010). Sulfuric acid, malonic acid, and oxalic acid were detected at m/z 160, 166, and 152 respectively (the molecules clustered with a nitrate ion). The Cluster CIMS measures those acids with unit mass resolution. The detection of sulfuric acid in the CIMS has been quantified and calibrated, and the uncertainties for the concentrations of the monomers and dimers of sulfuric acid are estimated to be factors of 1.5 and 3, respectively (Chen et al., 2013). However, the detection of oxalic acid and, to a much lesser extent, malonic acid may not be as efficient as sulfuric acid due to gas-phase proton affinities of the organic acids compared to that of nitric acid. A calibration comparison with a different Cluster CIMS using acetate ($CH_3CO_2H{\bullet}CH_3CO_2^-$) as the reagent ion (Jen et al., 2015) showed up to two orders of magnitude higher inferred oxalic acid concentration and approximately similar malonic concentrations as the nitrate Cluster CIMS. Therefore, the estimated systematic uncertainty in the oxalic acid concentration measured via nitrate chemical ionization is approximately up to a factor 100 times lower than reported, indicating that the actual concentration could be up to 100 times higher than observed. We explore the sensitivity of the model to these organic-acid uncertainties in this paper.

Ambient gas-phase amines and ammonia concentrations were measured using the Ambient pressure Proton transfer Mass Spectrometer (AmPMS) (Hanson et al., 2011; Freshour et al., 2014), a quadrupole instrument (unit mass resolution) with high sensitivities for ammonia and amines. Signals at the protonated parent masses for methylamine, dimethylamine, and trimethylamine (C1-C3 amines) were assigned with confidence; also detected was a suite of larger alkylamines with four to seven carbons (C4-C7). Less is known about the speciation of these larger amines, as ambient measurements of amines larger than C3 are not often made (e.g. Ge et al., 2011). Contribution of amides to the signals at the masses of the larger amines may also be significant; as such, no structure information was assigned to the C4-C7 amines, as many isomers are possible. Uncertainties in the AmPMS data for this campaign is discussed further in Freshour et al. (2014) and is estimated to be +150/-60%, overall.

A Proton Transfer Reaction Mass Spectrometer (PTR-MS) based on the design of Hanson et al. (2011) was operated unattended during the campaign and was set to measure a suite of volatile organic compounds (VOCs), including isoprene and monoterpenes. However, only one calibration was done for the PTR-MS on May 18, 35 days into the campaign, and during processing, unexplainable spikes were seen in the data at irregular intervals. Further, monoterpene mixing ratios were nearly always unreasonably high (often ranging between 10-100 ppbv). For comparison, a field site in Manitou, Colorado, comprised of a ponderosa pine stand, had maximum monoterpene mixing ratios of 1-2 ppbv during the mid-summer (Ortega et al., 2015), and we expect the monoterpene emissions near the SGP (with few trees) site in April and May to be lower than the forested Manitou site in summer. We thus lack confidence overall in the VOC data obtained by the PTR-MS, so we use an alternative method for estimating monoterpene concentrations, which is described below.

2.2 ELVOC estimate

Rather than using the PTR-MS for VOC data, which suffered from calibration issues, we estimate monoterpene emissions and concentrations using the Model of Emissions of Gases and Aerosols from Nature version 2.1 (MEGAN2.1) (Guenther et al, 2006; Guenther et al, 2012; Sindelarova et al., 2014) in the Goddard Earth Observing System chemical-transport model (GEOS-Chem; http://geos-chem.org). We ran MEGAN2.1 in GEOS-Chem at a 2x2.5 degree resolution to estimate monoterpene emissions rates (monoterpenes are not tracked as prognostic species in these GEOS-Chem simulations). The specific monoterpenes estimated are alpha-pinene, beta-pinene, limonene, sabinene, myrcene, 3-carene, ocimene, and the lumped sum of other monoterpenes (see Guenther et al., 2012 for a complete list). These GEOS-Chem simulations use GEOS-FP meteorological fields generated by the Goddard Modeling and Assimilation Office (GMAO, http://gmao.gsfc.nasa.gov/) and include biogenic emission-factor updates to MEGAN2.1 based on Guenther et al. (2012) and Sindelarova et al. (2014). For a discussion on the uncertainties associated with emissions from MEGAN2.1, see Guenther et al. (2012). We estimate pseudo-steady-state monoterpene concentrations by assuming that the emitted monoterpenes are well mixed up to the boundary-layer (BL) height measured at SGP, and that emissions are balanced by chemical loss by ozonolysis. (The BL height measurements were obtained by the ARM value-added product radiosonde (PBLHTSONDE) at the SGP Central Facility.) For ozonolysis, we used a rate constant, k, of 8.1×10^{-17} cm^3 $molecule^{-1}$ s^{-1} for all monoterpenes, from IUPAC (http://www.iupac.org). For the ozone concentrations, we used hourly ozone monitor measurements from the closest EPA monitoring site, at Dewey, OK, which is 120 miles (~190 km) SW of the SGP site. The uncertainty in ozone concentration due to the distance between measurements is a source of potential error in our monoterpene concentration calculation; however, since we expect ozone concentrations to be relatively homogeneous regionally, we expect other errors (such as ELVOC yields), to be more significant sources of ELVOC uncertainty.

Anna Hodshire 5/16/2016 4:29 PM
Deleted: ·

We estimate the gas-phase ELVOC from the oxidation of the monoterpene (MT) concentrations obtained from MEGAN, assuming a pseudo-steady state between its chemical production and loss by irreversible condensation and neglecting dry deposition as the condensation sink timescales are faster than the dry-deposition timescales (Pierce and Adams, 2009):

$$[ELVOC] = \frac{0.03\, k\, [O_3]\, [MT]}{CS} \quad (2)$$

where CS is the condensation sink, calculated from the SMPS aerosol size-distribution measurements. We note that the SMPS measurements only go up to ~650 nm mobility diameter, so the condensation sink calculated represents a lower limit on the actual condensation sink. The prefactor, 0.03, is the ELVOC molar yield from the α-pinene + ozone reaction found in Jokinen et al. (2015). Alpha-pinene represents ~30% of the MEGAN-estimated monoterpenes present at SGP during the campaign, which is the largest fraction by any of our estimated monoterpene species. Thus, we assume the α-pinene yield to be representative of all of the monoterpenes; in reality, some monoterpene species have higher or lower yields. We do not know the ELVOC yield from oxidation processes for all monoterpene species; thus, this estimate of the ELVOC concentration should be taken as one possible

outcome of monoterpene oxidation. We also acknowledge that our modelled monoterpene concentrations depend on the modelled ozone concentrations, whereas we used the measured ozone concentrations to determine the ELVOC yield. The errors in this assumption are likely small compared to our uncertainties in the ELVOC yield.

2.3.1 Model description

The Model for Acid-Base chemistry in NAnoparticle Growth (MABNAG) has been developed by Yli-Juuti, et al. (2013) to simulate the growth and composition of a single particle resulting from both condensation of low-volatility vapors and acid-base reactions in the particle phase. The version of MABNAG used for this study accepts as inputs the gas-phase concentrations and properties of water, sulfuric acid, a representative organic acid, ammonia, a representative amine, and a representative non-reactive organic, taken here to be an extremely-low-volatility organic compound (ELVOC). The organic compounds are represented in MABNAG with the chemical properties (e.g. pKa, molecular mass, equilibrium vapor pressure) of one organic acid, one amine, and one ELVOC; thus, we must make assumptions about the properties of the organic acid, amine, and ELVOC inputs that are representative for the wide ranges of organic-acid, amine, and ELVOC species. MABNAG also requires an initial particle size and composition; for simplicity in this study, the initial particle is formed from 20 molecules of each input species, creating a particle approximately 3 nm in diameter. The choice of molecules in forming the initial particle has negligible influence on the growth rate and composition in the 10-20 nm size range. We assume a particle density of 1.5 g cm^{-3} and a surface tension of 0.03 N m^{-1}. A sensitivity case using 0.05 N m^{-1} for the surface tension did not affect our results at the particle diameters where we compare to measurements (above 10 nm).

The uptake rates of sulfuric acid, the organic acid, and the ELVOC are calculated as gas-phase-diffusion-limited mass transfer based on their ambient vapor pressures, equilibrium vapor pressures, and gas-phase diffusivities. Water and the bases are assumed to instantly reach equilibrium between the gas and particle phases due to their higher diffusivities and pure-species vapor pressures. Upon uptake, subsequent acid dissociations and base protonations in the particle phase are calculated by the Extended Aerosol Inorganics Model (E-AIM) (http://www.aim.env.uea.ac.uk/aim/aim.php, Clegg et al., 1992; Clegg and Seinfeld, 2006a, b; Wexler and Clegg, 2002). It is assumed that the ELVOC does not dissociate in the particle phase. This vapor pressure is low enough that uptake of ELVOCs is essentially irreversible, even at the smallest simulated particle sizes. We do not consider any additional particle-phase reactions beyond the acid-base reactions: this includes possible accretion reactions that could contribute to growth. We have estimated ELVOC concentrations as they have been shown to have a direct oxidation pathway from monoterpene species to ELVOC species (e.g. Jokinen et al., 2015). On the other hand, the estimations of the concentrations of semivolatile organic compounds (SVOCs), organics with saturation concentrations of 10^{0}-10^{2} µg m^{-3} (Murphy et al., 2014), and the contribution to growth from oligomerization is much less constrained: one must know how the SVOCs are reversibly partitioning to the full aerosol size distribution (as opposed to irreversible condensation to the condensation sink for ELVOCs), and oligomerization rates and the involved SVOC species are highly uncertain. For these reasons, we will not attempt to estimate the SVOC concentration present at SGP and will neglect oligomerization reactions in this work. SVOCs may also directly contribute to particle growth through condensation, as can low-volatility organic compounds (LVOCs), organics

with saturation concentrations of 10^{-3}-10^{-1} μg m^{-3} (Murphy et al., 2014). The condensation of SVOCs and LVOCs depends on particle size; the likelihood of irreversible condensation increases with increasing particle size (Pierce et al., 2011). Pierce et al. (2011) estimates that SVOCs and LVOCs can begin contributing to particle growth at diameters as small as ~10 nm and ~3 nm, respectively, but there are still considerable uncertainties as to the extent in which LVOCs and SVOCs partition to these smaller particle sizes. Thus, omitting LVOCs, SVOCs and resultant condensational growth and/or oligomerization reactions from SVOCs that contribute to growth is a limitation of this study and will be discussed further in the conclusions.

MABNAG assumes that species that enter the particle are instantaneously and homogeneously mixed into a liquid particle phase. This ignores potential particle-phase diffusion limitations that can arise from heterogeneous particle phases. SOA has been observed to have solid and semi-solid phases in both the laboratory and the field (Virtanen et al., 2010; Virtanen et al., 2011). Riipinen et al. (2012) estimated the importance of potential diffusion limitations as a function of size: they argue that diffusion does not limit growth for particles smaller than 20 nm diameter but is potentially important for particles 20-50 nm. However, this remains an uncertainty, and we will address this later.

2.3.2 Model inputs

Inputs to MABNAG were: the gas-phase concentrations from observations or MEGAN-based modelling (Table 1) and chemical properties (Table 2) of water, sulfuric acid, ammonia, an amine, an organic acid, and a non-reactive organic. Relative humidity (RH) is used as a proxy for the water concentration and was obtained from the 60-m tower data maintained by ARM at the Central Facility. Atmospheric temperature was also obtained from the 60-m tower data. The SGP measurement data described earlier provides the gas-phase concentrations of sulfuric acid; ammonia; a suite of amines; and two organic acids, malonic and oxalic acid. The non-reactive organic input will be our ELVOC concentration estimate from the MEGAN monoterpene emissions. ELVOCs consist of a large range of high-molecular-weight compounds with currently unknown structures (Ehn et al., 2014). We assume that our representative ELVOC is one of the dominant ELVOC monomer peaks seen in the mass spectra measured by Ehn et al. (2014), $C_{10}H_{16}O_9$, molecular weight of 280 g mol^{-1}, with the possible structure of three COOH groups, 4 CH groups, 3 CH_2 groups, and 3 OH groups. (Chemical structure is required for the UNIFAC activity coefficient calculations in E-AIM in MABNAG.) However, as the vapor pressure of this ELVOC is extremely low (assumed to be 10^{-9} Pa), simulations are generally insensitive to ELVOC chemical structure. No direct measurements have been made for the saturation vapor pressure of ELVOCs; we assume a saturation vapor pressure of 1×10^{-9} Pa (corresponding to a saturation concentration (C*) of $1 \times 2 \cdot 10^{-4}$ μg m^{-3} at 283 K). This vapor pressure is low enough that uptake of ELVOCs is essentially irreversible, even at the smallest simulated particle sizes.

MABNAG currently simulates one amine and one organic acid, so we ran a suite of sensitivity cases to assess the range of atmospheric acid and base conditions that could help explain observed particle growth. For the amine input, we tested the chemical properties of two amines with single amino groups: dimethylamine (DMA) or trimethylamine (TMA). We denote these cases as DMA and TMA. The pKas of these species are 10.7 (DMA) to 9.8 (TMA), so amines within this pKa range are represented in our sensitivity studies. We tested the sensitivity to the

amine concentration input by using the sum of the light amines only (methylamine, DMA, and TMA only; denoted as Lam) or the sum of all the amines measured (including the C4-C7 amines but excluding the diamines; denoted as Tam) as the input. For the Lam cases, we used the chemical properties of DMA or TMA (denoted DMA_Lam and TMA_Lam, respectively). We assumed the larger amines, which made up over 50% of the total amines (by mass), have a lower pKa than the light amines, and therefore use properties similar to that of TMA for the Tam cases (denoted TMA_Tam). This prevents the over-estimation of the potential contribution of large amines due to salt formation. The assumption that all larger amines behave similarly with low pKas is likely true for alkylamines with a single amino group but does not apply for diamines. Future studies need to examine how diamines react with acids (e.g. dicarboxylic acids to form nylons) and contribute to nanoparticle growth. Regardless, the range of amine pKas and concentrations examined here illustrate the sensitivity of particles to various parameters. For the organic-acid input, we tested using the chemical properties of oxalic or malonic acid, as these were the organic-acid species measured at SGP. These cases are denoted as OX or MAL. We acknowledge that there is a large range of organic acids in the atmosphere, and other monocarboxylic and dicarboxylic acids have been measured in ambient particles (e.g. Rogge et al., 1993; Sempere et al., 1994; Khwaja et al. 1995; Kawamura et al., 1996; Limbeck and Puxbaum, 1999). However, aerosol data from urban, rural, and remote regions has shown that malonic acid tends to be among the dominant organic-acid species in the particle phase, with oxalic acid as the dominant organic-acid aerosol species at all measurement locations (e.g. Grosjean, 1978; Kawamura and Ikushima, 1993; Rogge et al., 1993; Sempere et al., 1994; Kawamura et al., 1995; Khwaja et al., 1995; Kawamura et al., 1996; Kawamura and Sakaguchi, 1999; Limbeck and Puxbaum et al., 1999; Kerminen et al., 2000; Narukawa et al., 2002; Mochida et al., 2003; Sempere and Kawamura, 2003). Thus, we estimate that the contribution of organic acids predicted by MABNAG represents a lower bound of the total contribution of organic acids to particle growth but might be a reasonable estimate.

There is uncertainty in the saturation vapor pressures of organic acids. A review of dicarboxylic acids and complex mixtures compiled by Bilde et al. (2015) shows the best fit saturation vapor pressure of the subcooled liquid states of malonic and oxalic acid as functions of temperature (Figures 7 and 8 of the review). As there are variations between different reported measurements at the same temperature, we have selected to use the saturation vapor pressure values for the subcooled liquid states of oxalic and malonic acid obtained from the best-fit functions in Bilde et al. (2015). Additionally, we include a sensitivity case of reducing the saturation vapor pressures by one order of magnitude below the values shown in Table 2. This reduction is within the range of uncertainty in Bilde et al. (2015). We denote simulations using the properties of oxalic acid with the saturation vapor pressure reduced by one order of magnitude as OX_LoVP; we use similar notation for the malonic-acid cases (MAL_LoVP).

We further performed sensitivity studies for the concentration of oxalic acid. Due to the uncertainty in the oxalic-acid detection efficiency from the Cluster CIMS, the real oxalic-acid concentration could be up to 100x the reported concentration (Figures 2, 4, and 6, panel a). Thus, we ran three sets of concentration input tests: the sum of the reported malonic and oxalic acids (denoted as 1ox), the sum of the reported malonic and 10x the oxalic-acid concentration (denoted as 10ox), and the sum of the reported malonic and 100x the oxalic-acid concentrations (denoted as 100ox). Note that since our simulations include the sum of the oxalic-acid and malonic-acid

concentrations, the scaling of the oxalic-acid concentrations implicitly also allows for testing uncertainties in malonic-acid uncertainties, although we believe these to be smaller (Eisele and Tanner, 1993). Thus, we tested three dimensions of sensitivities for the organic-acid inputs: pKa, vapor pressure, and organic-acid concentrations.

In total, there are 36 sensitivity cases for each day (Tables 4-6). We present the case MAL/10ox/DMA_Lam as the base case for each day, to which other cases will be compared to (Figures 2-4, (e)-(f)). The choice of this case is somewhat arbitrary, but it generally gives intermediate results relative to other simulations, as will be shown later. For each case, we set MABNAG to run until the particle reaches 40 nm in diameter or, if the mean particle growth rate is below 3.3 nm hr^{-1}, the model will stop after 12 hours of simulated time.

2.4 Growth rate calculations

2.4.1 Observed growth rate (SMPS)

We have calculated the observed growth rates between 10-20 nm for each day of our analysis from the SMPS data (Figure 1, a-c). This size range is used since we constrain our analysis of particle composition to the TDCIMS data. During the NPFS campaign, the TDCIMS was set to measure at ~40 nm mode diameter when new-particle formation events were not ongoing. Then, when the onset of a new-particle formation event was detected, the TDCIMS was set to measure smaller particle sizes, around 20 nm mode diameter, in order to determine what species were in the freshly growing particles. Thus, our growth rate calculations represent the size range that the TDCIMS measured in during the events of our analysis.

The plots for May 9 and May 11 indicate that there could be two separate nucleation events, whereas April 19 shows one event. Similar to May 9 and May 11, the SMPS data for May 12 shows what appears to be two nucleation events occurring at the surface where the SMPS collected size distributions. Tethered-balloon flight profiles for May 12 indicate that nucleation potentially occurred aloft. These observations will be described in detail in a manuscript currently in preparation (Craig, et al., 2016, in preparation), but are briefly described here: The balloon payload consisted of two portable condensation particle counters (model 3007, TSI, Inc.) operating at different minimum size-cut points, which allowed the vertically-resolved measurement of 10 to 20 nm diameter particle number concentrations, $N_{10\text{-}20nm}$. On May 12, high concentrations of particles in this size range were detected at 600 m above ground level, exactly coincident with, or slightly prior to, ground-level observations of high concentrations of $N_{10\text{-}20nm}$. We hypothesize the following explanation for the "double" nucleation events observed on May 9, 11, and 12: Nucleation and growth begins to occur aloft in the residual layer. Once the mixed-layer depth grows into the residual layer, these new particles (that may have already grown to ~10 nm) then mix down and are measured at the surface. This hypothesis is supported by the presence of a high concentration of larger particles (D_p = 10-30 nm) that have already undergone growth at the "beginning" of the first event as measured by the SMPS on May 9 and May 11. Then, the second event, which presumably begins near the surface, shows a high concentration of freshly growing particles (3-5 nm, close to the limit of the SMPS detection) before larger particles appear.

As a result, we decided to calculate the growth rate based only on the second growth event for May 9 and May 11, as the second growth events are likely more representative of our ground-based measurements. There is considerable noise in the SMPS data (Figure 1, a-c), especially for May 9 and May 11, due possibly to the

hypothesized mixing down of particles and possible inhomogeneities in the air mass. For this reason, we have calculated the growth rate between 10-20 nm for each using three different methods. The first method, referred to here as the leading-edge method, is adapted from Lehtipalo et al. (2014) and finds the time at which the binned aerosol distribution between 10-20 nm reaches one half of its maximum dN/dlogD_p for each bin. A linear fit between the bin's median diameter and the associated time determines the growth rate. The second method, referred to here as the D_p-mode method, tracks the change in diameter of the maximum dN/dlogD_p of the aerosol size distribution between 10-20 nm; a linear fit between the diameters and time determines the growth rate. When plotted against the size distribution (see supplement, Figures S1-S3), it is seen that the leading-edge and D_p-mode method both do not always track the growing size distribution well. For this reason, we have included a third method, which we call the visual method, in which we have made a linear growth rate between 10-20 nm for each day based upon visual inspection of the size distribution (see supplement, Figure S1-S3), using Eq. (3):

$$GR_{obs} = \frac{dDp}{dt} \cong \frac{\Delta Dp}{\Delta t} \quad (3)$$

These three methods provide a range of growth rates (Table 3) for the particles between 10-20 nm; the specific results for each day will be discussed in Section 3. We do not attempt to provide uncertainty estimates for each method, due to the overall noise in the data. Instead, we present the ranges of calculated growth rates as a possible range of the actual growth rates. May 9 and May 11 tend to have higher growth rates: this could be from the influence of the continued mixing down from nucleation aloft and not actually representative of the growth rates of the particles forming near the surface.

Anna Hodshire 6/23/2016 3:57 PM
Deleted: This method yields a range of growth rates (Table 3)

Jan Hamer 7/1/2016 9:49 AM
Deleted: The use of these three methods provides a range of growth rates (Table 3) for the particles between 10-20 nm; the specific results for each day will be discussed in section 3. .We do not attempt to provide uncertainty estimates for each method, due to the overall noise in the data. Instead, we present the ranges of growth rates as possible ranges of the actual growth rates. May 9 and May 11 tend to have higher maximum growth rates: (up to 8 nm hr^{-1}): this could be from the influence of the continued mixing down from nucleation aloft and not actually representative of the growth rates of the particles forming near the surface.

2.4.2 MABNAG growth rate

MABNAG provides the wet diameter as a function of time: we calculated the rate of change of these diameters using Eq. (3) to get the modelled growth rate. Growth rates in MABNAG generally increase with size due to the reduction of the Kelvin effect with size (gas-phase concentrations are held fixed). The growth rates generally do not change much at diameters larger than 10 nm, so we provide the average growth rate between diameters of 10-20 nm, the same range used to determine the observed growth rates.

2.5 HYSPLIT back trajectories

In order to assess the influence of air mass source upon each event, the NOAA HYbrid Single-Particle Lagrangian Integrated Trajectory (HYSPLIT) model (Draxler and Rolph, 2012; Rolph, 2012) with NAM meteorological data was used to obtain 48-hour air mass back trajectories (Figure 1d-f). The model was initialized at ~250 m above ground level (AGL) at the time of the observed NPF onset for each trajectory; a total of 24 trajectories were output for each event day using the HYSPLIT ensemble feature that perturbs the start height by small increments vertically and horizontally.

3. Results

3.1. April 19: Growth by primarily organics

On April 19, 2013, a NPF event was recorded by the SMPS beginning around 12:00 Central Daylight Time (CDT) (Figure 1a); the three growth rate methods (see section 2.4.1) provided a possible growth rate range of 1.6-8.8 nm hr^{-1} (Table 3). The gas-phase concentrations of each measured species, averaged through this 10-20 nm diameter growth period, are presented in Table 1, and the timeseries of these observations in Figure 2a-b. Note that oxalic acid was not measured by the Cluster CIMS for this day. The ratio of measured oxalic-acid concentration to measured malonic-acid concentration was approximately 0.1 throughout the campaign when oxalic acid data was available; thus, we assume that a baseline concentration of oxalic acid was present at 0.1 times the measured concentration of malonic acid for this day. Some notable features of the gas-phase data for April 19 (Figure 2a-b) include relatively low sulfuric-acid concentrations (~2×10^6 cm^{-3}), which should only contribute to growth rates of about 0.08 nm hr^{-1} (assuming kinetic regime growth, an accommodation coefficient of 1, and a temperature of 283 K), or approximately 10% of the observed rates. Conversely, the concentrations of ammonia and amines are sufficiently high (100-1000 pptv) that they could play a role in sulfuric-acid neutralization and organic-salt formation. The TDCIMS particle-phase ion-fraction data (Figure 2c-d) shows primarily organics with some amines present in the particle phase, indicating that growth by acid-base reactions of organic acids and amines and/or irreversible condensation of ELVOCs is possible. As mentioned previously, we currently have no unequivocal way to distinguish between organic acids and ELVOCs or higher-volatility non-reactive organics in the TDCIMS. The organics categories presented (organics, organics with S, and organics with N) should be taken as the sum total of organics (excluding amines) detected by the TDCIMS. The TDCIMS also shows a presence of nitrate (the nitrate (ox/inorg) category) later on in the growth event. We do not expect to see significant inorganic nitric acid in the growing of sub-50 nm particles, as ammonium nitrate tends to undergo equilibrium-limited growth in submicron particles and partition proportionally to the particle mass distribution (Zhang et al., 2012b). The possibility that much of the observed ox/inorg nitrate signal arises from decomposition or ion-molecule reactions of organic nitrates cannot be excluded. Furthermore, the TDCIMS shows heightened sensitivity to inorganic nitrate with respect to sulfate (Smith et al., 2004; Lawler et al., 2014). Due to all of these uncertainties, we hesitate to attribute significant growth from inorganic nitrate.

The 48-hour HYSPLIT trajectory for April 19 (Figure 1d) shows the flow coming from the northwest. The predicted trajectories appear to be subsiding from the free troposphere over the time period and thus likely only experience surface emissions during the last 18 hours before passing through the Central Facility at Lamont, OK. The surface emissions would likely be coming from central/western Kansas, through primarily agricultural regions and no major urban areas, consistent with the low sulfuric acid concentrations. Based on these back trajectories, we hypothesize that the air mass obtained biogenic SOA precursors from the region north of the SGP site as well as high levels of gas-phase bases due to emissions from agricultural practices.

The MABNAG simulations for this day are able to corroborate the predominance of organics in the particle phase. Our base simulation, MAL/10ox/DMA_Lam (Figure 2e-g; Figure 3) predicts a growth rate of 1.4 nm hr^{-1} with 16% mole fraction from sulfuric acid; <<1% from organic acid, 24% from ammonia; 9.1% from amines; and

Anna Hodshire 5/16/2016 4:29 PM
Deleted: ·

Anna Hodshire 6/10/2016 12:44 PM
Deleted: 2

Anna Hodshire 7/6/2016 11:37 AM
Formatted: Indent: First line: 0.5"

Anna Hodshire 6/9/2016 10:35 AM
Deleted: Table 4

50% from ELVOCs. Figure 3 shows the final dry particle compositions by mole fraction (left-hand bars) and mass fraction (right-hand bars) across our sensitivity cases. Details of MABNAG-predicted ion concentrations are given in Table S1 of the supplement. On a molar basis across cases, MABNAG shows (Figure 3) negligible (<5%) amounts of organic acid in the particle phase, except for MAL_LoVP/100ox cases (an upper bound for organic-acid uptake due to lowered vapor pressure and increased gas-phase concentration), which show up to 18% of the particle was composed of organic acid. Malonic acid has a lower vapor pressure than oxalic acid, and thus more malonic acid is able to enter the particle-phase than oxalic acid. The ELVOC mole fraction tends to be around 50% for most cases, corresponding to ELVOCs composing over 80% of the dry particle by mass fraction. There is a smaller (around 35%) ELVOC mole fraction predicted for the high organic-acid cases. Since we do not know the actual contributions to growth from ELVOCs (or higher-volatility non-reactive organics) versus organic acids from the TDCIMS data, we cannot determine the accuracy of these individual species predictions. However, as the TDCIMS shows very small particle-phase contributions from bases even though high gas-phase base concentrations were also observed, this corroborates that the growth may be dominated by non-reactive organics. We see that MABNAG predicts that approximately ~16% of the particle is composed of sulfuric acid by mole (with associated ammonia). No sulfuric acid appears directly in the TDCIMS ion spectra: thus, MABNAG appears to overpredict the contribution of sulfuric acid (and associated ammonia) for this day relative to the TDCIMS ion fractions. However, since sulfuric-acid vapor concentrations were non-zero, we expect some sulfuric acid in the particle phase. The most likely reason for the discrepancy is low signal-to-noise in the TDCIMS during this period, resulting from low collected particle mass. The TDCIMS data shows some amine/amides in the particle phase: the most amine was predicted with DMA_Lam cases (9-11% by mole) and this compares most closely to the TDCIMS ion fractions of the amine particle-phase predictions. All TMA_Lam cases predict less than 1% amines by moles in the particle phase and thus likely are not realistic inputs for this day. The majority of our simulations predict that less than 1% of the particle is organic acid by mole; thus, the contribution to particle growth from organic salt formation would be negligible, even when including the contribution from associated bases. Thus, we expect the majority of growth from organics to be coming from non-reactive organics (ELVOCs in our simulations) for this day.

The modelled growth rate is around 1.4 nm hr^{-1} for most cases with a few cases (MAL_LoVP/100ox cases) reaching up to 1.7 nm hr^{-1}. When we compare the modelled growth rates to our three growth rate methods that attempt to capture the observed growth rates, we see that the leading-edge method gave the highest growth rate estimate at 8.8 nm hr^{-1} and the D_p-mode method gave the lowest estimate, at 1.6 nm hr^{-1}. However, a visual inspection of the best-fit lines of these two methods (Figure S1) shows that the leading-edge method appears to overpredict the growth rate (the slope of the best fit line is the growth rate in nm hr^{-1}). The D_p-mode method could be slightly underpredicted the growth rate, but is not an unreasonable estimate. The visual method predicts a rate of 3.3 nm hr^{-1}. Therefore, we are more inclined to believe that the growth lies between these two latter estimates, e.g. 1.6-3.3 nm hr^{-1}. Thus, all MABNAG cases come close to or slightly underpredict the observed growth rates. We do note that the organics with N and N (ox/inorg) ion categories dominate the overall TDCIMS spectrum; as MABNAG currently does not account for nitrogen-containing species beyond ammonia and amines, this could account for some of the potential discrepancies in the particle growth rate and composition between model and

Anna Hodshire 6/9/2016 11:09 AM
Deleted: Across our sensitivity cases (Table 4),

Anna Hodshire 6/9/2016 10:51 AM
Deleted: with

Anna Hodshire 6/24/2016 12:45 PM
Deleted: cases underpredict the observed growth rates (3-4 nm hr^{-1}).

observations. As organics are a very important part of this day's particle growth, our results are sensitive to our precursor and yield assumptions of ELVOCs, and for this day where ELVOCs dominated growth, a 50% uncertainty in ELVOC yield would correspond to close to a 50% uncertainty in growth rate (ELVOCs dominate the simulated volume fraction). Having more-direct measurements of VOCs and associated ELVOC yields will better constrain the ELVOC budget. However, even a 50% underprediction of the contribution from ELVOCs to growth would lead to a maximum growth rate of 2.1 nm hr^{-1}, which is on the low end of the growth-rate range that we have calculated from the measurements. Thus, our low bias in growth rate for this day may not be from the ELVOC concentration uncertainties alone. Our lack of LVOCs, SVOCs, and accretion reactions from SVOCs likely also contribute to our potential underprediction, as these species will contribute more with increasing particle size.

Overall, the observations from April 19 clearly show that organic species contribute heavily to growth: the MABNAG results corroborate this, and further the MABNAG simulations show that ELVOCs dominate over organic acids for all sensitivity cases. As the TDCIMS shows small amounts of particle-phase ions from bases even though high gas-phase base concentrations were also observed, this corroborates that the growth may be dominated by non-reactive organics. Furthermore, as ELVOCs are larger molecules than the other species considered here, their contributions to growth rates are even larger than their contribution to mole or ion fractions. Finally, we hypothesize that LVOCs, and perhaps SVOCs or accretion reactions, are contributing to growth within the 10-20 nm diameter range, as MABNAG possibly underestimates growth without these species/reactions.

3.2 May 9: Growth by primarily sulfuric acid and ammonia

On May 9, 2013 (Figure 4), two growth events were observed; we focus our analysis on the second event, which began around 13:00 CDT. The SMPSs and Cluster CIMS both experienced instrument failure from 17:30 CDT onwards on this day; the Cluster CIMS was also not operational before 12:00 CDT. However, the two instruments captured enough of the event to inform our analysis and provide modelling inputs. By 17:30, the three growth rate methods provide a possible growth rate range of 2.4-11.3 nm hr^{-1}. The Cluster CIMS measured high sulfuric acid for this day (~2×10^7 cm^{-3}), sufficiently high for sulfuric acid to contribute significantly to condensational growth. The ammonia concentrations are somewhat higher than the amine concentrations. The TDCIMS shows a high amount of ammonia and sulfate, indicating the presence of ammonium sulfate contributing strongly to the growth of the particles. A small, but non-trivial, amount of organics and amines are seen in the particle phase as well.

The HYSPLIT back trajectory for May 9 (Figure 1e) shows flow from the south, through much of central/east central Texas. The predicted trajectories are entirely in the boundary layer, allowing for the possibility of the air mass experiencing surface emissions throughout the entire previous 48 hours. Many of the possible trajectories pass over or near the major metropolitan Dallas/Fort Worth region and extend into the industrial gulf-coast region; some of the trajectories extend towards the major metropolitan region of Houston. Both possible trajectory paths could contribute SO_2 emissions to the air mass. Local agricultural practices could have contributed ammonia and amines to the air mass, explaining the high base concentrations present at the SGP site.

Anna Hodshire 7/6/2016 9:41 AM
Formatted: Font:10 pt

Anna Hodshire 7/6/2016 9:41 AM
Deleted: ,Additionally, our

Anna Hodshire 7/6/2016 9:41 AM
Formatted: Font:(Default) Times, Font color: Auto

Anna Hodshire 6/9/2016 11:26 AM
Deleted: .

Anna Hodshire 6/9/2016 11:16 AM
Deleted: 3

Anna Hodshire 6/24/2016 12:52 PM
Deleted: particles grew to 20-40 nm diameter at a rate of 3.5-8 nm hr^{-1}.

Anna Hodshire 5/16/2016 4:29 PM
Deleted: ·

Anna Hodshire 6/9/2016 11:26 AM
Deleted: .

The MABNAG simulations for this day are able to capture ammonium-sulfate formation as the dominant growth pathway. Our base simulation, MAL/10ox/DMA_Lam, (Figure 4e-g; Figure 5.) predicts a growth rate of 3.2 nm hr^{-1} with 31% of the particle composition by moles from sulfuric acid; 2.2% from organic acid; 42% from ammonia; 20% from amines; and 4.3% from ELVOCs. Most sensitivity cases (Figure 5) predict approximately 60-90% of the particle is composed of sulfuric acid and ammonia by mole fraction. Only the MAL_LoVP/100ox (upper bound for organic-acid uptake) cases predict otherwise; these cases show over 60% of the particle to be organic acid by moles. However, these cases also show unrealistically high growth rates (~48-57 nm hr^{-1}). Based on these growth rates, we conclude that, at least for this day, growth cannot be realistically captured by the MAL_LoVP/100ox inputs; these cases will not be discussed further. The TDCIMS shows a small amount of organics and an even smaller amount of amine/amide in the particle composition. MABNAG predicts roughly 5-25% of the particle by moles to be organics (ELVOC plus organic acids) with less than 1% up to 5% of the organics by moles coming from ELVOCs. Thus, unlike April 19, organic acid is predicted to dominate the organics contribution for this day. However, given that most cases predict negligible (<3% by mole) of the particle to be composed of organic acid, the contribution to particle growth from organic-salt formation is still predicted to be minor for this day. On a molar basis, less than 1% up to 21% of the particle is predicted to be amines.

MABNAG predicts growth rates between 2.9-5 nm hr^{-1}, with the highest growth rates seen for LoVP cases. These LoVP cases tend to predict a moderate (~15-25% by mole fraction) amount of organics (organic acid + ELVOC) and (~<1% to 20% by mole fraction) amines in the particle phase, leading us to believe that the reduced vapor pressure of organic acids allows for the best fit simulations compared to the measurements of particle growth and composition. When we consider our three growth rate methods that attempt to capture the observed growth rates (Figure S2), we again see that the leading- edge method predicts the highest growth rates, at 11.3 nm hr^{-1}.and the D_p-mode method predicts the lowest, at 2.4 nm h^{-1}. However, again, the best-fit line shows that the leading-edge method appears to be again overpredicting the actual growth rate—some of the larger diameters appear to be influenced by the mixing down of the first nucleation event. The D_p-mode method could be slightly underpredicting the growth rates but the best-fit line does not seem unreasonable enough for us to preclude this growth rate. The visual method provides a growth rate of 5 nm hr^{-1}, but we acknowledge that there is still some uncertainty in this estimate.. If we consider the range provided by the D_p-mode and visual methods, 2.4 to 5.0 nm hr^{-1}, our MABNAG cases either match or slightly underpredict the observed growth rates. Any possible underprediction could again be from the uncertainty from the nitrogen-containing species that appear in the TDCIMS but are not accounted for in MABNAG, as well as our uncertainty in ELVOC concentrations and lack of LVOCs, SVOCs, and accretion reactions.

Overall, the observations from May 9 show a strong contribution from ammonia and sulfate (presumably ammonium sulfate), and the MABNAG simulations corroborate this growth pathway, with the highest average mole fractions of sulfuric acid and ammonia predicted in the particle phase of the three days. This growth pathway should be well represented in regional/global models provided that emissions are well resolved.

3.3 May 11: Growth by sulfuric-acid/bases/organics

Anna Hodshire 6/9/2016 11:16 AM
Deleted: 3

Anna Hodshire 6/9/2016 11:16 AM
Deleted: Table 5

Anna Hodshire 6/9/2016 11:16 AM
Deleted: Table 5

Anna Hodshire 5/5/2016 10:56 AM
Deleted: amines

May 11, 2013 (Figure 6), similar to May 9, shows two growth events; we focus our analysis on the second event, which began around 15:00 CDT. All instruments were fully operational during the growth event, which is observed to extend into May 12. The particles grow to about 25-35 nm in diameter, and our three growth-rate estimates provide a possible growth-rate range of 5.6-8.3 nm hr^{-1} in the 10-20 nm diameter range. The sulfuric-acid concentration on this day (~4x10^6 cm^{-3}) is in between those from the other two growth days. As with the other days, there are high ammonia and amines concentrations (100-10,000 pptv) throughout the event. The TDCIMS shows a mixed view of what is present in the particle phase during the growth event. There is a fairly constant and significant relative amount of sulfate present in the particle. However, at the beginning of the event, amines are the dominant base present, but by 21:00, the relative amine signal has decreased and at 23:00 ammonia is dominant. Both the positive and negative signals show significant contributions from organics. The TDCIMS negative ion data also indicate the presence of nitrate; as stated previously, we hesitate to attribute significant growth from nitrate due to the unknown sensitivity of the TDCIMS to nitrate. Overall, from the TDCIMS, it appears that both sulfate and organics, as well as bases, are important for growth, but we cannot assess the relative importance of ammonia to amines for growth from the observations.

The HYSPLIT back trajectory for May 11 originates primarily from the north, travelling through central Kansas and Nebraska before reaching SGP. Some of the predicted trajectories stay in the boundary layer for the full 48 hours; others show subsidence from the free troposphere, making it difficult to assess how much of the air mass was influenced from surface emissions over the previous 48 hours. Regardless, the air mass passed through primarily agricultural regions and no major urban areas, similar to April 19, but we are unsure of the source of the sulfate on May 11.

Similar to the TDCIMS data, the MABNAG simulations for this day show varying mixtures of sulfuric acid, organics, and bases. Our base simulation, MAL/10ox/DMA_Lam, (Figure 6e-g; Figure 7) predicts a growth rate of 0.9 nm hr^{-1} with 29% of the particle composition by mole from sulfuric acid; <<1% from organic acid; 46% from ammonia; 11% from amines; and 14% from ELVOCs. Across cases (Figure 7), we see that roughly 10-30% by mole fraction of the particle is predicted to be sulfuric acid, in reasonable agreement with the TDCIMS data. MAL_LoVP/100ox (upper bound for organic acid uptake) cases predict up to 46% of the particle moles to be organic acid; the rest of the cases predict less than 1% up to 5% of the particle moles to be organic acid. Conversely, MABNAG predicts roughly 5-25% of the moles in the particle to be from ELVOCs, with the lowest relative ELVOC contribution seen in MAL_LoVP/100ox cases. Since the TDCIMS shows a variable amount of organics throughout the event, and we do not know the actual individual contributions from ELVOCs and organic acids, nor are we accounting for any higher-volatility neutral organic species (e.g. LVOCs and SVOCs), we cannot conclude which set of organics inputs best captures this day and do not exclude any set of inputs for being unrealistic. MABNAG predicts mole fractions of 35-55% for ammonia and less than 1% up to 11% for amines (with less than 1% amines predicted for all TMA cases). As the TDCIMS shows a large amount of amine/amides at the beginning of the event and a large amount of ammonia at the end of the event, we cannot determine which set of base inputs best capture this day either. The majority of our simulations predict <5% by mole of the particle to be organic acid, thus again leading to only minor contributions from organic-salt formation to particle growth.

Anna Hodshire 6/9/2016 11:20 AM
Deleted: 4

Anna Hodshire 6/24/2016 2:21 PM
Deleted: at a rate of 3-8 nm hr^{-1}.

Anna Hodshire 6/9/2016 11:21 AM
Deleted: 4

Anna Hodshire 6/9/2016 11:21 AM
Deleted: Table 6

Similar to April 19 and May 9, MABNAG tends to underpredict the growth rate for this day, with most cases predicting growth at around 0.9-1 nm hr^{-1}. Our three growth-rate methods are in moderately close agreement with each other for this day, with a possible range of 5.6 to 7.5 nm hr^{-1}. It is difficult to distinguish between the first and second growth events for this day, and our observed growth rates could be biased high due to mixing from the first growth rate. However, the majority of MABNAG cases predict a growth rate of 0.9-1 nm hr^{-1}; even if our observed growth rates are biased high, it is still likely that MABNAG underpredicts growth rates for this day. We do note that the MAL_LowVP/100ox cases show slightly higher growth rates at 2.7-3.4 nm hr^{-1}, which come closer to the possible observed growth rates. We do note that as MABNAG appears to be underpredicting the growth rates more than for April 19 or May 9 that the MABNAG-predicted particle compositions (Figures 6 and 7) are possibly less representative of the actual particle compositions. However, we reiterate our hypothesis that the underpredictions could be from the nitrogen-containing species that are detected in the TDCIMS but are not accounted for in MABNAG, as well as our uncertainty in ELVOC concentrations and lack of LVOCs, SVOCs, and accretion reactions. Furthermore, this day shows a more variable particle-phase spectrum than April 19 or May 9, as well as a more poorly defined second growth event (Figure 1c), making the observed growth rates difficult to determine. The TDCIMS particle composition information is only qualitative. Thus, we will not speculate what differences are possible between observed and modelled particle composition.

Overall, the observations from May 11 show that organics, sulfate, and bases (either amines or ammonia) are all important for the evolution of this new-particle growth event. The MABNAG simulations corroborate this, with the organic contribution being from ELVOCs. Growth by LVOCs and/or SVOCs, or organic accretion may also be important, as MABNAG simulations generally underestimated growth and the mole fraction of organics on this day, relative to observations. The back trajectories on this day are similar to those from April 19, though we are unsure of the reason for the difference in sulfuric acid concentrations between the two days. Similar to April 19, the TDCIMS tends to show more organics than bases that would remain after neutralizing the observed particle-phase sulfuric acid, corroborating that the organics in the particle phase are likely dominated by non-reactive organics.

3.4 Synthesis across days

For the 3 days analyzed here, new-particle growth at SGP can be driven by combinations of sulfuric acid (with associated bases) and non-reactive organics, of which ELVOCs contribute a substantial fraction (at least for the yields assumed here). The exact mixture of these pathways depends on the airmass history. We found that the contribution of small organics and organic salts, such as oxalic and malonic acid and associated salts formed with ammonia and amines, to growth may be minor at SGP. However, decreasing the assumed vapor pressure and/or increasing the vapor-phase concentration of the organic acids (within uncertainty ranges) increased the contribution of the small organic acids on some days. Both modelling and measurements show that both ammonia and amines can act as the bases in growing nanoparticles at SGP. While the MABNAG simulations here are limited in the number of species and growth-processes considered, the model is capable of qualitatively differentiating the dominant particle-phase compositions between the 3 days: organics on April 19, inorganics on May 9, and a mixture on May 11. We do not see that one set of assumptions in MABNAG best captures all three days (Figures 3, 5, and

7), and instead present these results as a basis for further research, especially into the contribution of higher-volatility organic species to growth.

Although not discussed above, we also considered the effects of RH uncertainty on our results: April 19 and May 11 both have much lower relative humidities (32% and 36%, respectively) than May 9 (69%). MABNAG shows a moderate sensitivity to RH. We ran a simulation of all days and all cases at 80% RH (not shown); the simulations showed an increase in the dissociation of both malonic and oxalic acids as well as an increase in growth rate for all cases (in part due to increased water uptake), with most cases showing an associated increase in the mole fraction of organic acid. The increase in growth rate depended on the organic acid concentration input and vapor pressure, with the highest increases seen for LoVP/100ox cases. These higher-RH results may be applicable since the boundary layer was well-mixed on the three nucleation days, and the RH increases with height within well-mixed boundary layers. Thus, using surface-based measurements for RH may be a lower-bound for RH and cause growth underestimates.

3.5 Limitations of This Study

While we have shown that MABNAG can quantitatively capture the dominant species that contribute to growth for observed growth events, this study is limited in its scope due to the following uncertainties and limitations:

- There are significant uncertainties in both the measured organic-acid concentrations and chemical properties. The measured oxalic-acid concentrations could be up to 100 times too low due to the uncertainty in the oxalic-acid detection efficiency in the Cluster CIMS. Also, the malonic acid sensitivity is not known. The saturation vapor pressures of malonic and oxalic acid show variation amongst the reported values, and our simulation results are sensitive to their vapor pressures within the reported ranges.
- There is not yet a constrained ELVOC budget from the oxidation of atmospheric VOCs. The yields from different species and under different atmospheric conditions are just beginning to be quantified. The fixed, 3% yield that we used here is preliminary and must be refined as the community continues to learn more about ELVOCs. The confidence in our estimated ELVOC budget also is limited by uncertainties stemming from using MEGAN output for the monoterpene-concentration estimate, and by uncertainties in the local ozone concentrations.
- Large (greater than C3) amines are relatively unstudied in the field as of yet, and the exact identification of these molecules is difficult with current instrumentation. As a result, estimating the thermodynamic properties such as pKa and vapor pressure that determine abilities of these amines to participate in acid-base reactions is difficult, and we can only provide estimates of these contributions.
- Our particle-phase composition measurements from the TDCIMS provide only qualitative information for the organic species present in the growing particles. We do not know the exact molar contributions to the particles from each species, as the TDCIMS is not calibrated for each of the many organic compounds that are detected due to fragmentation during desorption as well as chemical ionization of desorbed gas phase ions. Perhaps more significantly, particle phase "matrix effects" may impact the efficiency by which

organic compounds are desorbed and ionized; such matrix effects are difficult to assess since they depend on the coexisting compounds in the particles and the phase of the particles.

- We did not know the parent molecule(s) of the nitrate signal in the TDCIMS ions that is classified as either inorganic or oxidized nitrate. This signal appears non-trivially during part of every growth event analyzed, but we are without knowledge of its origin.
- The MABNAG model, as used here, only simulates one organic acid and one amine in any individual simulation. This limits our ability to determine the contribution of combinations of organic acids and amines to growth through acid-base reactions and condensation (for the less-volatile organic acids). Instead, we present only limiting cases that inform us of the potential contributions of organic acids and amines if the sum of oxalic and malonic acid had the properties of one these species.
- We did not account for the contribution of LVOCs or SVOCs to condensational growth as there were no gas concentration measurements of such compounds. As particles grow beyond initial cluster sizes, the LVOCs will begin to contribute to growth, and likely are a significant contributor for particles as they approach diameters of 10 nm (Pierce et al., 2011). As the particle continues to grow, the SVOCs may also be a non-trivial contributor to growth (Pierce et al., 2011). Thus, the growth by non-reactive organics is likely underestimated in this study.
- We did not account for accretion reactions that could contribute to particle growth as there were no observations to constrain the contribution of accretion products to new-particle growth during this study. Accretion has been observed in the laboratory in particles greater than 4 nm in size (Wang et al., 2010) and thus has the potential to contribute to growth even at these smaller particle sizes.
- We assumed in MABNAG that all species in the particle phase instantaneously homogeneously mix into a liquid phase: this assumption ignores any particle-phase diffusion limitations that can arise from heterogeneous particle phases. It is estimated that such diffusion limitations can begin to matter at particle sizes greater than 20 nm in diameter.
- We use RH measured at the surface, which may be an underestimate of RH in other portions of a well-mixed boundary layer. MABNAG sensitivity simulations with increased RH showed increased growth rates and contributions from organic acids.

Anna Hodshire 6/24/2016 2:57 PM
Deleted: '

4. The Southern Great Plains: Comparison to other campaigns

The New Particle Formation Study provided unique insights into new-particle formation events for the region during the spring of 2013, as both gas-phase and particle-phase measurements were taken concurrently in order to assess the species contribution to growth. We see that from three days of the campaign where all instruments were running, three different dominant growth mechanisms are present, from growth by primarily organics to growth by primarily ammonium sulfate to a mixture of growth from organics, sulfuric acid, and bases.

Previous field campaigns have taken place to similarly assess the growth of new-particle formation events in the continental boundary layer. A review paper by Kulmala et al. (2004) and references therein considered over 100 field campaigns, both long-term and intensive, primarily at continental boundary layer sites. Growth

rates were found to be mainly within the 1-20 nm hr^{-1} range in the mid-latitudes, and our events are within this range. Furthermore, for campaigns in which growth rates and gas-phase sulfuric acid were measured, it was found that sulfuric acid tended to account for only 10-30% of the observed growth rates (Kulmala et al., 2004); although water and ammonia accounted for some of the remaining growth, organic compounds are thought to comprise the remaining growth. Studies within the past few years have reported growth from either primarily organics (e.g. Smith et al., 2008b; Kuang et al., 2010; Riipinen et al., 2011; Pierce et al., 2012) or inorganic components, primarily sulfate or ammonium sulfate (e.g. Bzdek et al., 2012).

On-line particle-composition measurements of sub-micron aerosols are a relatively new and still-evolving measurement technique. Smith et al. (2004) reported the first such measurements, using the TDCIMS to examine 6-20 nm particles. Another recently developed instrument is the Nano Aerosol Mass Spectrometer (NAMS) (Wang et al., 2006; Wang and Johnston et al., 2006; Pennington and Johnson, 2012), which reports quantitative elemental composition of nanoparticles in the 10-30 nm range. Of the recent studies that have used combined gas-phase measurements with particle-phase measurements (using either the TDCIMS, NAMS, or both) to determine dominant growth mechanisms (e.g. Smith et al., 2008b; Bzdek et al., 2012; Bzdek et al., 2014), this study is, to our knowledge, unique in reporting distinctly different dominant growth pathways for separate yet temporally closely spaced new-particle growth events. However, it is highly unlikely that SGP is truly unique in this regard; instead the findings of this paper point towards the value of investigating more field sites influenced by mixtures of anthropogenic and biogenic emission using similar combinations of gas-phase and particle-phase measurements.

5 Conclusions

Jan Hamer 5/12/2016 11:43 AM
Deleted: 4.

In this study, we sought to understand the species/mechanisms that contribute to the growth of newly formed particles at the US Department of Energy Atmospheric Radiation Measurement program Southern Great Plains (SGP) field site in Oklahoma, US, and to find closure in particle growth rates and composition between the SGP measurements and the growth model, MABNAG. We analyzed data collected from April 13-May 25, 2013 for the SGP New Particle Formation Study (NPFS). We focused the analysis on three new-particle formation and growth events occurring on April 19, May 9, and May 11. These days had different dominant species contributing to growth: April 19 was primarily from organics, May 9 was from ammonium sulfate, and May 11 was from organics, amines/ammonia, and sulfate. MABNAG was constrained by the measured gas-phase concentrations of key atmospheric species present during the growth event for each day, and we found that MABNAG qualitatively simulated the observed dominant species for each day under certain sets of assumptions. We saw that during the NPFS campaign, new-particle growth events can be explained by either sulfuric acid forming salts with atmospheric bases (either ammonia or amines) or the condensation of primarily non-reactive organics, or a combination of these two. MABNAG can qualitatively capture different dominant growth pathways. It appears from the TDCIMS that most of the organics measured are likely non-reactive: if we assume equivalent detection efficiencies, there are

generally more organics than there are bases. The MABNAG simulations support that the organics in the growing particles are likely non-reactive, with the non-reactive-organic ELVOC input species dominating the organic contribution to the particle growth over the organic acid input species in almost every sensitivity case.

MABNAG tends to underpredict the observed growth rates. Due to the strong organics signals in the TDCIMS, we propose that these low growth rates are mainly due to an underrepresentation of organic uptake in MABNAG, either by non-reactive condensation of LVOCs or SVOCs or particle-phase accretion. Furthermore, the discovery of ELVOCs is relatively new and the ELVOC budget remains largely unconstrained.

Although we have not achieved complete closure in particle growth rates and composition between the SGP measurements and MABNAG simulations, we present this work as an important step towards understanding new-particle formation and growth events. We find that the relatively poorly understood ELVOC species can play a key role in the growth of particles through non-reactive condensation. Yet, organics of higher but still sufficiently low vapor pressures ($\sim<10^{0}$ μg m^{-3} saturation mass concentration) are likely also important for growth, and increase in importance with increasing particle size. Based on these findings, we encourage more field-based measurements that focus on the speciation and properties of organics, both in the gas phase and in particles. In particular, gas-phase ELVOC, LVOC, and SVOC measurements, found either through speciation or volatility measurements, would greatly inform future modelling efforts. These measurements are exceedingly challenging but as experimental techniques evolve, they will be invaluable in understanding and modelling both aerosol fundamentals and aerosol impacts on climate and human health.

6. Data Availability

The data from the New Particle Formation Study campaign that was used in the analysis of this paper is available on the ARM DOE website by request (http://www.arm.gov/campaigns/sgp2013npfs). E-AIM is freely available on-line, at http://www.aim.env.uea.ac.uk/aim/aim.php.

Acknowledgements

This research was supported by the U.S. Department of Energy's Atmospheric System Research, an Office of Science, Office of Biological and Environmental Research program, under Grant No. DE-SC0011780 and Grant No. DE-SC0014469. We acknowledge the cooperation of the U.S. Department of Energy as part of the Atmospheric Radiation Measurement (ARM) Climate Research Facility in hosting the New Particle Formation Study (NPFS) at the Central Facility. In addition to data from the NPFS data, we acknowledge the access of atmospheric condition data (temperature and relative humidity) from routine measurements at the Central Facility. Coty Jen was supported under a NSF AGS Postdoctoral Fellowship. Taina Yli-Juuti was supported by the Academy of Finland Centre of Excellence (grant no. 272041) and strategic funding from University of Eastern Finland.

References

Almeida, J., Schobesberger, S., Kurten, A., Ortega, I. K., Kupiainen-Maatta, O., Praplan, A. P., Adamov, A., Amorim, A., Bianchi, F., Breitenlechner, M., David, A., Dommen, J., Donahue, N. M., Downard, A., Dunne, E., Duplissy, J., Ehrhart, S., Flagan, R. C., Franchin, A., Guida, R., Hakala, J., Hansel, A., Heinritzi, M., Henschel, H., Jokinen, T., Junninen, H., Kajos, M., Kangasluoma, J., Keskinen, H., Kupc, A., Kurten, T., Kvashin, A. N., Laaksonen, A., Lehtipalo, K., Leiminger, M., Leppa, J., Loukonen, V., Makhmutov, V., Mathot, S., McGrath, M. J., Nieminen, T., Olenius, T., Onnela, A., Petaja, T., Riccobono, F., Riipinen, I., Rissanen, M., Rondo, L., Ruuskanen, T., Santos, F. D., Sarnela, N., Schallhart, S., Schnitzhofer, R., Seinfeld, J. H., Simon, M., Sipila, M., Stozhkov, Y., Stratmann, F., Tome, A., Trostl, J., Tsagkogeorgas, G., Vaattovaara, P., Viisanen, Y., Virtanen, A., Vrtala, A., Wagner, P. E., Weingartner, E., Wex, H., Williamson, C., Wimmer, D., Ye, P., Yli-Juuti, T., Carslaw, K. S., Kulmala, M., Curtius, J., Baltensperger, U., Worsnop, D. R., Vehkamaki, H. and Kirkby, J.: Molecular understanding of sulphuric acid-amine particle nucleation in the atmosphere, Nature, 502(7471), 359–363 [online] Available from: http://dx.doi.org/10.1038/nature12663, 2013.

Barsanti, K. C. and Pankow, J. F.: Thermodynamics of the formation of atmospheric organic particulate matter by accretion reactions—Part 1: aldehydes and ketones, Atmos. Environ., 38(26), 4371–4382, doi:10.1016/j.atmosenv.2004.03.035, 2004.

Barsanti, K. C. and Pankow, J. F.: Thermodynamics of the formation of atmospheric organic particulate matter by accretion reactions—2. Dialdehydes, methylglyoxal, and diketones, Atmos. Environ., 39(35), 6597–6607, doi:10.1016/j.atmosenv.2005.07.056, 2005.

Barsanti, K. C. and Pankow, J. F.: Thermodynamics of the formation of atmospheric organic particulate matter by accretion reactions—Part 3: Carboxylic and dicarboxylic acids, Atmos. Environ., 40(34), 6676–6686, doi:10.1016/j.atmosenv.2006.03.013, 2006.

Barsanti, K. C., McMurry, P. H. and Smith, J. N.: The potential contribution of organic salts to new particle growth, Atmos. Chem. Phys., 9(9), 2949–2957, doi:10.5194/acp-9-2949-2009, 2009.

Bilde, M., Barsanti, K., Booth, M., Cappa, C. D., Donahue, N. M., Emanuelsson, E. U., McFiggans, G., Krieger, U. K., Marcolli, C., Topping, D., Ziemann, P., Barley, M., Clegg, S., Dennis-Smither, B., Hallquist, M., Hallquist, Å. M., Khlystov, A., Kulmala, M., Mogensen, D., Percival, C. J., Pope, F., Reid, J. P., Ribeiro da Silva, M. A. V, Rosenoern, T., Salo, K., Soonsin, V. P., Yli-Juuti, T., Prisle, N. L., Pagels, J., Rarey, J., Zardini, A. A. and Riipinen, I.: Saturation vapor pressures and transition enthalpies of low-volatility organic molecules of atmospheric relevance: from dicarboxylic acids to complex mixtures., Chem. Rev., 115(10), 4115–56, doi:10.1021/cr5005502, 2015.

Boucher, O., Randall, D., Artaxo, P., Bretherton, C., Feingold, G., Forster, P., Kerminen, V.M., Kondo, Y., Liao, H., Lohmann, U., Rasch, P., Satheesh, S. K., Sherwood, S., Stevens, B., and Zhang, X. Y.: Clouds and Aerosols, in: Climate Change 2013: The Physical Science Basis. Contribution of Working Group I to the Fifth Assessment Report of the Intergovernmental Panel on Climate Change, edited by: Stocker, T. F., Qin, D., Plattner, G.K., Tignor, M., Allen, S. K., Boschung, J., Nauels, A., Xia, Y., Bex, V., and Midgley, P. M., Cambridge University Press, Cambridge, UK, and New York, NY, USA, 2013.

Bzdek, B. R., Zordan, C. a, Pennington, M. R., Luther III, G. W. and Johnston, M. V: Quantitative Assessment of the Sulfuric Acid Contribution to New Particle Growth, Environ. Sci. Technol., 46(8), 4365–4373, doi:10.1021/es204556c, 2012.

Bzdek, B. and Lawler, M.: Molecular constraints on particle growth during new particle formation, Geophys. …, 1–10, doi:10.1002/2014GL060160.Received, 2014.

Carlton, A. G., Bhave, P. V, Napelenok, S. L., Edney, E. O., Sarwar, G., Pinder, R. W., Pouliot, G. A. and Houyoux, M.: Model representation of secondary organic aerosol in CMAQv4.7., Environ. Sci. Technol., 44(22), 8553–60, doi:10.1021/es100636q, 2010.

Campaign: New Particle Formation Study 2013 (NPFS 2013): http://www.arm.gov/campaigns/sgp2013npfs, last access: 18 Feb. 2016.

Charlson, R. J., Schwartz, S. E., Hales, J. M., Cess, R. D., Coakley, J. A., Hansen, J. E., and Hofmann, D. J.: Climate forcing by anthropogenic aerosols, Science, 255, 423–430, 1992.

Chen, M., Titcombe, M., Jiang, J., Jen, C., Kuang, C., Fischer, M. L., Eisele, F. L., Siepmann, J. I., Hanson, D. R., Zhao, J. and McMurry, P. H.: Acid-base chemical reaction model for nucleation rates in the polluted atmospheric boundary layer., Proc. Natl. Acad. Sci. U. S. A., 109(46), 18713–8, doi:10.1073/pnas.1210285109, 2012.

Chen, M., Titcombe, M., Jiang, J., Jen, C., Kuang, C., Fischer, M. L., Eisele, F. L., Siepmann, J. I., Hanson, D. R., Zhao, J. and McMurry, P. H.: Acid-base chemical reaction model for nucleation rates in the polluted atmospheric boundary layer, AIP Conf. Proc., 1527(46), 647–650, doi:10.1063/1.4803354, 2013.

Cheng, Y., Su, H., Koop, T., Mikhailov, E. and Pöschl, U.: Size dependence of phase transitions in aerosol nanoparticles., Nat. Commun., 6, 5923, doi:10.1038/ncomms6923, 2015.

Clegg, S. L., Pitzer, K. S. and Brimblecombe, P.: Thermodynamics of Multicomponent, Misclble, Ionic Solutions. 2. Mixtures Including Unsymmetrical Electrolytes, J. Phys. Chem., 96(23), 9470–9479, doi:10.1021/j100202a074, 1992.

Clegg, S. L. and Seinfeld, J. H.: Thermodynamic models of aqueous solutions containing inorganic electrolytes and dicarboxylic acids at 298.15 K. 1. The acids as non-dissociating components, J. Phys. Chem. A, 110, 5692–5717, 2006a.

Clegg, S. L. and Seinfeld, J. H.: Thermodynamic models of aqueous solutions containing inorganic electrolytes and dicarboxylic acids at 298.15 K. 2. Systems including dissociation equilibria, J. Phys. Chem. A, 110, 5718–5734, 2006b.

Clement, A. C., Burgman, R., and Norris, J. R.: Observational and Model Evidence for Positive Low-Level Cloud Feedback, Science, 325, 460–464, 2009.

Craig, et al.: in preparation, 2016.

D'Andrea, S. D., Häkkinen, S. A. K., Westervelt, D. M., Kuang, C., Levin, E. J. T., Kanawade, V. P., Leaitch, W. R., Spracklen, D. V., Riipinen, I. and Pierce, J. R.: Understanding global secondary organic aerosol amount and size-resolved condensational behavior, Atmos. Chem. Phys., 13(22), 11519–11534, doi:10.5194/acp-13-11519-2013, 2013.

Donahue, N. M., Trump, E. R., Pierce, J. R. and Riipinen, I.: Theoretical constraints on pure vapor-pressure driven condensation of organics to ultrafine particles, Geophys. Res. Lett., 38(16), n/a–n/a, doi:10.1029/2011GL048115, 2011.

Draxler, R. R. and Rolph, G. D.: HYSPLIT (HYbrid Single-Particle Lagrangian Integrated Trajectory) Model access via NOAA ARL READYWebsite, NOAA Air Resources Laboratory, Silver Spring, MD, 2012.

Ehn, M., Kleist, E., Junninen, H., Petäjä, T., Lönn, G., Schobesberger, S., Dal Maso, M., Trimborn, A., Kulmala, M., Worsnop, D. R., Wahner, A., Wildt, J. and Mentel, T. F.: Gas phase formation of extremely oxidized pinene reaction products in chamber and ambient air, Atmos. Chem. Phys., 12(11), 5113–5127, doi:10.5194/acp-12-5113-2012, 2012.

Ehn, M., Thornton, J. a, Kleist, E., Sipilä, M., Junninen, H., Pullinen, I., Springer, M., Rubach, F., Tillmann, R., Lee, B., Lopez-Hilfiker, F., Andres, S., Acir, I.-H., Rissanen, M., Jokinen, T., Schobesberger, S., Kangasluoma, J., Kontkanen, J., Nieminen, T., Kurtén, T., Nielsen, L. B., Jørgensen, S., Kjaergaard, H. G., Canagaratna, M., Maso, M. D., Berndt, T., Petäjä, T., Wahner, A., Kerminen, V.-M., Kulmala, M., Worsnop, D. R., Wildt, J. and Mentel, T. F.: A large source of low-volatility secondary organic aerosol., Nature, 506, 476–9, doi:10.1038/nature13032, 2014.

Eisele, F. L. and Tanner, D. J.: Measurement of the gas phase concentration of H 2 SO 4 and methane sulfonic acid and estimates of H 2 SO 4 production and loss in the atmosphere, J. Geophys. Res., 98(D5), 9001, doi:10.1029/93JD00031, 1993.

Ervens, B. and Volkamer, R.: Glyoxal processing by aerosol multiphase chemistry: towards a kinetic modeling framework of secondary organic aerosol formation in aqueous particles, Atmos. Chem. Phys., 10(17), 8219–8244, doi:10.5194/acp-10-8219-2010, 2010.

Extended AIM Aerosol Thermodynamics model: http://www.aim.env.uea.ac.uk/aim/aim.php, last access: 18 Feb. 2016.

Forster, P., Ramaswamy, V., Artaxo, P., Berntsen, T., Betts, R., Fahey, D. W., Haywood, J., Lean, J., Lowe, D. C., Myhre, G., Nganga, J., Prinn, R., Raga, G., Schulz, M., and Dorland, R. V.: Changes in atmospheric constituents and in radiative forcing, in: Climate Change 2007: The Physical Science Basis. Contribution of Working Group I to the Fourth Assessment Report of the Intergovernmental Panel on Climate Change, edited by: Solomon, S., Qin, D., Manning, M., Chen, Z., Marquis, M.,Averyt, K. B., Tig- nor, M., and Miller, H. L., Cambridge University Press, Cambridge, UK and New York, NY, USA, 129–234, 2007.

Freshour, N. A., Carlson, K. K., Melka, Y. A., Hinz, S., Panta, B. and Hanson, D. R.: Amine permeation sources characterized with acid neutralization and sensitivities of an amine mass spectrometer, Atmos. Meas. Tech., 7(10), 3611–3621, doi:10.5194/amt-7-3611-2014, 2014.

Gao, S., Keywood, M., Ng, N. L., Surratt, J., Varutbangkul, V., Bahreini, R., Flagan, R. C. and Seinfeld, J. H.: Low-Molecular-Weight and Oligomeric Components in Secondary Organic Aerosol from the Ozonolysis of Cycloalkenes and α-Pinene, J. Phys. Chem. A, 108(46), 10147–10164, doi:10.1021/jp047466e, 2004.

Ge, X., Wexler, A. S. and Clegg, S. L.: Atmospheric amines – Part I. A review, Atmos. Environ., 45(3), 524–546, doi:10.1016/j.atmosenv.2010.10.012, 2011.

GEOS-Chem Model: http://geos-chem.org, last access: 18 Feb. 2016.

Grosjean, D., Van Cauwenberghe, K., Schmid, J. P., Kelley, P. E. and Pitts, J. N.: Identification of C3-C10 aliphatic dicarboxylic acids in airborne particulate matter, Environ. Sci. Technol., 12(3), 313–317, doi:10.1021/es60139a005, 1978.

Guenther, A., Karl, T., Harley, P., Wiedinmyer, C., Palmer, P. I. and Geron, C.: Estimates of global terrestrial isoprene emissions using MEGAN (Model of Emissions of Gases and Aerosols from Nature), Atmos. Chem. Phys., 6(11), 3181–3210, doi:10.5194/acp-6-3181-2006, 2006.

Guenther, a. B., Jiang, X., Heald, C. L., Sakulyanontvittaya, T., Duhl, T., Emmons, L. K. and Wang, X.: The model of emissions of gases and aerosols from nature version 2.1 (MEGAN2.1): An extended and updated framework for modeling biogenic emissions, Geosci. Model Dev., 5(6), 1471–1492, doi:10.5194/gmd-5-1471-2012, 2012.

Haar, L. and Gallagher, J. S.: Thermodynamic properties of ammonia, J. Phys. Chem., 7(3), 635–792, doi:10.1063/1.3159398, 1978.

Hall, W. a. and Johnston, M. V.: Oligomer Content of α-Pinene Secondary Organic Aerosol, Aerosol Sci. Technol., 45(1), 37–45, doi:10.1080/02786826.2010.517580, 2011.

Hanson, D. R., McMurry, P. H., Jiang, J., Tanner, D. and Huey, L. G.: Ambient pressure proton transfer mass spectrometry: detection of amines and ammonia., Environ. Sci. Technol., 45(20), 8881–8, doi:10.1021/es201819a, 2011.

Heaton, K. J., Dreyfus, M. A., Wang, S. and Johnston, M. V: Oligomers in the early stage of biogenic secondary organic aerosol formation and growth., Environ. Sci. Technol., 41(17), 6129–36, doi:10.1021/es070314n, 2007.

Iida, K., Stolzenburg, M. R., McMurry, P. H. and Smith, J. N.: Estimating nanoparticle growth rates from size-dependent charged fractions: Analysis of new particle formation events in Mexico City, J. Geophys. Res. Atmos., 113(5), 897–901, doi:10.1029/2007JD009260, 2008.

International Union of Pure and Applied Chemistry: http://www.iupac.org/, last access: 18 Feb. 2016.

Jaeschke, W., Dierssen, J. P., Gunther, A., and Schumann, M.: Phase partitioning of ammonia and ammonium in a multiphase system studied using a new vertical wet denuder technique, At- mos. Environ., 32, 365–371, 1998.

Jen, C. N., Bachman, R., Zhao, J., McMurry, P. H. and Hanson, D. R.: Diamine-sulfuric acid reactions are a potent source of new particle formation, Geophys. Res. Lett., n/a–n/a, doi:10.1002/2015GL066958, 2015.

Jiang, J., Chen, M., Kuang, C., Attoui, M. and McMurry, P. H.: Electrical Mobility Spectrometer Using a Diethylene Glycol Condensation Particle Counter for Measurement of Aerosol Size Distributions Down to 1 nm, Aerosol Sci. Technol., 45(4), 510–521, doi:10.1080/02786826.2010.547538, 2011.

Jokinen, T., Sipilä, M., Richters, S., Kerminen, V.-M., Paasonen, P., Stratmann, F., Worsnop, D., Kulmala, M., Ehn, M., Herrmann, H. and Berndt, T.: Rapid Autoxidation Forms Highly Oxidized RO2 Radicals in the Atmosphere, Angew. Chemie Int. Ed., 53, 14596–14600, doi:10.1002/anie.201408566, 2014.

Jokinen, T., Berndt, T., Makkonen, R., Kerminen, V., Junninen, H. and Paasonen, P.: Production of extremely low volatile organic compounds from biogenic emissions : Measured yields and atmospheric implications, , 1–6, doi:10.1073/pnas.1423977112, 2015.

Kalberer, M., Paulsen, D., Sax, M., Steinbacher, M., Dommen, J., Prevot, A. S. H., Fisseha, R., Weingartner, E., Frankevich, V., Zenobi, R. and Baltensperger, U.: Identification of polymers as major components of atmospheric organic aerosols., Science, 303(5664), 1659–62, doi:10.1126/science.1092185, 2004.

Kawamura, K. and Ikushima, K.: Seasonal changes in the distribution of dicarboxylic acids in the urban atmosphere, Env. Sc. Tec., 27, 10, 2227–2235, 1993.

Kawamura, K., Kasukabe, H., Yasui, O., and Barrie, L. A.: Production of dicarboxylic acids in the arctic atmosphere at polar sunrise, Geophys. Res. Lett., 22, 10, 1253–1256, 1995.

Kawamura, K., Seméré, R., Imai, Y., Fujii, Y. and Hayashi, M.: Water soluble dicarboxylic acids and related compounds in Antarctic aerosols, J. Geophys. Res., 101(D13), 18721, doi:10.1029/96JD01541, 1996.

Kawamura, K. and Sakaguchi, F.: Molecular distributions of water soluble dicarboxylic acids in marine aerosols over the Pacific Ocean including tropics, J. Geophys. Res. A, 104, D3, 3501– 3509, 1999.

Kerminen, V.-M., Ojanen, C., Pakkanen, T., Hillamo, R., Aurela, M. and Meriläinen, J.: Low-Molecular-Weight Dicarboxylic Acids in an Urban and Rural Atmosphere, J. Aerosol Sci., 31(3), 349–362, doi:10.1016/S0021-8502(99)00063-4, 2000.

Kerminen, V. M., Lehtinen, K. E. J., Anttila, T., and Kulmala, M.: Dynamics of atmospheric nucleation mode particles: a timescale analysis, Tellus Ser. B-Chem. Phys. Meteorol., 56, 135–146, 2004.

Khwaja, H. A.: Atmospheric concentrations of carboxylic acids and related compounds at a semiurban site, Atmos. Environ., 29(1), 127–139, doi:10.1016/1352-2310(94)00211-3, 1995.

Kirkby, J., Curtius, J., Almeida, J., Dunne, E., Duplissy, J., Ehrhart, S., Franchin, A., Gagne, S., Ickes, L., Kurten, A., Kupc, A., Metzger, A., Riccobono, F., Rondo, L., Schobesberger, S., Tsagkogeorgas, G., Wimmer, D., Amorim, A., Bianchi, F., Breitenlechner, M., David, A., Dommen, J., Downard, A., Ehn, M., Flagan, R. C., Haider, S., Hansel, A., Hauser, D., Jud, W., Junninen, H., Kreissl, F., Kvashin, A., Laaksonen, A., Lehtipalo, K., Lima, J., Lovejoy, E. R., Makhmutov, V., Mathot, S., Mikkila, J., Minginette, P., Mogo, S., Nieminen, T., Onnela, A., Pereira, P., Petaja, T., Schnitzhofer, R., Seinfeld, J. H., Sipila, M., Stozhkov, Y., Stratmann, F., Tome, A., Vanhanen, J., Viisanen, Y., Vrtala, A., Wagner, P. E., Walther, H., Weingartner, E., Wex, H., Winkler, P. M., Carslaw, K. S., Worsnop, D. R., Baltensperger, U. and Kulmala, M.: Role of sulphuric acid, ammonia and galactic cosmic rays in atmospheric aerosol nucleation, Nature, 476(7361), 429–433 [online] Available from: http://dx.doi.org/10.1038/nature10343, 2011.

Kuang, C., McMurry, P. H. and McCormick, a. V.: Determination of cloud condensation nuclei production from measured new particle formation events, Geophys. Res. Lett., 36(April), 1–5, doi:10.1029/2009GL037584, 2009.

Kuang, C., Riipinen, I., Sihto, S.-L., Kulmala, M., McCormick, A. V. and McMurry, P. H.: An improved criterion for new particle formation in diverse atmospheric environments, Atmos. Chem. Phys., 10(17), 8469–8480, doi:10.5194/acp-10-8469-2010, 2010.

Kulmala, M., Vehkamäki, H., Petäjä, T., Dal Maso, M., Lauri, A., Kerminen, V.-M., Birmili, W. and McMurry, P. H.: Formation and growth rates of ultrafine atmospheric particles: a review of observations, J. Aerosol Sci., 35(2), 143–176, doi:10.1016/j.jaerosci.2003.10.003, 2004.

Khwaja, H.A.: Atmospheric concentrations of carboxylic acids and related compounds at a semiurban site. Atmos. Environ., 29, 127—139, 1995.

Lawler, M. J., Whitehead, J., O'Dowd, C., Monahan, C., McFiggans, G. and Smith, J. N.: Composition of 15–85 nm particles in marine air, Atmos. Chem. Phys., 14(21), 11557–11569, doi:10.5194/acp-14-11557-2014, 2014.

Limbeck, A. and Puxbaum, H.: Organic acids in continental background aerosols, Atmos. Environ., 33(12), 1847–1852, doi:10.1016/S1352-2310(98)00347-1, 1999.

Limbeck, A., Kulmala, M., Puxbaum, H.: Secondary organic aerosol formation in the atmosphere via heterogeneous reaction of gaseous isoprene on acidic particles, Geophys. Res. Lett., 30(19), 4–7, doi:10.1029/2003GL017738, 2003.

Mäkelä, J., Yli□Koivisto, S. and Hiltunen, V.: Chemical composition of aerosol during particle formation events in boreal forest, Tellus B, 380–393 [online] Available from: http://onlinelibrary.wiley.com/doi/10.1034/j.1600-0889.2001.530405.x/abstract, 2001.

Marti, J. J., Jefferson, A., Cai, X. P., Richert, C., McMurry, P. H. and Eisele, F.: H 2 SO 4 vapor pressure of sulfuric acid and ammonium sulfate solutions, J. Geophys. Res. Atmos., 102(D3), 3725–3735, doi:10.1029/96JD03064, 1997.

Matsunaga, S. N., Wiedinmyer, C., Guenther, a. B., Orlando, J. J., Karl, T., Toohey, D. W., Greenberg, J. P. and Kajii, Y.: Isoprene oxidation products are a significant atmospheric aerosol component, Atmos. Chem. Phys. Discuss., 5(6), 11143–11156, doi:10.5194/acpd-5-11143-2005, 2005.

Mochida, M., Kawabata, A., Kawamura, K., Hatsushika, H., and Yamazaki, K.: Seasonal variation and origins of dicarboxylic acids in the marine atmosphere over the western North Pacific, J. Geophys. Res. A., 108, D6, AAC7/1–AAC7/11, 2003.

Murphy, B. N., Donahue, N. M., Robinson, A. L. and Pandis, S. N.: A naming convention for atmospheric organic aerosol, Atmos. Chem. Phys., 14(11), 5825–5839, doi:10.5194/acp-14-5825-2014, 2014.

Narukawa, M., Kawamura, K., Li, S. M., and Bottenheim, J. W.: Dicarboxylic acids in the Arctic aerosols and snowpacks collected during ALERT 2000, Atmos. Envir., 36, 15–16, 2491– 2499, 2002.

Ortega, J., Turnipseed, A., Guenther, A. B., Karl, T. G., Day, D. A., Gochis, D., Huffman, J. A., Prenni, A. J., Levin, E. J. T., Kreidenweis, S. M., DeMott, P. J., Tobo, Y., Patton, E. G., Hodzic, A., Cui, Y. Y., Harley, P. C., Hornbrook, R. S., Apel, E. C., Monson, R. K., Eller, A. S. D., Greenberg, J. P., Barth, M. C., Campuzano-Jost, P., Palm, B. B., Jimenez, J. L., Aiken, A. C., Dubey, M. K., Geron, C., Offenberg, J., Ryan, M. G., Fornwalt, P. J., Pryor, S. C., Keutsch, F. N., DiGangi, J. P., Chan, A. W. H., Goldstein, A. H., Wolfe, G. M., Kim, S., Kaser, L., Schnitzhofer, R., Hansel, A., Cantrell, C. A., Mauldin, R. L., and Smith, J. N.: Overview of the Manitou Experimental Forest Observatory: site description and selected science results from 2008 to 2013, Atmos. Chem. Phys., 14, 6345-6367, doi:10.5194/acp-14-6345-2014, 2014.

Pankow, J. F.: Gas/particle partitioning of neutral and ionizing compounds to single and multi-phase aerosol particles. 1. Unified modeling framework, Atmos. Environ., 37, 3323–3333, 2003.

Pennington, M. R. and Johnston, M. V.: Trapping charged nanoparticles in the nano aerosol mass spectrometer (NAMS), Int. J. Mass Spectrom., 311, 64–71, doi:10.1016/j.ijms.2011.12.011, 2012.

Pierce, J. R. and Adams, P. J.: Efficiency of cloud condensation nuclei formation from ultrafine particles, Atmos. Chem. Phys., 7(5), 1367–1379, doi:10.5194/acp-7-1367-2007, 2007.

Pierce, J. R. and Adams, P. J.: Uncertainty in global CCN concentrations from uncertain aerosol nucleation and primary emission rates, Atmos. Chem. Phys., 9(4), 1339–1356, doi:10.5194/acp-9-1339-2009, 2009.

Pierce, J. R., Riipinen, I., Kulmala, M., Ehn, M., Petäjä, T., Junninen, H., Worsnop, D. R. and Donahue, N. M.: Quantification of the volatility of secondary organic compounds in ultrafine particles during nucleation events, Atmos. Chem. Phys., 11(17), 9019–9036, doi:10.5194/acp-11-9019-2011, 2011.

Pierce, J. R., Leaitch, W. R., Liggio, J., Westervelt, D. M., Wainwright, C. D., Abbatt, J. P. D., Ahlm, L., Al-Basheer, W., Cziczo, D. J., Hayden, K. L., Lee, A. K. Y., Li, S.-M., Russell, L. M., Sjostedt, S. J., Strawbridge, K. B., Travis, M., Vlasenko, A., Wentzell, J. J. B., Wiebe, H. A., Wong, J. P. S. and Macdonald, A. M.: Nucleation and condensational growth to CCN sizes during a sustained pristine biogenic SOA event in a forested mountain valley, Atmos. Chem. Phys., 12(7), 3147–3163, doi:10.5194/acp-12-3147-2012, 2012.

Pinder, R.W., Adams, P. J., and Pandis, S. N.: Ammonia emission controls as a cost-effective strategy for reducing atmospheric particulate matter in the eastern United States, Environ. Sci. Technol., 41, 380–386, 2007.

Poling, B. E., Prausnitz, J. M., and O'Connell, J. P.: Properties of gases and liquids, 5th Edn., McGraw-Hill, New York, 2001.

Pöschl, U., Rudich, Y. and Ammann, M.: Kinetic model framework for aerosol and cloud surface chemistry and gas-particle interactions – Part 1: General equations, parameters, and terminology, Atmos. Chem. Phys., 7(23), 5989–6023, doi:10.5194/acp-7-5989-2007, 2007.

Pun, B. K. and Seigneur, C.: Investigative modeling of new pathways for secondary organic aerosol formation, Atmos. Chem. Phys., 7(9), 2199–2216, doi:10.5194/acp-7-2199-2007, 2007.

Riccobono, F., Schobesberger, S., Scott, C. E., Dommen, J., Ortega, I. K., Rondo, L., Almeida, J., Amorim, A., Bianchi, F., Breitenlechner, M., David, A., Downard, A., Dunne, E. M., Duplissy, J., Ehrhart, S., Flagan, R. C., Franchin, A., Hansel, A., Junninen, H., Kajos, M., Keskinen, H., Kupc, A., Kurten, A., Kvashin, A. N., Laaksonen, A., Lehtipalo, K., Makhmutov, V., Mathot, S., Nieminen, T., Onnela, A., Petaja, T., Praplan, A. P., Santos, F. D., Schallhart, S., Seinfeld, J. H., Sipila, M., Spracklen, D. V., Stozhkov, Y., Stratmann, F., Tome, A., Tsagkogeorgas, G., Vaattovaara, P., Viisanen, Y., Vrtala, A., Wagner, P. E., Weingartner, E., Wex, H., Wimmer, D., Carslaw, K. S., Curtius, J., Donahue, N. M., Kirkby, J., Kulmala, M., Worsnop, D. R. and Baltensperger, U.: Oxidation Products of Biogenic Emissions Contribute to Nucleation of Atmospheric Particles, Science (80-.)., 344(6185), 717–721, doi:10.1126/science.1243527, 2014.

Riipinen, I., Sihto, S.-L., Kulmala, M., Arnold, F., Dal Maso, M., Birmili, W., Saarnio, K., Teinilä, K., Kerminen, V.-M., Laaksonen, A. and Lehtinen, K. E. J.: Connections between atmospheric sulphuric acid and new particle formation during QUEST III–IV campaigns in Heidelberg and Hyytiälä, Atmos. Chem. Phys., 7(8), 1899–1914, doi:10.5194/acp-7-1899-2007, 2007.

Riipinen, I., Pierce, J. R., Yli-Juuti, T., Nieminen, T., Häkkinen, S., Ehn, M., Junninen, H., Lehtipalo, K., Petäjä, T., Slowik, J., Chang, R., Shantz, N. C., Abbatt, J., Leaitch, W. R., Kerminen, V.-M., Worsnop, D. R., Pandis, S. N., Donahue, N. M. and Kulmala, M.: Organic condensation: a vital link connecting aerosol formation to cloud

condensation nuclei (CCN) concentrations, Atmos. Chem. Phys., 11(8), 3865–3878, doi:10.5194/acp-11-3865-2011, 2011.

Riipinen, I., Yli-Juuti, T., Pierce, J. R., Petäjä, T., Worsnop, D. R., Kulmala, M. and Donahue, N. M.: The contribution of organics to atmospheric nanoparticle growth, Nat. Geosci., 5(7), 453–458, doi:10.1038/ngeo1499, 2012.

Rissanen, M. P., Kurtén, T., Sipilä, M., Thornton, J. A., Kangasluoma, J., Sarnela, N., Junninen, H., Jørgensen, S., Schallhart, S., Kajos, M. K., Taipale, R., Springer, M., Mentel, T. F., Ruuskanen, T., Petäjä, T., Worsnop, D. R., Kjaergaard, H. G. and Ehn, M.: The formation of highly oxidized multifunctional products in the ozonolysis of cyclohexene., J. Am. Chem. Soc., 136(44), 15596–606, doi:10.1021/ja507146s, 2014.

Rogge,W. F.,Mazurek, M. A., Hildemann, L. M., Cass, G. R., and Simoneit, B. R. T.: Quantification of urban organic aerosols at a molecular level: identification, abundance and seasonal variation, Atmos. Envir., Part A: General Topics, 27A, 8, 1309–1330, 1993.

Rolph, G. D.: Real-time Environmental Applications and Display sYstem (READY), NOAA Air Resources Laboratory, Silver Spring, MD, 2012.

Rosenfeld, D., Lohmann, U., Raga, G. B., O'Dowd, C. D., Kulmala, M., Fuzzi, S., Reissell, A., and Andreae, M. O.: Flood or Drought: How Do Aerosols Affect Precipitation?, Science, 312, 1309–1313, 2008.

Scott, C. E., Spracklen, D. V., Pierce, J. R., Riipinen, I., D'Andrea, S. D., Rap, A., Carslaw, K. S., Forster, P. M., Kulmala, M., Mann, G. W. and Pringle, K. J.: Impact of gas-to-particle partitioning approaches on the simulated radiative effects of biogenic secondary organic aerosol, Atmos. Chem. Phys. Discuss., 15(4), 4145–4172, doi:10.5194/acpd-15-4145-2015, 2015.

Seinfeld, J. H. and Pandis, S. N.: Atmospheric chemistry and physics: From air pollution to climate change, John Wiley & Sons, Inc., New York, USA, 523–538, 1998.

Seinfeld, J. H. and Pandis, S. N.: Atmospheric Chemistry and Physics, 2nd ed., John Wiley and Sons, New York, 2006.

Sempére, R. and Kawamura, K.: Comparative distributions of dicarboxylic acids and related polar compounds in snow, rain and aerosols from urban atmosphere, Atmos. Environ., 28(3), 449–459, doi:10.1016/1352-2310(94)90123-6, 1994.

Sempére, R. and Kawamura, K.: Trans-hemispheric contribution of C2–C10 a, w-dicarboxylic acids, and related polar compounds to water-soluble organic carbon in the western Pacific aerosols in relation to photochemical oxidation reactions, Glob. Biogeochem. Cycl., 17, 2, 38/1–38/15, 2003.

Shiraiwa, M., Garland, R. M. and Pöschl, U.: Kinetic double-layer model of aerosol surface chemistry and gas-particle interactions (K2-SURF): Degradation of polycyclic aromatic hydrocarbons exposed to O_3, NO_2, H_2O, OH and NO_3, Atmos. Chem. Phys., 9(24), 9571–9586, doi:10.5194/acp-9-9571-2009, 2009.

Shiraiwa, M., Pfrang, C. and Pöschl, U.: Kinetic multi-layer model of aerosol surface and bulk chemistry (KM-SUB): the influence of interfacial transport and bulk diffusion on the oxidation of oleic acid by ozone, Atmos. Chem. Phys., 10(8), 3673–3691, doi:10.5194/acp-10-3673-2010, 2010.

Shiraiwa, M., Pfrang, C., Koop, T. and Pöschl, U.: Kinetic multi-layer model of gas-particle interactions in aerosols and clouds (KM-GAP): linking condensation, evaporation and chemical reactions of organics, oxidants and water, Atmos. Chem. Phys., 12(5), 2777–2794, doi:10.5194/acp-12-2777-2012, 2012.

Sindelarova, K., Granier, C., Bouarar, I., Guenther, A., Tilmes, S., Stavrakou, T., Müller, J.-F., Kuhn, U., Stefani, P. and Knorr, W.: Global data set of biogenic VOC emissions calculated by the MEGAN model over the last 30 years, Atmos. Chem. Phys., 14(17), 9317–9341, doi:10.5194/acp-14-9317-2014, 2014.

Smith, J. N., Moore, K. F., McMurry, P. H. and Eisele, F. L.: Atmospheric Measurements of Sub-20 nm Diameter Particle Chemical Composition by Thermal Desorption Chemical Ionization Mass Spectrometry, Aerosol Sci. Technol., 38(2), 100–110, doi:10.1080/02786820490249036, 2004.

Smith, J. N. and Rathbone, G. J.: Carboxylic acid characterization in nanoparticles by thermal desorption chemical ionization mass spectrometry, Int. J. Mass Spectrom., 274(1-3), 8–13, doi:10.1016/j.ijms.2008.04.008, 2008a.

Smith, J. N., Dunn, M. J., VanReken, T. M., Iida, K., Stolzenburg, M. R., McMurry, P. H. and Huey, L. G.: Chemical composition of atmospheric nanoparticles formed from nucleation in Tecamac, Mexico: Evidence for an important role for organic species in nanoparticle growth, Geophys. Res. Lett., 35(4), 2–6, doi:10.1029/2007GL032523, 2008b.

Smith, J. N., Barsanti, K. C., Friedli, H. R., Ehn, M., Kulmala, M., Collins, D. R., Scheckman, J. H., Williams, B. J. and McMurry, P. H.: Observations of aminium salts in atmospheric nanoparticles and possible climatic implications., Proc. Natl. Acad. Sci. U. S. A., 107(15), 6634–9, doi:10.1073/pnas.0912127107, 2010.

Southern Great Plains: http://www.arm.gov/sites/sgp, last access: 18 Feb. 2016.

Spracklen, D. V., Carslaw, K. S., Kulmala, M., Kerminen, V.-M., Sihto, S.-L., Riipinen, I., Merikanto, J., Mann, G. W., Chipperfield, M. P., Wiedensohler, A., Birmili, W. and Lihavainen, H.: Contribution of particle formation to global cloud condensation nuclei concentrations, Geophys. Res. Lett., 35(6), L06808, doi:10.1029/2007GL033038, 2008.

Spracklen, D. V., Carslaw, K. S., Merikanto, J., Mann, G. W., Reddington, C. L., Pickering, S., Ogren, J. A., Andrews, E., Baltensperger, U., Weingartner, E., Boy, M., Kulmala, M., Laakso, L., Lihavainen, H., Kivekäs, N., Komppula, M., Mihalopoulos, N., Kouvarakis, G., Jennings, S. G., O'Dowd, C., Birmili, W., Wiedensohler, A., Weller, R., Gras, J., Laj, P., Sellegri, K., Bonn, B., Krejci, R., Laaksonen, A., Hamed, A., Minikin, A., Harrison, R. M., Talbot, R. and Sun, J.: Explaining global surface aerosol number concentrations in terms of primary emissions and particle formation, Atmos. Chem. Phys., 10(10), 4775–4793, doi:10.5194/acp-10-4775-2010, 2010.

Spracklen, D. V., Jimenez, J. L., Carslaw, K. S., Worsnop, D. R., Evans, M. J., Mann, G. W., Zhang, Q., Canagaratna, M. R., Allan, J., Coe, H., McFiggans, G., Rap, A. and Forster, P.: Aerosol mass spectrometer constraint on the global secondary organic aerosol budget, Atmos. Chem. Phys., 11(23), 12109–12136, doi:10.5194/acp-11-12109-2011, 2011.

Stolzenburg, M. R., McMurry, P. H., Sakurai, H., Smith, J. N., Mauldin, R. L., Eisele, F. L. and Clement, C. F.: Growth rates of freshly nucleated atmospheric particles in Atlanta, J. Geophys. Res., 110(D22), D22S05, doi:10.1029/2005JD005935, 2005.

Tao, Ye Ye, Xinguan Jiang, S.: Effects of amines on particle growth observed in new particle formation events, , 3510–3532, doi:10.1002/2014JD022145.Received, 2015.

Tolocka, M. P., Jang, M., Ginter, J. M., Cox, F. J., Kamens, R. M. and Johnston, M. V: Formation of oligomers in secondary organic aerosol., Environ. Sci. Technol., 38(5), 1428–34, doi:10.1021/es035030r, 2004.

Virtanen, A., Joutsensaari, J., Koop, T., Kannosto, J., Yli-Pirilä, P., Leskinen, J., Mäkelä, J. M., Holopainen, J. K., Pöschl, U., Kulmala, M., Worsnop, D. R. and Laaksonen, A.: An amorphous solid state of biogenic secondary organic aerosol particles, Nature, 467(7317), 824–827, doi:10.1038/nature09455, 2010.

Virtanen, A., Kannosto, J., Kuuluvainen, H., Arffman, A., Joutsensaari, J., Saukko, E., Hao, L., Yli-Pirilä, P., Tiitta, P., Holopainen, J. K., Keskinen, J., Worsnop, D. R., Smith, J. N. and Laaksonen, A.: Bounce behavior of freshly nucleated biogenic secondary organic aerosol particles, Atmos. Chem. Phys., 11(16), 8759–8766, doi:10.5194/acp-11-8759-2011, 2011.

Voisin, D., Smith, J. N., Sakurai, H., McMurry, P. H. and Eisele, F. L.: Thermal desorption chemical ionization mass spectrometer for ultrafine particle chemical composition, Aerosol Sci. Technol., 37(6), 471–475, doi:10.1080/02786820300959, 2003.

Wang, S. and Johnston, M. V.: Airborne nanoparticle characterization with a digital ion trap-reflectron time of flight mass spectrometer, Int. J. Mass Spectrom., 258(1-3), 50–57, doi:10.1016/j.ijms.2006.07.001, 2006.

Wang, S., Zordan, C. A. and Johnston, M. V.: Chemical characterization of individual, airborne sub-10-nm particles and molecules, Anal. Chem., 78(6), 1750–1754, doi:10.1021/ac052243l, 2006.

Wang, L., Khalizov, A. F., Zheng, J., Xu, W., Ma, Y., Lal, V. and Zhang, R.: Atmospheric nanoparticles formed from heterogeneous reactions of organics, Nat. Geosci., 3(4), 238–242, doi:10.1038/ngeo778, 2010.

Weber, R. J., Marti, J. J., McMurry, P. H., Eisele, F. L., Tanner, D. J. and Jefferson, A.: Measurements of new particle formation and ultrafine particle growth rates at a clean continental site, J. Geophys. Res., 102(D4), 4375, doi:10.1029/96JD03656, 1997.

Westervelt, D. M., Pierce, J. R., Riipinen, I., Trivitayanurak, W., Hamed, A., Kulmala, M., Laaksonen, A., Decesari, S. and Adams, P. J.: Formation and growth of nucleated particles into cloud condensation nuclei: model–measurement comparison, Atmos. Chem. Phys., 13(15), 7645–7663, doi:10.5194/acp-13-7645-2013, 2013.

Westervelt, D. M., Pierce, J. R. and Adams, P. J.: Analysis of feedbacks between nucleation rate, survival probability and cloud condensation nuclei formation, Atmos. Chem. Phys., 14(11), 5577–5597, doi:10.5194/acp-14-5577-2014, 2014.

Wexler, A. S. and Clegg, S. L.: Atmospheric aerosol models for systems including the ions H+, NH4+, Na+, SO42−, NO3−, Cl−, Br−, and H2O, J. Geophys. Res. Atmos., 107(D14), ACH–14–1–ACH 14–14, doi:10.1029/2001JD000451, 2002.

Winkler, P. M., Ortega, J., Karl, T., Cappellin, L., Friedli, H. R., Barsanti, K., McMurry, P. H. and Smith, J. N.: Identification of the biogenic compounds responsible for size-dependent nanoparticle growth, Geophys. Res. Lett., 39(20), doi:10.1029/2012GL053253, 2012.

Xu, L., Suresh, S., Guo, H., Weber, R. J. and Ng, N. L.: Aerosol characterization over the southeastern United States using high-resolution aerosol mass spectrometry: spatial and seasonal variation of aerosol composition and

sources with a focus on organic nitrates, Atmos. Chem. Phys., 15(13), 7307–7336, doi:10.5194/acp-15-7307-2015, 2015.

Yli-Juuti, T., Barsanti, K., Hildebrandt Ruiz, L., Kieloaho, A.-J., Makkonen, U., Petäjä, T., Ruuskanen, T., Kulmala, M. and Riipinen, I.: Model for acid-base chemistry in nanoparticle growth (MABNAG), Atmos. Chem. Phys., 13(24), 12507–12524, doi:10.5194/acp-13-12507-2013, 2013.

Yu, F.: A secondary organic aerosol formation model considering successive oxidation aging and kinetic condensation of organic compounds: global scale implications, Atmos. Chem. Phys., 11(3), 1083–1099, doi:10.5194/acp-11-1083-2011, 2011.

Yu, H., Ortega, J., Smith, J. N., Guenther, A. B., Kanawade, V. P., You, Y., Liu, Y., Hosman, K., Karl, T., Seco, R., Geron, C., Pallardy, S. G., Gu, L., Mikkilä, J. and Lee, S.-H.: New Particle Formation and Growth in an Isoprene-Dominated Ozark Forest: From Sub-5 nm to CCN-Active Sizes, Aerosol Sci. Technol., 6826 (April 2015), 1285–1298, doi:10.1080/02786826.2014.984801, 2014.

Zaveri, R. A., Easter, R. C., Fast, J. D. and Peters, L. K.: Model for Simulating Aerosol Interactions and Chemistry (MOSAIC), J. Geophys. Res., 113(D13), D13204, doi:10.1029/2007JD008782, 2008.

Zhang, R., Khalizov, A., Wang, L., Hu, M. and Xu, W.: Nucleation and growth of nanoparticles in the atmosphere, Chem. Rev., 112(3), 1957–2011, doi:10.1021/cr2001756, 2012a.

Zhang, X., Pandis, S. N. and Seinfeld, J. H.: Diffusion-Limited Versus Quasi-Equilibrium Aerosol Growth, Aerosol Sci. Technol., 46(8), 874–885, doi:10.1080/02786826.2012.679344, 2012b.

Zhao, J., Ortega, J., Chen, M., McMurry, P. H., and Smith, J. N.: Dependence of particle nucleation and growth on high-molecular-weight gas-phase products during ozonolysis of α-pinene, Atmos. Chem. Phys., 13, 7631-7644, doi:10.5194/acp-13-7631-2013, 2013.

Appendix A: List of abbreviations

AGL	Above Ground Level
AmPMS	Ambient pressure Proton transfer Mass Spectrometer
ARM	Atmospheric Radiation Measurement
BL	Boundary Layer
BVOC	Biological Volatile Organic Compound
CCN	Cloud Condensation Nuclei
CDT	Central Daylight Time
CIMS	Chemical Ionization Mass Spectrometer
CPC	Condensation Particle Counter
CS	Condensation Sink
DMA	Dimethylamine
DOE	Department of Energy

D_p	Particle Diameter
E-AIM	Extended Aerosol Inorganics Model
ELVOC	Extremely Low-Volatility Organic Compound
EPA	Environmental Protection Agency
GR	Growth Rate
HYSPLIT	HYbrid Single-Particle Lagrangian Integrated Trajectory
IUPAC	International Union of Pure and Applied Chemistry
Lam	sum of Light (C1-C3) amines measured at SGP
Lo-VP	reducing the vapor pressure of the organic acid input in MABNAG by 10^{-1}
LVOC	Low-Volatile Organic Compound
MABNAG	Model for Acid-Base chemistry in NAnoparticle Growth
MAL	Malonic acid
MEGAN	Model of Emissions of Gases and Aerosols in Nature
NAM	North American Mesoscale model
NAMS	Nano Aerosol Mass Spectrometer
NOAA	National Oceanic and Atmospheric Administration
NPF	New-Particle Formation
NPFS	New-Particle Formation Study
OX	Oxalic acid
PTR-MS	Proton Transfer Reaction-Mass Spectrometer
RH	Relative Humidity
SGP	Southern Great Plains
SMPS	Scanning Mobility Particle Sizer
SOA	Secondary Organic Aerosol
SVOC	Semi-Volatile Organic Compound
Tam	sum of Total amines measured at SGP
TDCIMS	Thermal Decomposition Chemical Ionization Mass Spectrometer
TMA	Trimethylamine
UNIFAC	UNIquac Functional-group Activity Coefficient method
VOC	Volatile Organic Compounds

Anna Hodshire 6/22/2016 9:34 AM
Deleted: -

Anna Hodshire 6/22/2016 9:34 AM
Deleted: -

Anna Hodshire 6/22/2016 9:34 AM
Deleted: -

Table 1. Gas-phase concentration and temperature inputs to MABNAG for each day.

Day	T [C]	RH (%)	Sulfuric Acid [cm^{-3}]	Organic Acid: mal+ox / mal+10ox / mal + 100ox [cm^{-3}]	Ammonia [cm^{-3}]	Amine: Light / Total [cm^{-3}]	EL-VOC [cm^{-3}]
4/19/13	11.6	32	2.4×10^{6}	1.17×10^{7} / 2.17×10^{7} / 1.10×10^{8}	2.98×10^{10}	2.91×10^{9} / 4.8×10^{10}	1.22×10^{7}
5/09/13	12.7	69	1.97×10^{7}	7.15×10^{7} / 1.49×10^{8} / 9.11×10^{8}	8.94×10^{9}	1.01×10^{9} / 2.41×10^{10}	4.3×10^{6}
5/11/13	16.4	36	5.3×10^{6}	2.66×10^{7} / 6.43×10^{7} / 4.14×10^{8}	1.11×10^{10}	1.54×10^{9} / 1.85×10^{10}	4.1×10^{6}

Anna Hodshire 5/16/2016 4:29 PM
Deleted: ·
Anna Hodshire 5/16/2016 4:28 PM
Deleted: ·
Anna Hodshire 5/16/2016 4:29 PM
Deleted: ·
Anna Hodshire 5/16/2016 4:29 PM
Deleted: ·
Anna Hodshire 5/16/2016 4:29 PM
Deleted: ·
Anna Hodshire 5/16/2016 4:29 PM
Deleted: ·
Anna Hodshire 5/16/2016 4:29 PM
Deleted: ·
Anna Hodshire 5/16/2016 4:29 PM
Deleted: ·
Anna Hodshire 5/16/2016 4:29 PM
Deleted: ·
Anna Hodshire 5/16/2016 4:29 PM
Deleted: ·
Anna Hodshire 5/16/2016 4:29 PM
Deleted: ·
Anna Hodshire 5/16/2016 4:29 PM
Deleted: ·
Anna Hodshire 5/16/2016 4:29 PM
Deleted: ·
Anna Hodshire 5/16/2016 4:29 PM
Deleted: ·
Anna Hodshire 5/16/2016 4:29 PM
Deleted: ·
Anna Hodshire 5/16/2016 4:29 PM
Deleted: ·
Anna Hodshire 5/16/2016 4:29 PM
Deleted: ·
Anna Hodshire 5/16/2016 4:29 PM
Deleted: ·
Anna Hodshire 5/16/2016 4:29 PM
Deleted: ·
Anna Hodshire 5/16/2016 4:29 PM
Deleted: ·
Anna Hodshire 5/16/2016 4:29 PM
Deleted: ·
Anna Hodshire 5/16/2016 4:29 PM
Deleted: ·
Anna Hodshire 5/16/2016 4:29 PM
Deleted: ·

Table 2. Chemical properties for each species input in MABNAG.

Species	Molar Mass [g/mol]	pKa 1	pKa 2	Vapor Pressure of pure compound [Pa] (µg m-3)	Henry's Law Constant [mol kg-1 atm-1]	Diffusion Coefficient [m2 s-1]
Sulfuric Acid	98.1	-3	1.99	0	n/a	9.4×10^{-6}
Malonic Acid	104.1	2.85	5.7	4×10^{-5} (1.8×10^{-5})	n/a	8.4×10^{-6} [a]
Oxalic Acid	90.03	1.46	4.4	4×10^{-3} (1.5×10^{-3})	n/a	8.4×10^{-6} [b]
Ammonia	17.03	9.25	n/a	n/a	60.7[c]	n\a
DMA	45.1	10.7	n/a	n/a	31.41[d]	n\a
TMA	59.1	9.8	n/a	n/a	9.6[d]	n\a
ELVOC[e]	280	n/a	n/a	1×10^{-9} (1.2×10^{-3})	n/a	5×10^{-6}

[a]Calculated using the Fuller et al., method (Eq. 11-4.4 in Poling et al., 2014)

[b]Assumed to be the same as malonic acid

[c]Haar and Gallagher, 1978

[d] http://webbook.nist.gov/chemistry/

[e]Assumed properties of the ELVOC species

Anna Hodshire 5/16/2016 4:29 PM
Deleted: ·

Anna Hodshire 5/16/2016 4:29 PM
Deleted: ·

Anna Hodshire 5/16/2016 4:29 PM
Deleted: ·

Anna Hodshire 5/16/2016 4:29 PM
Deleted: ·

Anna Hodshire 5/16/2016 4:29 PM
Deleted: ·

Anna Hodshire 5/16/2016 4:29 PM
Deleted: ·

Anna Hodshire 5/16/2016 4:29 PM
Deleted: ·

Anna Hodshire 5/16/2016 4:29 PM
Deleted: ·

Anna Hodshire 5/16/2016 4:29 PM
Deleted: ·

Table 3. Observed growth-rate ranges between 10-20 nm for each day.

Day	Leading-edge method [nm hr^{-1}]	Dp-mode method [nm hr^{-1}]	Visual method [nm hr^{-1}]
April 19	8.8	1.6	3.3
May 9	11.3	2.4	5.0
May 11	7.5	5.6	8.3

May 9
2.5
5.0
11.3

May 11
7.5
5.6
8.3

Day
Leading-edge method [nm hr^{-1}]
Dp(mode) method
[nm hr^{-1}]
Visual method [nm hr^{-1}]

April 19
8.8
1.6
3.3

May 9
2.5
5.0
11.3

May 11
7.5
5.6
8.3

Day
Leading-edge method [nm hr^{-1}]
Dp(mode) method
[nm hr^{-1}]
Visual method [nm hr^{-1}]

Anna Hodshire 6/23/2016 2:44 PM
Deleted: Day ... [1]

Anna Hodshire 6/23/2016 2:44 PM
Deleted: April 19 ... [2]

Anna Hodshire 6/23/2016 2:44 PM
Deleted: 3-4 ... [3]

Anna Hodshire 6/23/2016 2:44 PM
Deleted: May 11 ... [4]

Anna Hodshire 6/23/2016 2:44 PM
Deleted: 3-8 ... [5]

Anna Hodshire 6/23/2016 2:50 PM
Formatted Table

Jan Hamer 7/1/2016 9:54 AM
Deleted: Dp mode

Anna Hodshire 6/8/2016 9:48 AM
Deleted: Table 4. Modelled Growth Rates and final mole fractions for April 19. The base case (MAL/10ox/DMA_L) is in bold. The observed growth rate for this day is 2-4 nm hr^{-1}. ... [6]

Anna Hodshire 6/8/2016 9:48 AM
Deleted:

Anna Hodshire 6/8/2016 9:48 AM
Deleted:

Anna Hodshire 6/8/2016 9:48 AM
Deleted:

Anna Hodshire 6/8/2016 9:48 AM
Deleted: Case ... [7]

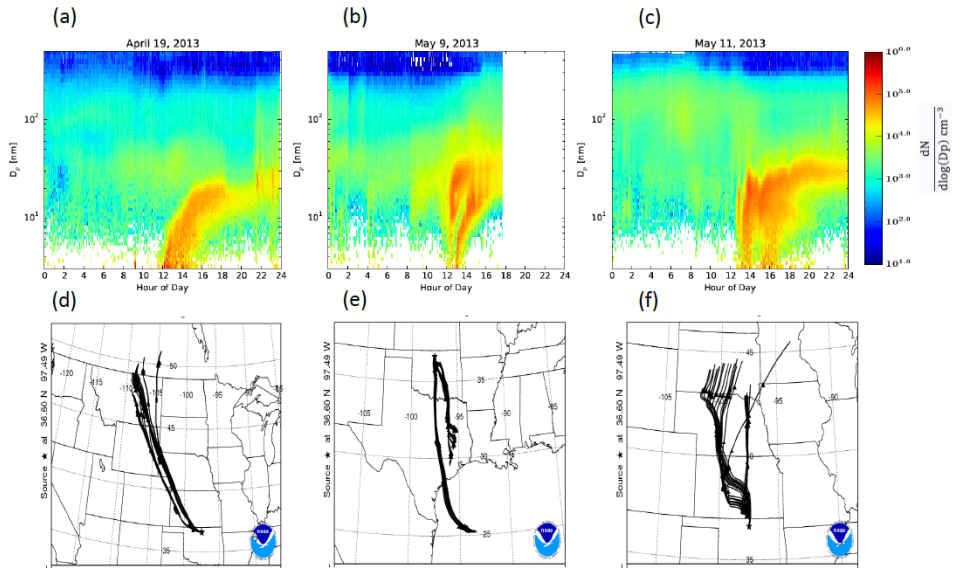

Figure 1 (a-c) The growth events for April 19, May 9, and May 11, 2013, as captured by a scanning mobility particle sizer at SGP. Each plot shares the same colorbar. (d-f) The associated 48 hour Hysplit back trajectories for each day as calculated using the NOAA Hysplit Model with NAM meteorological data, initialized at 250 m AGL.

Unknown
Formatted: Font:(Default) Times New Roman, 10 pt

Anna Hodshire 6/8/2016 10:16 AM
Deleted: :

Anna Hodshire 6/22/2016 9:36 AM
Deleted: 0

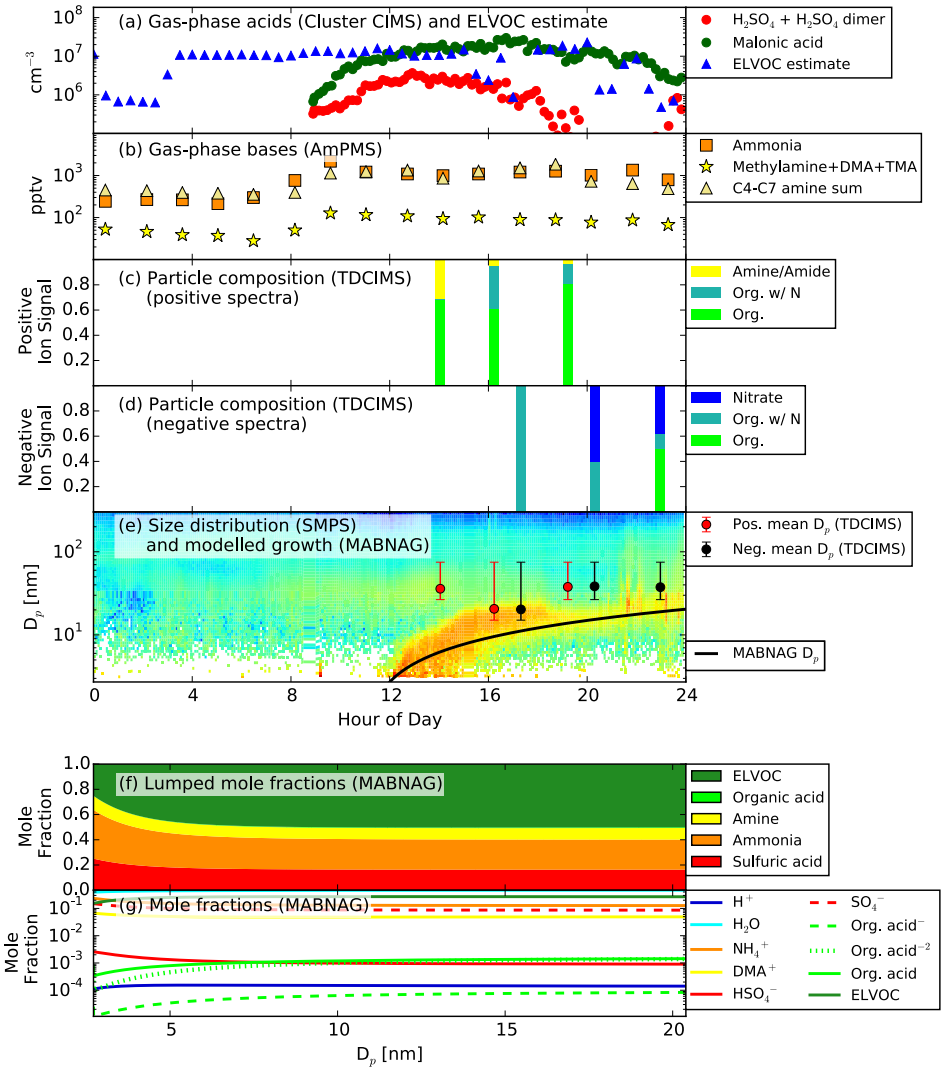

Figure 2. Measurements and MABNAG predictions for the base-case simulation, MAL/10ox/DMA_Lam, for April 19, 2013. (a) Gas-phase acids and ELVOC estimate. Oxalic acid was not measured for this day; the cluster CIMS was not operational before 9:00 CDT for this day. (b) Gas phase bases. (c)-(d) Particle-phase data. The TDCIMS was not operational before 14:00 CDT (e) Size distribution from the three merged SMPSs with the modeled growth rate (black line). Overlaid is the mean collection diameter from the TDCIMS for the positive (red points) and negative (black points) signals . (f)-(g) Modelled particle composition as a function of size. (f) shows the lumped

Anna Hodshire 6/8/2016 10:16 AM
Deleted: :

mole fractions (excluding water) of each species, including any dissociation products. (g) shows the individual mole fractions of each species and its dissociation products. NH_3 and DMA are not shown as both species dissociate almost entirely to NH_4^+ and DMA^+, respectively. OH- is not shown as its concentration is extremely low (~10^{-15}).

5

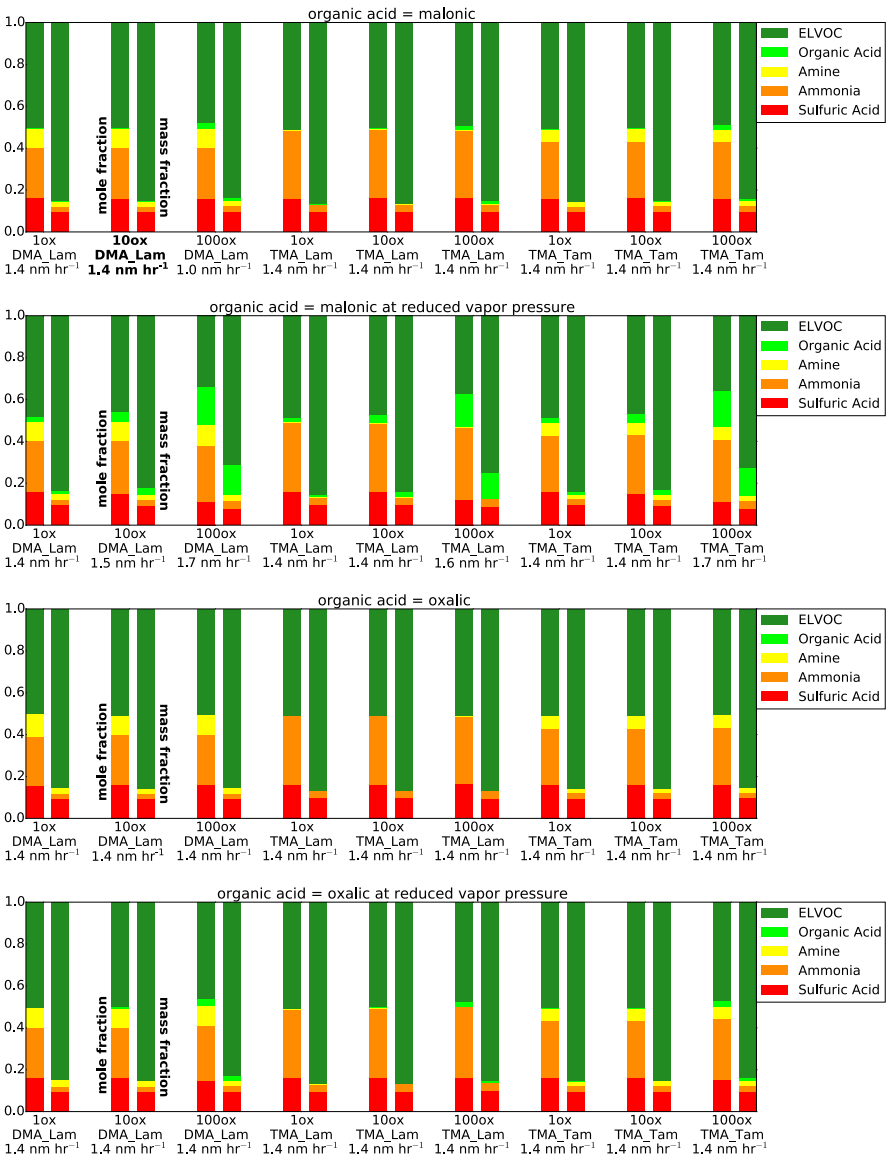

Figure 3. The final dry particle composition for each sensitivity case for April 19, 2013, as both lumped mole fraction (left-hand bars) and lumped mass fraction (right-hand bars). The top and third rows represent each case that uses the properties of malonic acid and oxalic acid, respectively, at the best-fit vapor pressure from Bilde et al. (2015) for the chemical properties of the organic acid inputs. The second and forth rows represent each case that uses the properties of malonic acid and oxalic acid, respectively, at one order of magnitude less in vapor pressure

than the best-fit value for the chemical properties organic acid inputs. 1ox, 10ox, and 100ox refer to cases using the measured (1ox) concentration, 10 times (10ox) the measured concentration, and 100 times (100ox) the measured concentration of oxalic acid, respectively, each summed with the measured malonic acid concentration, for the organic acid concentration input. DMA and TMA refer to cases using the properties of dimethylamine and trimethylamine, respectively, for the chemical properties of the amine inputs. Lam and Tam refer to cases using the sum of the concentrations of only the light amines measured (methylamine, DMA, and TMA) and the sum of the concentrations of the total amines measured (including C4-C7 amines but excluding diamines), respecitively, for the amine concentration input. The bottom row of each case label shows the growth rate for that case in nm hr^{-1}. The bolded case label (first row, second case) represent our base case (see Figure 2 and text).

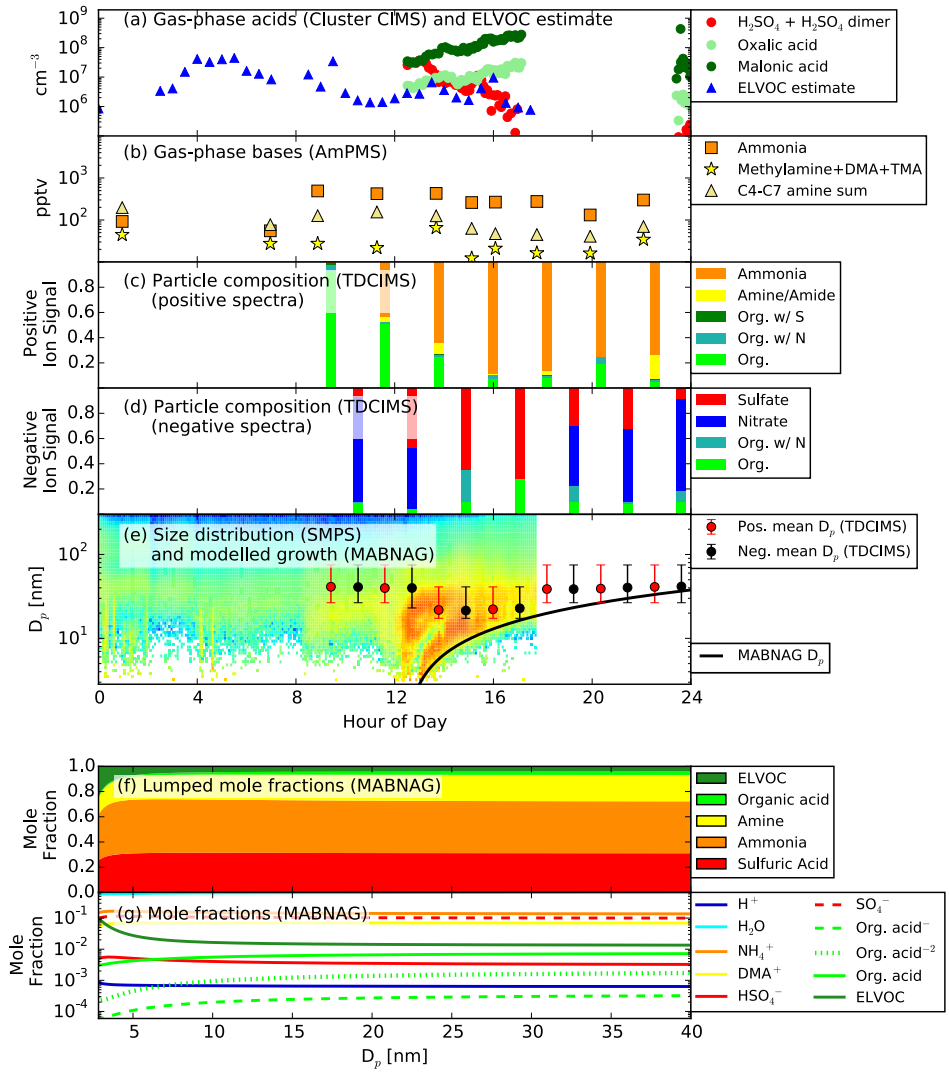

Figure 4. Measurements and MABNAG predictions for the base-case simulation, MAL/10ox/DMA_Lam, for May 9, 2013. (a) Gas-phase acids and ELVOC estimate. The Cluster CIMS was not operational between 17:30-23:00 CDT for this day. (b) Gas phase bases. The AmPMS was not operational between 2:00-6:00 CDT for this day.(c)-(d)

Anna Hodshire 6/8/2016 10:06 AM
Deleted: 3

Particle-phase data. The TDCIMS was not operational before 9:00 CDT for this day. (e) Size distribution from the three merged SMPSs with the modeled growth rate (black line). Overlaid is the mean collection diameter from the TDCIMS for the positive (red points) and negative (black points) signals. The SMPSs were not operational after 17:30 CDT for this day. (f)-(g) Modelled particle composition as a function of size. (f) shows the lumped mole fractions (excluding water) of each species, including any dissociation products. (g) shows the individual mole fractions of each species and its dissociation products. NH_3 and DMA are not shown as both species dissociate almost entirely to NH_4^+ and DMA^+, respectively. OH- is not shown as its concentration is extremely low ($\sim 10^{-15}$).

Anna Hodshire 6/8/2016 1:34 PM
Formatted: Normal, Line spacing: single

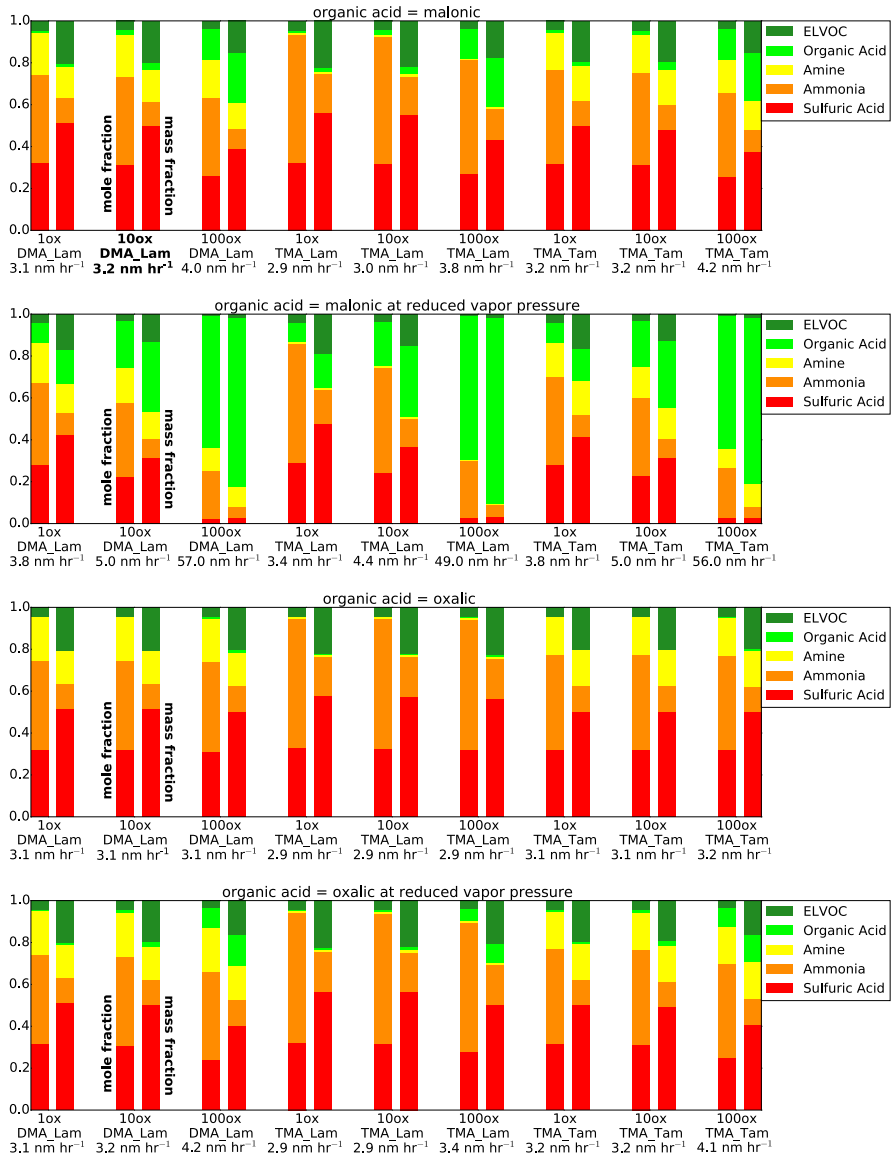

Figure 5. The final dry particle composition for each sensitivity case for May 9, 2013, as both lumped mole fraction (left-hand bars) and lumped mass fraction (right-hand bars). The top and third rows represent each case that uses the properties of malonic acid and oxalic acid, respectively, at the best-fit vapor pressure from Bilde et al. (2015) for the chemical properties of the organic acid inputs. The second and forth rows represent each case that uses the

Anna Hodshire 6/8/2016 1:34 PM
Deleted: ... [8]
Unknown
Formatted: Font:(Default) Times New Roman, 10 pt

properties of malonic acid and oxalic acid, respectively, at one order of magnitude less in vapor pressure than the best-fit value for the chemical properties organic acid inputs. 1ox, 10ox, and 100ox refer to cases using the measured (1ox) concentration, 10 times (10ox) the measured concentration, and 100 times (100ox) the measured concentration of oxalic acid, respectively, each summed with the measured malonic acid concentration, for the organic acid concentration input. DMA and TMA refer to cases using the properties of dimethylamine and trimethylamine, respectively, for the chemical properties of the amine inputs. Lam and Tam refer to cases using the sum of the concentrations of only the light amines measured (methylamine, DMA, and TMA) and the sum of the concentrations of the total amines measured (including C4-C7 amines but excluding diamines), respecitively, for the amine concentration input. The bottom row of each case label shows the growth rate for that case in nm hr^{-1}. The bolded case label (first row, second case) represent our base case (see Figure 4 and text).

Anna Hodshire 6/8/2016 1:33 PM
Formatted: Normal, Line spacing: single

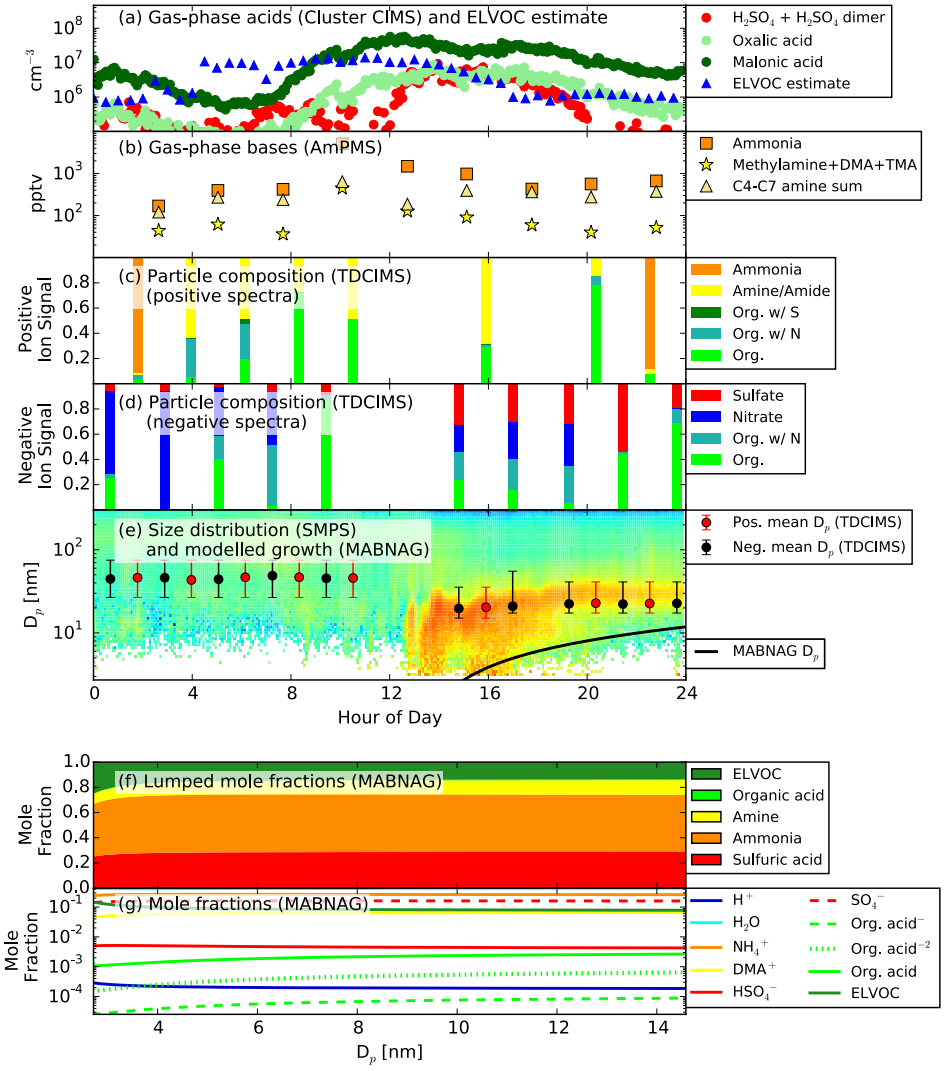

Figure 6. Measurements and MABNAG predictions for the base-case simulation, MAL/10ox/DMA_Lam, for May 11, 2013. (a) Gas-phase acids and ELVOC estimate. (b) Gas phase bases. (c)-(d) Particle-phase data. (e) Size distribution from the three merged SMPSs with the modeled growth rate (black line). Overlaid is the mean collection diameter from the TDCIMS for the positive (red points) and negative (black points) signals . (f)-(g) Modelled particle composition as a function of size. (f) shows the lumped mole fractions (excluding water) of each species, including any dissociation products. (g) shows the individual mole fractions of each species and its

Anna Hodshire 6/8/2016 10:11 AM
Deleted: 4

Anna Hodshire 6/8/2016 10:15 AM
Deleted: :

dissociation products. NH_3 and DMA are not shown as both species dissociate almost entirely to NH_4^+ and DMA^+, respectively. OH- is not shown as its concentration is extremely low ($\sim 10^{-15}$).

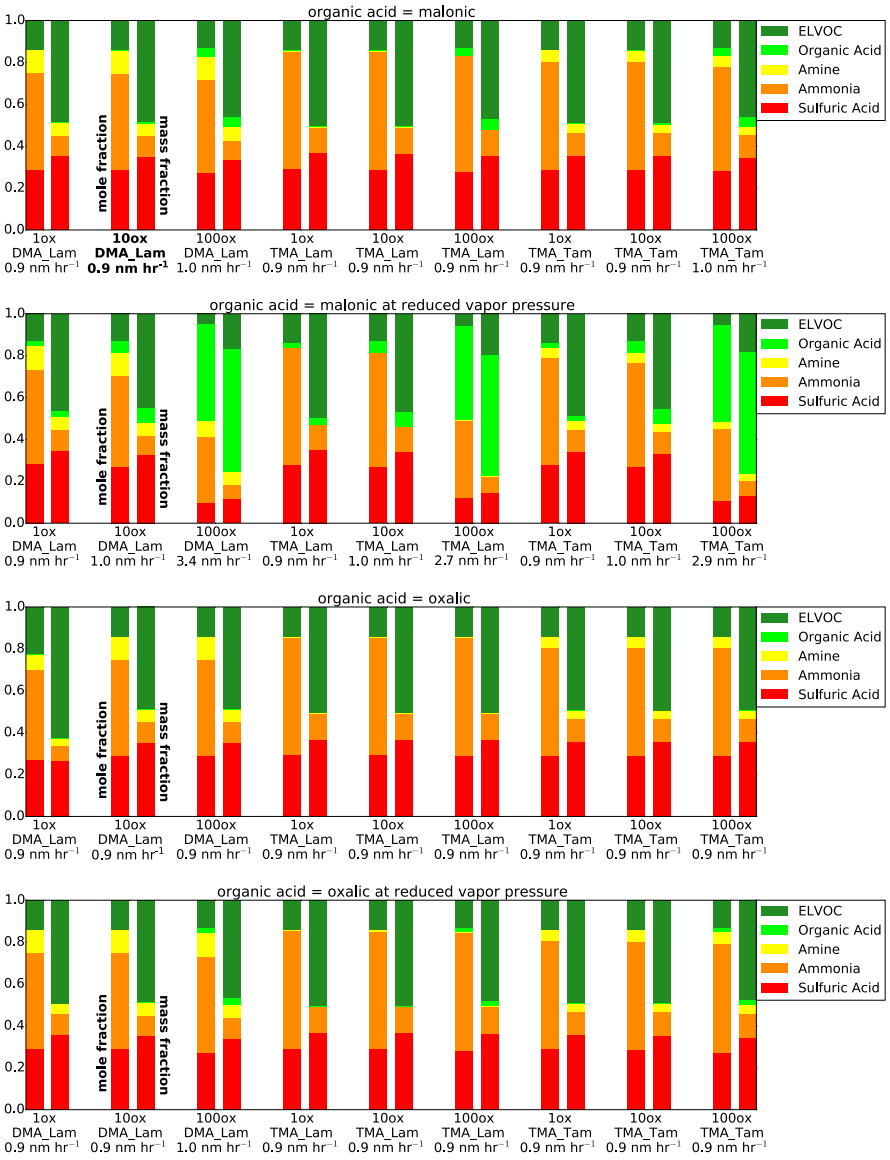

Figure 7. The final dry particle composition for each sensitivity case for May 11, 2013, as both lumped mole fraction (left-hand bars) and lumped mass fraction (right-hand bars). The top and third rows represent each case that uses the properties of malonic acid and oxalic acid, respectively, at the best-fit vapor pressure from Bilde et al. (2015) for the chemical properties of the organic acid inputs. The second and forth rows represent each case that uses the properties of malonic acid and oxalic acid, respectively, at one order of magnitude less in vapor pressure

Unknown

Formatted: Font:(Default) Times New Roman, 10 pt

than the best-fit value for the chemical properties organic acid inputs. 1ox, 10ox, and 100ox refer to cases using the measured (1ox) concentration, 10 times (10ox) the measured concentration, and 100 times (100ox) the measured concentration of oxalic acid, respectively, each summed with the measured malonic acid concentration, for the organic acid concentration input. DMA and TMA refer to cases using the properties of dimethylamine and trimethylamine, respectively, for the chemical properties of the amine inputs. Lam and Tam refer to cases using the sum of the concentrations of only the light amines measured (methylamine, DMA, and TMA) and the sum of the concentrations of the total amines measured (including C4-C7 amines but excluding diamines), respecitively, for the amine concentration input. The bottom row of each case label shows the growth rate for that case in nm hr^{-1}. The bolded case label (first row, second case) represent our base case (see Figure 6 and text).

Anna Hodshire 7/7/2016 11:49 AM
Deleted: ... [9]

Anna Hodshire 7/7/2016 11:49 AM
Formatted: Normal, Line spacing: single

Supplementary Information

S1 Growth Rate Methods

Three methods were employed for determining a range of possible growth rates from the SMPS data. The first method, referred to here as the leading-edge method, is adapted from Lehtipalo et al. (2014) and finds the time at which the binned aerosol distribution between 10-20 nm reaches one-half of its maximum concentration for each bin. A linear fit between the bins' median diameter and the associated times determines the growth rate. The second method, referred to here as the D_p-mode method, tracks the change in diameter of the maximum concentration of the aerosol size distribution between 10-20 nm; a linear fit between peak diameters and the associated times determines the growth rate. When plotted against the size distribution (Figures S1-S3), it is seen that the leading-edge and D_p-mode methods do not tend to track the growing size distribution for every days. For this reason, we have included a third method, which we call the visual method, in which we have made a linear growth-rate estimate between 10-20 nm for each day based upon visual inspection of the size distribution.

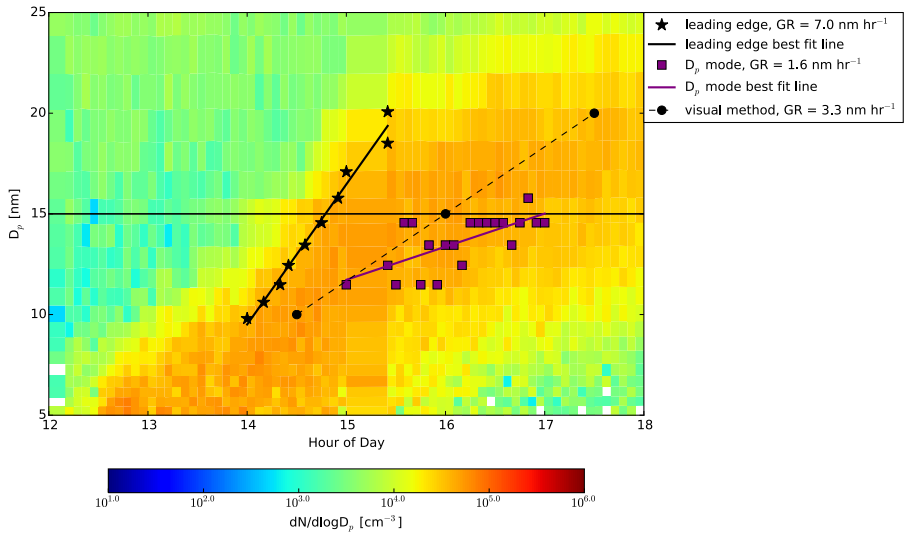

Figure S1. The results of the three growth rate calculations for April 19, 2013. The x-axis represents CDT time. The line at 15 nm D_p is to guide the eye.

Unknown
Formatted: Font:(Default) Times New Roman, 10 pt

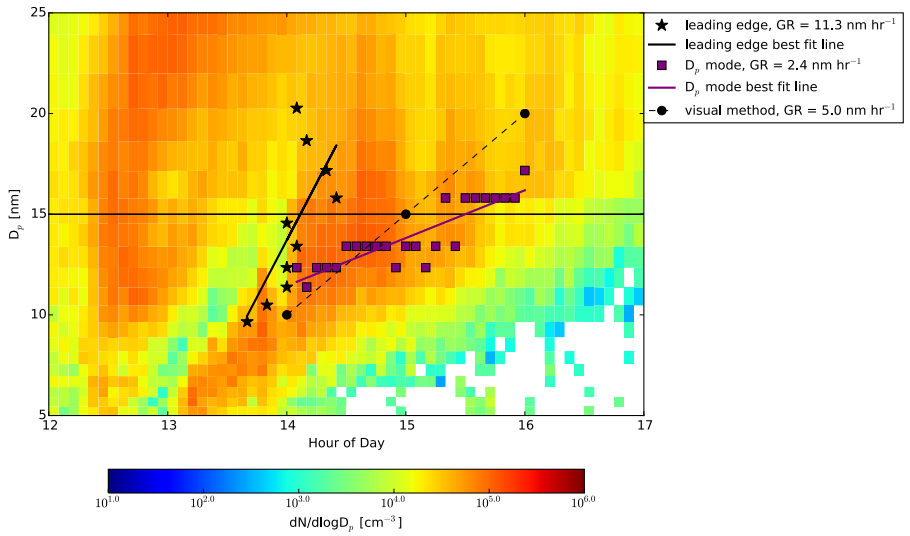

Figure S2. The results of the three growth rate calculations for May 9, 2013. The x-axis represents CDT time. The line at 15 nm D_p is to guide the eye.

Unknown

Formatted: Font:(Default) Times New Roman, 10 pt

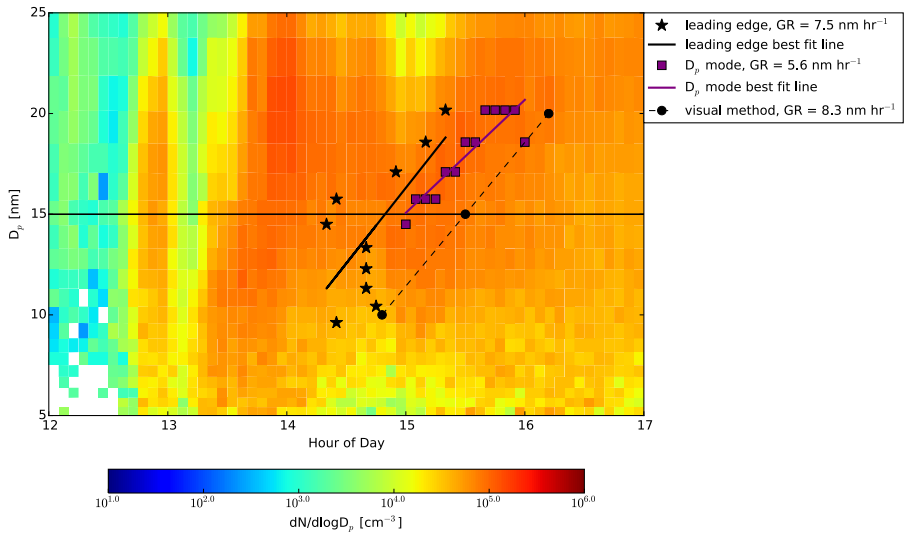

Figure S3. The results of the three growth rate calculations for May 11, 2013. The x-axis represents CDT time. The line at 15 nm D_p is to guide the eye.

Unknown

Formatted: Font:(Default) Times New Roman, 10 pt

Table S1. Breakdown of the percent dissociations of H_2SO_4 to HSO_4^{-1} to HSO_4^{-1} and SO_4^{-2} ; the organic acid (malonic or oxalic) to its first and second dissociation products; NH_3 to NH_4^+; and the amine (DMA or TMA) to its dissociation product for the model output of April 19, 2013. In MABNAG, sulfuric acid is assumed to dissociate completely.

Case	HSO_4^{-1}	SO_4^{-2}	Org. Acid	Org. $Acid^{-1}$	Org. $Acid^{-2}$	NH_3	NH_4^+	Amine	$Amine^+$
MAL/1ox/DMA_L	0.01	0.99	0.49	0.029	0.48	8.6E-09	1	3.1E-10	1
MAL/10ox/DMA_L	**0.01**	**0.99**	**0.49**	**0.029**	**0.48**	**8.6E-09**	**1**	**3.1E-10**	**1**
MAL/100ox/DMA_L	0.011	0.99	0.5	0.028	0.47	8.3E-09	1	3E-10	1
MAL/1ox/TMA_L	0.018	0.98	0.64	0.027	0.33	6.3E-09	1	2.3E-09	1
MAL/10ox/TMA_L	0.018	0.98	0.64	0.027	0.33	6.3E-09	1	2.3E-09	1
MAL/100ox/TMA_L	0.018	0.98	0.64	0.027	0.33	6.2E-09	1	2.3E-09	1
MAL/1ox/TMA_T	0.013	0.99	0.55	0.028	0.42	7.6E-09	1	2.8E-09	1
MAL/10ox/TMA_T	0.013	0.99	0.55	0.028	0.42	7.6E-09	1	2.8E-09	1
MAL/100ox/TMA_T	0.013	0.99	0.56	0.028	0.41	7.4E-09	1	2.7E-09	1
OX/1ox/DMA_L	0.016	0.98	0.071	0.1	0.83	4.2E-09	1	1.5E-10	1
OX/10ox/DMA_L	0.01	0.99	0.028	0.066	0.91	8.6E-09	1	3.2E-10	1
OX/100ox/DMA_L	0.01	0.99	0.028	0.066	0.91	8.5E-09	1	3.1E-10	1
OX/1ox/TMA_L	0.024	0.98	0.1	0.11	0.78	3.6E-09	1	1.4E-09	1
OX/10ox/TMA_L	0.025	0.97	0.11	0.12	0.77	3.1E-09	1	1.3E-09	1
OX/100ox/TMA_L	0.018	0.98	0.05	0.086	0.86	6.3E-09	1	2.3E-09	1
OX/1ox/TMA_T	0.019	0.98	0.085	0.11	0.81	3.9E-09	1	1.5E-09	1
OX/10ox/TMA_T	0.013	0.99	0.035	0.074	0.89	7.6E-09	1	2.8E-09	1
OX/100ox/TMA_T	0.013	0.99	0.035	0.074	0.89	7.5E-09	1	2.8E-09	1
MAL_LoVP/1ox/DMA_L	0.011	0.99	0.5	0.028	0.47	8.3E-09	1	3E-10	1
MAL_LoVP/10ox/DMA_L	0.011	0.99	0.51	0.028	0.46	8.1E-09	1	2.9E-10	1
MAL_LoVP/100ox/DMA_L	0.011	0.99	0.56	0.028	0.41	6.9E-09	1	2.3E-10	1
MAL_LoVP/1ox/TMA_L	0.018	0.98	0.64	0.027	0.33	6.2E-09	1	2.3E-09	1

jrpierce 7/5/2016 12:51 PM
Deleted: S2

Anna Hodshire 7/6/2016 12:18 PM
Deleted: B/O represents the molar ratio of the remaining bases left after neutralizing HSO_4^{-1} and SO_4^{-2} to the total dissociated organic acid

Anna Hodshire 7/6/2016 12:17 PM
Formatted Table

MAL_LoVP/10ox/TMA_L	0.018	0.98	0.65	0.027	0.32	6.1E-09	1	2.3E-09	1
MAL_LoVP/100ox/TMA_L	0.018	0.98	0.68	0.026	0.3	5.6E-09	1	1.9E-09	1
MAL_LoVP/1ox/TMA_T	0.013	0.99	0.56	0.028	0.41	7.4E-09	1	2.7E-09	1
MAL_LoVP/10ox/TMA_T	0.013	0.99	0.57	0.028	0.4	7.2E-09	1	2.7E-09	1
MAL_LoVP/100ox/TMA_T	0.013	0.99	0.61	0.027	0.37	6.3E-09	1	2.2E-09	1
OX_LoVP/1ox/DMA_L	0.01	0.99	0.028	0.066	0.91	8.5E-09	1	3.1E-10	1
OX_LoVP/10ox/DMA_L	0.01	0.99	0.028	0.067	0.9	8.4E-09	1	3.1E-10	1
OX_LoVP/100ox/DMA_L	0.011	0.99	0.031	0.07	0.9	7.7E-09	1	2.8E-10	1
OX_LoVP/1ox/TMA_L	0.018	0.98	0.05	0.086	0.86	6.3E-09	1	2.3E-09	1
OX_LoVP/10ox/TMA_L	0.018	0.98	0.05	0.086	0.86	6.2E-09	1	2.3E-09	1
OX_LoVP/100ox/TMA_L	0.019	0.98	0.053	0.089	0.86	5.9E-09	1	2.2E-09	1
OX_LoVP/1ox/TMA_T	0.013	0.99	0.035	0.074	0.89	7.5E-09	1	2.8E-09	1
OX_LoVP/10ox/TMA_T	0.013	0.99	0.036	0.074	0.89	7.5E-09	1	2.8E-09	1
OX_LoVP/100ox/TMA_T	0.013	0.99	0.039	0.077	0.88	6.9E-09	1	2.6E-09	1

Table S2. Breakdown of the percent dissociations of H_2SO_4 to HSO_4^{-1} to HSO_4^{-1} and SO_4^{-2} ; the organic acid (malonic or oxalic) to its first and second dissociation products; NH_3 to NH_4^+; and the amine (DMA or TMA) to its dissociation product for the model output of May 9, 2013. In MABNAG, sulfuric acid is assumed to dissociate completely.

Case	HSO_4^{-1}	SO_4^{-2}	Org Acid	Org. $Acid^{-1}$	Org. $Acid^{-2}$	NH_3	NH_4^+	Amine	$Amine^{\pm}$
MAL/1ox/DMA_L	0.032	0.97	0.78	0.035	0.18	3.3E-09	1	1.4E-10	1
MAL/10ox/DMA_L	**0.031**	**0.97**	**0.78**	**0.035**	**0.19**	**3.3E-09**	**1**	**1.4E-10**	**1**
MAL/100ox/DMA_L	0.028	0.97	0.77	0.035	0.19	3.7E-09	1	1.4E-10	1
MAL/1ox/TMA_L	0.062	0.94	0.88	0.026	0.092	2.2E-09	1	1.2E-09	1
MAL/10ox/TMA_L	0.061	0.94	0.88	0.025	0.092	2.2E-09	1	1.2E-09	1
MAL/100ox/TMA_L	0.055	0.95	0.88	0.025	0.097	2.5E-09	1	1.0E-09	1
MAL/1ox/TMA_T	0.035	0.97	0.8	0.034	0.17	3.1E-09	1	1.6E-09	1
MAL/10ox/TMA_T	0.035	0.97	0.8	0.033	0.17	3.1E-09	1	1.6E-09	1
MAL/100ox/TMA_T	0.031	0.97	0.79	0.033	0.18	3.5E-09	1	1.4E-09	1
OX/1ox/DMA_L	0.032	0.97	0.13	0.16	0.71	3.2E-09	1	1.4E-10	1
OX/10ox/DMA_L	0.032	0.97	0.13	0.16	0.71	3.2E-09	1	1.4E-10	1
OX/100ox/DMA_L	0.032	0.97	0.13	0.16	0.71	3.2E-09	1	1.4E-10	1
OX/1ox/TMA_L	0.062	0.94	0.24	0.19	0.57	2.2E-09	1	1.2E-09	1
OX/10ox/TMA_L	0.062	0.94	0.24	0.19	0.57	2.2E-09	1	1.2E-09	1
OX/100ox/TMA_L	0.062	0.94	0.24	0.2	0.57	2.2E-09	1	1.2E-09	1
OX/1ox/TMA_T	0.035	0.97	0.14	0.17	0.69	3.0E-09	1	1.6E-09	1
OX/10ox/TMA_T	0.035	0.97	0.14	0.17	0.69	3.0E-09	1	1.6E-09	1
OX/100ox/TMA_T	0.035	0.97	0.14	0.17	0.69	3.1E-09	1	1.6E-09	1
MAL_LoVP/1ox/DMA_L	0.03	0.97	0.78	0.034	0.19	3.5E-09	1	1.4E-10	1
MAL_LoVP/10ox/DMA_L	0.027	0.97	0.76	0.035	0.2	4.0E-09	1	1.4E-10	1
MAL_LoVP/100ox/DMA_L	0.016	0.98	0.71	0.04	0.25	5.4E-09	1	1.6E-10	1
MAL_LoVP/1ox/TMA_L	0.057	0.94	0.88	0.025	0.094	2.4E-09	1	1.1E-09	1
MAL_LoVP/10ox/TMA_L	0.051	0.95	0.87	0.026	0.1	2.7E-09	1	9.9E-10	1
MAL_LoVP/100ox/TMA_L	0.025	0.98	0.81	0.037	0.16	4.5E-09	1	9.7E-10	1

Anna Hodshire 7/6/2016 12:18 PM
Deleted: . B/O represents the molar ratio of the remaining bases left after neutralizing HSO_4^{-1} and SO_4^{-2} to the total dissociated organic acid. Simulations labeled "acidic" under the B/O column represent cases in which there was not enough base in the particle to fully neutralize the sulfuric and organic acids.

Anna Hodshire 7/6/2016 12:18 PM
Formatted Table

MAL_LoVP/1ox/TMA_T	0.033	0.97	0.8	0.033	0.17	3.3E-09	1	1.5E-09	1
MAL_LoVP/10ox/TMA_T	0.029	0.97	0.78	0.034	0.18	3.8E-09	1	1.3E-09	1
MAL_LoVP/100ox/TMA_T	0.017	0.98	0.73	0.04	0.23	5.2E-09	1	1.2E-09	1
OX_LoVP/1ox/DMA_L	0.032	0.97	0.13	0.16	0.71	3.2E-09	1	1.4E-10	1
OX_LoVP/10ox/DMA_L	0.032	0.97	0.13	0.16	0.71	3.2E-09	1	1.4E-10	1
OX_LoVP/100ox/DMA_L	0.029	0.97	0.12	0.16	0.71	3.3E-09	1	1.3E-10	1
OX_LoVP/1ox/TMA_L	0.062	0.94	0.24	0.2	0.57	2.2E-09	1	1.2E-09	1
OX_LoVP/10ox/TMA_L	0.062	0.94	0.23	0.2	0.57	2.2E-09	1	1.2E-09	1
OX_LoVP/100ox/TMA_L	0.058	0.94	0.23	0.2	0.58	2.3E-09	1	1.1E-09	1
OX_LoVP/1ox/TMA_T	0.035	0.97	0.14	0.17	0.69	3.0E-09	1	1.6E-09	1
OX_LoVP/10ox/TMA_T	0.035	0.97	0.14	0.17	0.69	3.1E-09	1	1.6E-09	1
OX_LoVP/100ox/TMA_T	0.032	0.97	0.14	0.17	0.69	3.1E-09	1	1.4E-09	1

Table S3. Breakdown of the percent dissociations of H_2SO_4 to HSO_4^{-1} to HSO_4^{-1} and SO_4^{-2} ; the organic acid (malonic or oxalic) to its first and second dissociation products; NH_3 to NH_4^+; and the amine (DMA or TMA) to its dissociation product for the model output of May 11, 2013. In MABNAG, sulfuric acid is assumed to dissociate completely.

Case	HSO_4^{-1}	SO_4^{-2}	Org Acid	Org. $Acid^{-1}$	Org. $Acid^{-2}$	NH_3	NH_4^+	Amine	$Amine^+$
MAL/1ox/DMA_L	0.026	0.97	0.78	0.026	0.19	3.9E-09	1	1.8E-10	1
MAL/10ox/DMA_L	**0.026**	**0.97**	**0.78**	**0.026**	**0.19**	**3.9E-09**	**1**	**1.8E-10**	**1**
MAL/100ox/DMA_L	0.027	0.97	0.78	0.026	0.19	4.1E-09	1	1.8E-10	1
MAL/1ox/TMA_L	0.039	0.96	0.84	0.023	0.13	3.2E-09	1	2.1E-09	1
MAL/10ox/TMA_L	0.039	0.96	0.84	0.023	0.13	3.2E-09	1	2.1E-09	1
MAL/100ox/TMA_L	0.04	0.96	0.84	0.022	0.13	3.3E-09	1	2.0E-09	1
MAL/1ox/TMA_T	0.033	0.97	0.82	0.024	0.16	3.5E-09	1	2.3E-09	1
MAL/10ox/TMA_T	0.033	0.97	0.82	0.024	0.16	3.5E-09	1	2.3E-09	1
MAL/100ox/TMA_T	0.033	0.97	0.82	0.024	0.16	3.6E-09	1	2.2E-09	1
OX/1ox/DMA_L	0.033	0.97	0.15	0.14	0.71	3.3E-09	1	1.4E-10	1
OX/10ox/DMA_L	0.026	0.97	0.1	0.13	0.77	3.9E-09	1	1.8E-10	1
OX/100ox/DMA_L	0.026	0.97	0.1	0.13	0.77	3.9E-09	1	1.8E-10	1
OX/1ox/TMA_L	0.046	0.95	0.19	0.16	0.66	2.8E-09	1	1.6E-09	1
OX/10ox/TMA_L	0.039	0.96	0.14	0.15	0.71	3.2E-09	1	2.2E-09	1
OX/100ox/TMA_L	0.04	0.96	0.15	0.15	0.71	3.2E-09	1	2.2E-09	1
OX/1ox/TMA_T	0.041	0.96	0.17	0.15	0.68	3.0E-09	1	1.6E-09	1
OX/10ox/TMA_T	0.033	0.97	0.13	0.14	0.73	3.5E-09	1	2.3E-09	1
OX/100ox/TMA_T	0.033	0.97	0.13	0.14	0.73	3.5E-09	1	2.3E-09	1
MAL_LoVP/1ox/DMA_L	0.026	0.97	0.78	0.026	0.19	4.0E-09	1	1.8E-10	1
MAL_LoVP/10ox/DMA_L	0.027	0.97	0.78	0.026	0.19	4.1E-09	1	1.7E-10	1
MAL_LoVP/100ox/DMA_L	0.017	0.98	0.75	0.024	0.22	6.2E-09	1	1.6E-10	1
MAL_LoVP/1ox/TMA_L	0.04	0.96	0.84	0.022	0.13	3.3E-09	1	2.1E-09	1
MAL_LoVP/10ox/TMA_L	0.04	0.96	0.84	0.022	0.13	3.4E-09	1	1.9E-09	1
MAL_LoVP/100ox/TMA_L	0.028	0.97	0.82	0.021	0.16	5.2E-09	1	1.1E-09	1

Anna Hodshire 7/6/2016 12:18 PM
Deleted: B/O represents the molar ratio of the remaining bases left after neutralizing HSO_4^{-1} and SO_4^{-2} to the total dissociated organic acid. Simulations labeled "acidic" under the B/O column represent cases in which there was not enough base in the particle to fully neutralize the sulfuric and organic acids.

Anna Hodshire 7/6/2016 12:18 PM
Formatted Table

MAL_LoVP/1ox/TMA_T	0.033	0.97	0.82	0.024	0.16	3.6E-09	1	2.2E-09	1
MAL_LoVP/10ox/TMA_T	0.034	0.97	0.82	0.024	0.16	3.7E-09	1	2.1E-09	1
MAL_LoVP/100ox/TMA_T	0.022	0.98	0.79	0.022	0.19	5.7E-09	1	1.1E-09	1
OX_LoVP/1ox/DMA_L	0.026	0.97	0.1	0.13	0.77	3.9E-09	1	1.8E-10	1
OX_LoVP/10ox/DMA_L	0.026	0.97	0.1	0.13	0.77	3.9E-09	1	1.8E-10	1
OX_LoVP/100ox/DMA_L	0.028	0.97	0.1	0.13	0.77	3.9E-09	1	1.8E-10	1
OX_LoVP/1ox/TMA_L	0.039	0.96	0.14	0.15	0.71	3.2E-09	1	2.2E-09	1
OX_LoVP/10ox/TMA_L	0.04	0.96	0.15	0.15	0.71	3.2E-09	1	2.2E-09	1
OX_LoVP/100ox/TMA_L	0.042	0.96	0.15	0.15	0.71	3.2E-09	1	2.1E-09	1
OX_LoVP/1ox/TMA_T	0.033	0.97	0.13	0.14	0.73	3.5E-09	1	2.3E-09	1
OX_LoVP/10ox/TMA_T	0.033	0.97	0.13	0.14	0.73	3.5E-09	1	2.3E-09	1
OX_LoVP/100ox/TMA_T	0.035	0.97	0.13	0.14	0.73	3.4E-09	1	2.3E-09	1